

© 2017

Ana Filipa Miguel Carvalho

ALL RIGHTS RESERVED

COUPLED PHYSICAL AND PHYTOPLANKTON DYNAMICS IN COASTAL ANTARCTICA

by

ANA FILIPA MIGUEL CARVALHO

A dissertation submitted to the

Graduate School-New Brunswick

Rutgers, The State University of New Jersey

In partial fulfillment of the requirements

For the degree of

Doctor of Philosophy

Graduate Program in Oceanography

Written under the direction of

Josh Kohut and Oscar Schofield

and approved by

New Brunswick, New Jersey

May 2017

ABSTRACT OF THE DISSERTATION

COUPLED PHYSICAL AND PHYTOPLANKTON DYNAMICS IN COASTAL ANTARCTICA

By ANA FILIPA MIGUEL CARVALHO

Dissertation Directors: Josh Kohut and Oscar Schofield

The biophysical processes regulating primary productivity and biomass of phytoplankton in Antarctic coastal seas are both highly variable in time and space. This dissertation integrates multi-platform observations to understand the physical drivers of phytoplankton in coastal waters of Antarctica, with a greater focus in the West Antarctic Peninsula (WAP). The heads of cross-shelf canyons in the WAP are considered biological “hotspots”, yet the physiology and composition of the phytoplankton blooms and the physical mechanisms driving them are not well understood. Incubation experiments were conducted at three of the WAP canyons to test the role of light availability and upwelling of mUCDW in the increased productivity observed at those locations. Results showed that light, and in particular photoadaptation mechanisms are responsible for increased phytoplankton. This work determined an ecologically relevant MLD for coastal Antarctica to further investigate the role of light in these canyon systems. The mixed layer depth (MLD) determined by the maximum of the buoyancy frequency criteria was found to correlate the best with the vertical distribution of phytoplankton estimated by chlorophyll fluorescence. This metric was then applied to a high-resolution glider dataset with the aim to characterize the dynamics of the spring phytoplankton bloom in submarine canyons in the WAP. Both stability, due to increased freshwater input, and

mixed layer depth (MLD), and therefore light availability, have been linked to increased chlorophyll fluorescence.

To evaluate how the photophysiology of phytoplankton respond to physical forcing, the glider was equipped with a PAR sensor and integrated with a Fluorescence Induction and Relaxation (FIRe) sensor, the first sensor of its kind to be integrated in a glider. The concurrent high-resolution, vertically-resolved and autonomous measurements of physiological variables together with physical oceanographic data allows investigations on how photosynthetic processes are affected by environmental factors, as it is highly sensitive to environmental stresses. Analyses comparing different MLD regimes have shown different photoadaptations resulting from differences in solar radiation exposure conditions (both time and intensity), reflected in the depth of the ML. Potentially different photoacclimation regimes can be evaluated by comparing light saturation parameters (E_k) determined based on the relationship between Photosynthetic Available Radiation (PAR) and photosystem II photosynthetic efficiency (F_v/F_m). With decreasing sea ice trends and increased winds reported for some Antarctic coastal regions undergoing rapid climatic changes, the increased phytoplankton exposure to highly dynamic irradiance levels, especially with deeper MLD, have significant ecological and biogeochemical implications, particularly in the carbon cycling.

Acknowledgments

I am grateful to my committee for their guidance throughout this dissertation. I would like to thank Josh Kohut for being an incredible mentor. His dedication and friendship are, in large part, reasons why I decided to pursue this Ph.D. at Rutgers and I am happy to have brought some biology to his “furniture moving” life. I would also like to thank Oscar Schofield for all the support, mentorship and for pushing me to think outside the box. To both I owe my love for Antarctica and polar oceanography and I now hope to inspire the next generation the way they inspired me. I would also like to thank Matt Oliver and Max Gorbunov, who have been extremely supportive throughout my PhD and helped me speed up the process of scientific publication. Your guidance has definitely made me a better scientist.

I am also grateful for the support of the Palmer Long Term Ecological Research family, with a special thanks to Hugh Ducklow for accommodating my water needs for all the incubation experiments conducted over the years in Antarctica.

I would like to thank present and past members of the Department of Marine and Coastal Sciences, in particular my colleagues of the Rutgers University Center for Ocean Observing Leadership (RUCOOL, formerly known as Coastal Ocean Observation Lab). I thank Dave Aragon, Chip Haldeman, Tina Haskins, John Kerfoot, Laura Nazarro for helping me navigate the glider world, both on the hardware and software sides. Thanks to Janice McDonnell, Carrie Ferraro and Kristin Hunter-Thompson for training me to be a better science communicator and an advocate for scientific outreach. And Patty Gillen, for making the RUCOOL a functional family I love being a part of.

I'm grateful for Liz Sikes, John Wilkin, Bob Chant and Kay Bidle for taking the time to guide and support my research and education and for providing me with opportunities to expand my scientific experience outside my direct field of research. The students of the Graduate Program in Oceanography and DMCS post-docs provided a supportive community to adjust to the life of a graduate student living abroad. I'm thankful for having been part of the best cohort the GPO has seen: Nicole Couto, Nicole Waite, Jack McSweeney, Christien Laber, Alex Lopez, Brittany Schieler, Kevin Crum and Katie Harazin. Grad school would not have been the same without them.

I would like to give a special thanks to Amber Annett, Mehul Vora and Guangyu Xu for their friendship and for being there, especially in this last marathon run. I am very fortunate to have shared many adventures with them under and above water and hope to share many more no matter which continent we end up living on. A big thanks to Amber for all the "caffeination" breaks and lunches that helped my sanity during the writing process as well as for her energy, humor and enthusiasm.

Thank you to all friends inside and outside the graduate program, who kept me sane throughout ups and downs. Thanks Angela, Andreia, Jess for your friendship, and my teammates from volleyball, softball and soccer for keeping me sane through ball kicking. I'm also thankful for my scuba family here at Rutgers that allowed me to continue my passion of diving. I'm grateful for my amazing friends from college: Joana Boura, Ricardo Correia, Catarina Costa and Ricardo Maia; and despite the distance and the fact that we are all in different countries, we still support each other no matter what. A special thanks to Ana Martins for introducing me to the world of oceanography

and the support that led to my internship at Rutgers. The passion and enthusiasm with which she covered 300 slides every class made me fall in love with oceanography, and a few years later here I am excited to inspire the next generation of oceanographers. Many thanks to all my friends in the Azores for their support and friendship.

Finally, a heartfelt thanks to my family for their faith in my perseverance. I am extremely grateful to my parents for cultivating my love for the ocean and encouraging all my adventures that led to where I am today. I am truly fortunate to have the unconditional support from my mom, my sister Sofia, Paulo, and my grandma. Their support and encouragement were key to my success. And finally to my dad who, despite no longer being with us, was always the first one to encourage me to follow my dreams, always cheering me on from the sidelines. The one who supported me unconditionally and from whom I inherited my curiosity and love for science. I owe to him the person I am today.

During this Ph.D. I have been funded by a doctoral fellowship from the Portuguese Foundation for Science and Technology (DFRH - SFRH/BD/72705/2010), the NSF funded Palmer Long-Term Ecological Research (PAL-LTER) Project and a Teledyne Marine Graduate Research Fellowship.

Dedication

To my dad, Justino Carvalho, who always encouraged me to follow my dreams ...

Table of Contents

Abstract of the Dissertation	ii
Acknowledgments	iv
Dedication	vii
Table of Contents	viii
List of Tables	xii
List of Figures	xiv
 Chapter 1: INTRODUCTION.....	 1
 Chapter 2: BOTTOM-UP CONTROLS OF THE PHYTOPLANKTON SPRING BLOOM IN BIOLOGICAL HOTSPOTS IN THE WEST ANTARCTIC PENINSULA.....	 6
2.1 Abstract.....	7
2.2 Introduction.....	8
2.3 Materials and Methods:	11
2.3.1 Experimental approach and water collection	11
2.3.2 Physical measurements	14
2.3.3 Nutrient addition experiments	15
2.3.4 Light experiments.....	16
2.3.5 Chlorophyll <i>a</i> and accessory pigments.....	17
2.3.6 Macro- and micro-nutrient analysis.....	18
2.3.7 Trace-metal clean methodology.....	18
2.3.8 In vivo Chlorophyll <i>a</i> Fluorescence Kinetics.....	20
2.3.9 Statistical analyses	21
2.4 Results and Discussion.....	21

2.4.1	Palmer Deep Canyon	22
2.4.2	Margarite Trough.....	25
2.4.3	Charcot Island	28
2.4.4	Canyon dynamics and ecosystem implications	30
2.5	Conclusions	34
2.6	Acknowledgements	35

Chapter 3: DEFINING THE ECOLOGICALLY RELEVANT MIXED LAYER DEPTH FOR ANTARCTICA'S COASTAL SEAS 36

3.1	Abstract	37
3.2	Introduction.....	37
3.3	Data and Methods	39
3.3.1	Slocum gliders.....	39
3.3.2	Mixed layer depth.....	41
3.3.3	Chlorophyll-a Fluorescence	43
3.4	Results and Discussion.....	45
3.5	Conclusions	54
3.6	Acknowledgements	54

Chapter 4: MIXING AND PHYTOPLANKTON DYNAMICS IN A SUBMARINE CANYON IN THE WEST ANTARCTIC PENINSULA..... 56

4.1	Abstract	57
4.2	Introduction.....	58
4.3	Materials and Methods:	60
4.3.1	Slocum gliders.....	60
4.3.2	Sampling overview.....	61

4.3.3	Mixed layer depth estimation.....	63
4.3.4	Optical Measurements.....	64
4.3.4.1	ML averaged and integrated chlorophyll.....	64
4.3.4.2	Chlorophyll Depth	65
4.3.5	Climatology.....	65
4.3.6	Seawater iron methods	66
4.3.7	Cross-canyon analysis	67
4.4	Results	68
4.4.1	Physical properties around the Palmer Deep Canyon.....	68
4.4.2	Coupled dynamics at Palmer Deep Canyon.....	70
4.4.2.1	Seasonal climatology of MLD and chlorophyll.....	70
4.4.2.2	Cross-canyon variability.....	72
4.5	Discussion.....	79
4.5.1	The seasonal cycle at Palmer Deep canyon.....	80
4.5.1.1	Primary water masses.....	80
4.5.1.2	Phytoplankton seasonal dynamics.....	81
4.5.2	Palmer Deep cross-canyon spatial analysis	84
4.6	Conclusions	87
4.7	Acknowledgements.....	89

Chapter 5: MAPPING *IN SITU* CHLOROPHYLL VARIABLE FLUORESCENCE USING AUTONOMOUS UNDERWATER GLIDERS

5.1	Abstract.....	91
5.2	Introduction.....	91
5.3	Autonomous Platform and Sensor integration.....	93
5.3.1	Utility of Slocum gliders.....	93

5.3.2	Integrating variable fluorescence measurements into a glider.....	94
5.3.3	Other sensors pairings	97
5.4	Reference Profile Calibration	97
5.5	Post-deployment processing.....	98
5.5.1	Blanks	98
5.5.2	Functional absorption cross-sections (σ_{PSII}).....	99
5.5.3	Determination of chlorophyll concentrations.....	99
5.6	Hardware configurations	100
5.7	Mission designs.....	102
5.7.1	The “drift mission”	102
5.7.2	The “station keeping mission”	104
5.8	Photoacclimation mechanisms evaluation	106
5.9	Funding.....	110
5.10	Acknowledgements	110
Chapter 6:	Conclusions	111
Acknowledgement of Previous Publications.....		116
References.....		117

List of Tables

<i>Table 2.1: Incubation source waters parameters for all three sites (PD: Palmer Deep Canyon, MT: Margarite Trough, C: Charcot Is). Relevant initial parameters from the incubation water collection casts, including water source (S: near surface, D: deep), depth of sampling for incubation setup, chlorophyll a concentration (Chl a). Initial F_v/F_m measured on water collected for incubation are reported. For each cast, we report mixed layer depth (MLD) and corresponding Quality index (QI, following Carvalho et al. [2017]) as well as 1% light level. Macronutrients and iron (Fe) concentrations for the source waters are also presented.</i>	<i>13</i>
<i>Table 2.2: Average incident Photosynthetic Available Radiation (PAR, $\mu\text{Ein m}^{-2} \text{s}^{-1}$) for the 2-day period prior to incubation start and for the 4-day incubation duration for all 2 sites (PD: Palmer Deep Canyon, MT: Margarite Trough, C: Charcot Is). Modeled mixed layer depth averaged PAR (MLD_{ave}) indicates phytoplankton light acclimation history. Average light for each screening used (75%, 50%, 25%) is also shown, considering the 4-day average incident PAR during incubation.....</i>	<i>16</i>
<i>Table 2.3: Physiological parameters collected during light incubation experiments for the three canyon systems (PD: Palmer Deep Canyon, MT: Margarite Trough, C: Charcot Is). F_v/F_m is presented for the starting population (T_i). Changes in F_v/F_m and the functional absorption cross-section of PSII ($\Delta\sigma_{\text{PSII}}$) are reported in percentage as the difference between T_i and T_f, normalized by T_i.....</i>	<i>21</i>

<i>Table 3.1: Model-2 regressions between MLD as determined by the $\max(N^2)$ method and chlorophyll depth for the three regions. Statistics show regression coefficients for both MLD quality indices thresholds ($QI>0.8$, $QI>0.5$) determined by Lorbacher et al. [2006] tested as well as for all the data points (no QI filtering). Results are shown for a chlorophyll quality index (QC) of $QC>0.8$, $QC>0.5$ and no QC filtering.</i>	<i>48</i>
<i>Table 3.2: Examples of criteria used to define MLD in waters around Antarctica.....</i>	<i>50</i>
<i>Table 3.3: Comparison between the most commonly used MLD calculations ($QI>0.8$) and chlorophyll depth ($QC>0.5$) for all three regions. Statistics presented include regression coefficients (slope and intercept) in the linear Model II, 95% confidence intervals, R^2 and p-value.</i>	<i>52</i>
<i>Table 5.1: Notation of important FIRE variables</i>	<i>95</i>

List of Figures

Figure 2.1: (a) Bathymetry maps overlaid with the location of the water collection for the incubation experiments conducted along submarine canyons in the West Antarctic Peninsula: Palmer Deep Canyon (blue), Margarite Trough (red) and Charcot (purple). (b) Temperature, (c) salinity and (d) chlorophyll fluorescence depth profiles from CTD casts of source waters at the three incubation sites. Top 50 m of the water are zoomed in on the grey box for each depth profile. Colors denote cast location..... 12

Figure 2.2: Surface Photosynthetically Available Radiation (PAR, $\mu\text{Ein m}^{-2} \text{s}^{-1}$) for the period preceding and during each experiment: (a) Palmer Deep Canyon, (b) Margarite Trough and (c) Charcot. Incubation periods indicated by the colored box. Average PAR corresponding to the 2 day period prior to incubation casts (dashed colored arrow) sets the phytoplankton light history and the 4-day average incident PAR (solid black arrow), used to calculate the light levels at each light treatment (Table 2.2), are also reported..... 15

Figure 2.3: Photosynthetically Available Radiation (PAR, black line) profiles from collection casts for all three regions modeled using HydroLight: (a) Palmer Deep Canyon, (b) Margarite Trough and (c) Charcot Is. Vertical lines indicate average light level when screened to 75% (purple), 50% (green) and 25% (orange) of the incident radiation during the incubation experiment, where incident radiation is the average surface PAR during the 4-day incubation. Blue dotted and black solid horizontal lines

indicate MLD and 1% light level for each region, respectively. The blue vertical line represents the average PAR within the mixed layer (from Table 2.2)..... 17

Figure 2.4: Light (L1-5) and nutrient (N1-3) manipulation experiments at Palmer Deep Canyon. Total chlorophyll (T_{chl} , L1 and N1), relative change (%) in photosynthetic efficiency ($\Delta F_v/F_m$) at T_{final} (L2 and N2) and community composition from CHEMTAX (L3 and N3) are presented for the light and nutrient experiments, respectively. Light treatments are shown as the percentage of light screened from surface irradiance (75%, 50% and 25%). Nutrient controls are shown as surface (S) and mix (M) with the correspondent iron addition treatments (S+ and M+). Photoprotective pigment ratios, $DD+DT)/T_{chl}$ and $DT/(DT+DD)$, are shown for light experiment only. Different symbols (top 2 rows) denote treatments and timepoints that were found to be significantly different ($p<0.05$)..... 24

Figure 2.5: Light (L1-5) and nutrient (N1-3) manipulation experiments at Margarite Trough. Total chlorophyll (T_{chl} , L1 and N1), relative change (%) in photosynthetic efficiency ($\Delta F_v/F_m$) at T_{final} (L2 and N2) and community composition from CHEMTAX (L3 and N3) are presented for the light and nutrient experiments, respectively. Light treatments are shown as the percentage of light screened from surface irradiance (75%, 50% and 25%). Nutrient controls are shown as surface (S) and mix (M) with the correspondent iron addition treatments (S+ and M+). Photoprotective pigment ratios, $DD+DT)/T_{chl}$ and $DT/(DT+DD)$, are shown for light experiment only. Different symbols (top 2 rows) denote treatments and timepoints that were found to be significantly different ($p<0.05$)..... 26

Figure 2.6: Light (L1-5) and nutrient (N1-3) manipulation experiments at Charcot Is. Total chlorophyll (T_{chl} , L1 and N1), relative change (%) in photosynthetic efficiency ($\Delta F_v/F_m$) at T_{final} (L2 and N2) and community composition from CHEMTAX (L3 and N3) are presented for the light and nutrient experiments, respectively. Light treatments are shown as the percentage of light screened from surface irradiance (75%, 50% and 25%). Nutrient controls are shown as surface (S) and mix (M) with the correspondent iron addition treatments (S+ and M+). Photoprotective pigment ratios, $DD+DT/T_{chl}$ and $DT/(DT+DD)$, are shown for light experiment only. Different symbols (top 2 rows) denote treatments and timepoints that were found to be significantly different ($p < 0.05$). 29

Figure 3.1: Location of glider data used in the analysis: (a) glider tracks in the three main regions. Panels 1b-d show bathymetry maps overlaid with the detailed location of each individual glider profile (dots) for the regions shown in the first panel: (b) Ross Sea, (c) Amundsen Sea and (d) WAP. Red dots – MLD Quality index (QI) > 0.5 (see Section 2.2 for details); blue dots, remaining profiles not considered for the MLD analysis (QI < 0.5). 40

Figure 3.2: Determination of mixed layer depth (MLD) and chl-a depth (Z_{chl}) from a glider profile (located at 64.827°S, 64.286°W at GMT 4:29 on January 6th, 2014). (a) density profile (solid blue line) with MLD (dashed blue) calculated by max (N^2) and range of MLD (shaded blue) calculated using methods described in Table 3.2; (b) calculated buoyancy frequency (N^2) profile and MLD; (c) chl-a profile (solid green

line) with Z_{chl} (dotted line) defined by the maximum angle method [Chu and Fan, 2011], or the $\max(\tan\theta_{(chl)})$, and (d) calculated $\tan\theta_{(chl)}$ and Z_{chl} 41

Figure 3.3: θ -S scatters plots for all 3 areas shown in Figure 1: (a) Ross Sea, (b) Amundsen Sea and (c) WAP. Color indicates depth of the water column measurement in the upper 100 m of the water column. All data between 100-1000 meters are plotted in black. Primary water masses sampled are indicated and labeled (WW = Winter Water; MSW = Modified Shelf Water; AASW = Antarctic (summer) Surface Water; m(U)CDW = modified (Upper) Circumpolar Deep Water..... 45

Figure 3.4: Correlation between MLD and Z_{chl} for all glider profiles with Quality Index (QI) over 0.5 (open marker) and over 0.8 (filled marker) for all 3 regions: (a) Ross Sea (triangle); (b) Amundsen Sea (square); (c) WAP (circle); (d) comparison between all three Antarctic regions (QI>0.5) with normalized stability frequency colored and markers representing region. 95% confidence intervals (shaded area) and model-2 regression line are shown for QI>0.8 (dashed line). A quality index (QC) was also applied to chl-a profiles and only profiles with QC>0.8 are shown above. Line 1:1 is shown in green. 46

Figure 3.5: Model-2 regression comparison between most commonly used MLD calculations and Chlorophyll depth for all 3 regions: Ross Sea (left, red); Amundsen Sea (middle, black) and WAP (right, blue). Each row indicates one method. 95% confidence intervals (shaded area) and regression line are shown for quality index (QI)>0.8 (dashed line). Statistics summary presented in Table 3.3. Line 1:1 is shown in green.. 51

Figure 3.6: Example of profiles when MLD was not determined ($QI < 0.5$). Left: Density (Kg m^{-3}). Right: Chlorophyll-a fluorescence ($\mu\text{g L}^{-1}$). Horizontal lines indicate MLD for the most commonly used definitions in Antarctica's coastal seas. Shaded area denotes range of calculated MLD..... 53

Figure 4.1: Bathymetry maps overlaid with location of the glider profiles (red – MLD Quality index (QI) > 0.5 ; blue dots, remaining profiles where MLD was not determined and therefore not included in the analysis, i.e., $QI < 0.5$) for the regions, WAP (left) and PD (right). Cross-canyon transects highlighted in yellow from the 2015 mission (gliders ru05 and ud134). White line separates the head of the canyon into northern and southern flanks. Green square indicates location of Station E where dissolved iron data were collected. 62

Figure 4.2: Top row: θ -S for the two areas shown in Figure 1: (a, c) WAP, and (b, d) Palmer Deep Canyon. All data collected below 100 meters are plotted in black. Color indicates depth of the water column measurement (upper 100 m of the water column). Primary water masses sampled are indicated and labeled (WW = Winter Water; AASW = Antarctic (summer) Surface Water; mUCDW = modified Upper Circumpolar Deep Water; and the regional ACC-core UCDW. Bottom row: Scatter plots comparing depth of the mixed layer (MLD) with the depth of the lower boundary of the chlorophyll profile for all glider profiles with Quality Index (QI) over 0.5. Shaded region represents 95% confidence intervals (CI) for each region. Trend lines are shown for each area and each quality index. Line 1:1 shown in green. A quality index of 0.5 was also applied to chlorophyll (QI_{chl}) profiles and only profiles with $QI_{chl} > 0.5$ are shown above. Color of

the dots represents normalized stability, i.e., the stability frequency at that the depth of the ML ($\max(N^2)$) divided by the median stability of that region. 69

Figure 4.3: Mixed Layer Depth (MLD) in the Palmer Deep region showing evolution on MLD throughout the spring/summer season. Color denotes ML averaged: (a) temperature, (b) chlorophyll, (c), salinity and (d) ML integrated chlorophyll. Marker size represents the standard error of the variable in color (larger marker represents lower standard error, and vice-versa). Standard error of depth MLD is shown in the vertical bars. Averages were calculated using 13,972 individual glider profiles collected during 2010-2015 deployments. Daily averages of wind and surface PAR are shown in panels (a) and (b), respectively. Surface iron measurements at Station E are shown in panel (d) from 2014-2015 season. 71

Figure 4.4: Water stability in the Palmer Deep region using daily averages: (a) salinity and maximum of stability frequency ($\max N^2$); (b) seasonal climatology of MLD with $\max(N^2)$. Averages were calculated using 13,972 individual glider profiles collected during 2010-2015 deployments. 72

Figure 4.5: θ -S scatter plots from ru05/ud134 gliders, comparing the water masses of Northern (N, top) and Southern (S, bottom) flanks of the head of the Palmer Deep canyon through time (panels left to right). Black dots represent all glider measurements (both areas) for the entire deployment. Color denotes depth of the water column measurement. 73

Figure 4.6: Decomposition of the θ -S diagrams from Figure 4.5, for Northern (red) and Southern (blue) flanks of the head of the Palmer Deep canyon: (a1-4) average θ -S diagram with average (center points) and standard deviation (horizontal bars for salinity; vertical bars for temperature), (b1-4) average temperature profile, (c1-4) average salinity profile, with standard deviation (shaded area), per depth for each time point. 74

Figure 4.7. Relationship between the depth of the mixed layer (defined by the maximum water column buoyancy frequency, N^2) and: (a) ML integrated and (b) ML averaged chlorophyll concentrations. Comparison between the northern (filled marker, solid line) and southern (open marker, dashed line) flanks. The colors indicate time. Lines represent the trends seen between Jan 6 – Jan 21 (blue) and Jan 22 – Feb 9 (red). 76

Figure 4.8. Time averaged transect (Jan 6 - Jan 28, 2015) Northern and Southern regions are separated by the dashed vertical line at km 6.2 in the along-track distance. Variables plotted are time averaged transect of: (a) temperature, where warm layer at the surface represents AASW, dark blue denotes WW, bottom layer in red indicates possibly mUCDW intrusion; (b) salinity and (c) mixed layer depth (MLD; blue dotted line) with integrated chlorophyll (upper 100m; green solid line) and canyon bathymetry (black solid line)..... 77

Figure 4.9. Top panels: Bathymetry of the cross-canyon transect performed by ru05 (yellow, Figure 4.1). Bottom panels: Hovmöller diagram of the temporal evolution of each transect by ru05 regarding: (a) mixed layer depth, (b-d) ML averaged (b)

temperature, (c) salinity, (d) chlorophyll and (e) ML integrated chlorophyll. Dashed line separates northern and southern flanks of the head of the Palmer Deep canyon.. 78

Figure 5.1: An example of FRe profile. The quantum yield of photochemistry in PSII (i.e., photosynthetic efficiency) is deduced from a relative change in fluorescence yield (F_v/F_m) and the functional absorption cross-section of PSII (σ_{PSII}) - from the rate of fluorescence rise during fluorescence induction (100 μ s phase). The subsequent relaxation in fluorescence yield on millisecond time scale reflects the rates of photosynthetic electron transport down to carbon fixation. Minimum (F_o) and maximum (F_m) fluorescence yields corresponding to the states with open and closed reaction centers of PSII, respectively..... 95

Figure 5.2: Top (a) and side (b) view of the Fluorescence Induction and Relaxation (FRe) and Photosynthetic Active Radiation (PAR) sensors integrated into a Slocum glider FRe bay (black section). c) Optional add-on cap used to evaluate physiological stress in a dark-adapted state. d) Extended Slocum glider with double science bay configuration with FRe bay in front and Optics bay with Wetlab ECO pucks (measuring chlorophyll fluorescence, backscatter and colored dissolved organic matter, CDOM) in the aft, Conductivity-Temperature Depth (CTD) sensor and oxygen optode. The glider is shown without its two lateral wings that connect to the black FRe bay..... 96

Figure 5.3: Example of irradiance dependence of chlorophyll fluorescence yields recorded in two different FRe glider configurations. Measurements in: (a) light-adapted state, i.e., the optical chamber with cap “off” and (b) dark-adapted state, i.e.,

the optical chamber with cap “on”. F_o and F_m are minimum (open reaction centers) and maximum (closed reaction centers) fluorescence yields measured in dark-adapted cells. F_o' and F_m' are the minimum and maximum fluorescence yields in a light adapted state. F' is the actual fluorescence yield measured under ambient light. PQ and NPQ are photochemical quenching and non-photochemical quenching, respectively. Top grey arrows indicate example irradiances and its corresponding fraction of NPQ and PQ.

.....101

Figure 5.4: Example of diel cycles collected during the drift mission for shallow (left panels) and deeper (right panels) mixing regimes. The depth of the mixed layer is shown with a black line. Gaps in data show times where glider was drifting at the surface. One profile was collected every hour. Effects of high irradiance periods (hours 10-16) shown in yellow in the Photosynthetically Active Radiation panels (E) are evident by the low values seen in F_v'/F_m' (B, photosynthetic efficiency), F_m' (C, proxy for biomass) and σ_{PSII} (D, functional absorption cross-section). This is evidence of Non-Photochemical Quenching (NPQ), with the deepest penetration occurring during peak irradiance (hour 13-14). A warming of the upper ocean (A, Temperature) is also seen during the highest irradiances.....103

Figure 5.5: Two diel cycles (as outlined in the surface PAR, G) collected in two regions with different oceanographic conditions. Direction and magnitude of the dominant surface currents (A, from HF Radars) are in part responsible for changes in the vertical structure of the water column as demonstrated by the temperature (B) and salinity (C) panels and the depth of the ML (black line). Remaining rows report F_{IR}e

measurements - F_m' (C, relative units), F_v'/F_m' (D, dimensionless) and σ_{PSII} (E, functional absorption cross-section of PSII, \AA^2). While the irradiance effect is not very clear in the noisy F_v'/F_m' data (likely due to lower biomass), a depth-dependent diel signal is present in σ_{PSII} (showing high values during nighttime and a decrease during daytime). By analyzing high-resolution photophysiology data in context of our concurrent physical data we can better understand and evaluate the role of mixing and the water column vertical structure in phytoplankton primary production.....106

Figure 5.6: Top: Scatter plots of F_v/F_m and PAR with curve fits (Equation 5.2) for the two MLD regimes collected during the drift mission (Section 5.7.1; Figure 5.4). Left, 1: average MLD is 15 m (shallower). Right, 2: average MLD is 30 m (deeper). Three depth bins (surface to MLD1 – orange, MLD1 to MLD2 – black, and surface to MLD2 – purple) were created to evaluate potential different phytoplankton photoacclimation regimes. Light saturation parameter (E_k) for each fitting are also presented. Bottom: schematics on difference in photoacclimation regimes presented in the plots on top, evaluating E_k in relation to the MLD (black dashed line). 95% confidence intervals are presented in brackets for the E_k parameter estimation. Under a shallow MLD regime, where the light penetration (yellow layer in bottom panel) reaches closer to the bottom of the ML, there is likelihood of two potential different physiological communities (i.e., communities with different photoacclimation regimes) as evaluated by the different E_k (compare orange and purple layers). The much higher E_k seen at the surface gives an indication of phytoplankton acclimated to high irradiances while the lower E_k seen below the MLD shows low light acclimation. Under deeper MLD

conditions, Ek values are much closer indicating photoacclimation is similar between the 2 layers.....108

Chapter 1: Introduction

Cross-shelf canyon systems in the West Antarctic Peninsula (WAP) are considered biological “hotspots” by providing predictable food resource and driving penguin foraging locations [Erdmann *et al.*, 2011; Fraser and Trivelpiece, 1996] as penguin colonies are located near these deep submarine structures [Fraser and Trivelpiece, 1996]. The association of penguin colonies with deep submarine canyons has led to the hypothesis that phytoplankton productivity is enhanced due to canyon dynamics [Schofield *et al.*, 2013]. These canyons are known to provide a conduit to Upper Circumpolar Deep Water (UCDW), a nutrient enriched, warmer and more saline water mass than Antarctic surface waters onto the shelf [Martinson and McKee, 2012; Martinson *et al.*, 2008]. The presence of modified UCDW has been linked to increased phytoplankton productivity [Prézelin *et al.*, 2000; Prézelin *et al.*, 2004; Schofield *et al.*, 2010], which supports a productive regional food web [Schofield *et al.*, 2010]. Yet the physiology and composition of phytoplankton blooms in these canyons and the physical mechanisms driving them are not yet well understood. Globally, both light and nutrient availability have been identified as key drivers of phytoplankton blooms but their relative importance depends heavily the strength of stratification and mixed layer depth. Shallow mixed layer depths and increased water stability [Mitchell and Holm-Hansen, 1991] provide a relative stable light environment that allow photoacclimation and photoadaptation to become important processes regulating primary production, especially in polar regions [Moline, 1998; Schofield *et al.*, 1995].

The overarching theme of this thesis is to explore the dynamics of the phytoplankton spring bloom in the WAP canyons. Here, we conduct a multi-platform

field study to investigate the impact of canyon-driven physical processes on phytoplankton growth and physiology. The first research chapter (Chapter 2) focuses on testing the ‘Canyon Hypothesis’ [Schofield *et al.*, 2013]. Incubation experiments were conducted at three canyon systems along the WAP to evaluate the light vs. nutrients (macro- and micro-) question as to which factor is responsible for driving the phytoplankton spring bloom over the canyons. Different source waters were mixed (simulating upwelling of nutrient enriched mUCDW) and incubated at different light levels (simulating different mixed layer depths). Light was identified as the main driver of the bloom with phytoplankton showing the capacity to, given a relatively stable light environment (just like a shallow MLD), photoacclimate in a matter of a few days.

Given the results from the incubation experiments where light was identified as the main driver of the phytoplankton bloom, Chapter 3 came about from the need to standardize the mixed layer depth (MLD) definition, a widely used metric linked to light availability and phytoplankton dynamics. Historically several MLD definitions have been used, making inter-comparisons among region-specific studies difficult and sometimes inaccurate. Here we evaluate and present an ecologically relevant MLD for the coastal seas of Antarctica. Using several deployments of underwater gliders throughout three main coastal Antarctic regions (Ross Sea, Amundsen Sea and West Antarctic Peninsula), the MLD definition based on the maximum of buoyancy frequency was found to be the one that best describes the depth to which phytoplankton can be mixed in coastal Antarctic seas.

To further investigate the canyon dynamics effect on phytoplankton (Chapter 4), we apply the previously determined MLD metric to a case study in Palmer Deep Canyon (PD), a highly sampled region in the WAP (NSF PAL-LTER, NSF CONVERGE), surveyed using several oceanographic platforms. Glider deployments in the PD region were used to examine both the seasonal and spatial variability in phytoplankton, with a focus on how it relates to the light availability and thus, the MLD. Both water column stability and MLD were linked to the seasonal increase in chlorophyll fluorescence. Spatial variability in phytoplankton dynamics was associated with water masses present and water column structure driven by local circulation.

Previous chapters evaluated the biophysical controls on phytoplankton in the WAP submarine canyons. Chapter 5 describes a new advance using autonomous robotic underwater gliders with integrated variable fluorescence sensors that now make it possible to conduct underwater spatial surveys for mapping phytoplankton physiology remotely. The integration of a Fluorescence Induction and Relaxation (FIRe) sensor in a Slocum glider allows autonomous high-resolution and vertically-resolved measurements of physiological variables together with physical oceanographic data. The potential for this new technology is demonstrated with deployments in the PD region and documented biophysical controls of photosynthesis, the significant presence of nonphotochemical quenching *in situ*, and the relative light-acclimation states of the phytoplankton communities.

This dissertation is a compilation of two published manuscripts in *Geophysical Research Letters* and *Journal of Geophysical Research: Oceans* (Chapters 3 and 4, respectively), one manuscript that is currently under review for publication in *Optics Express* (Chapter 5) and one manuscript that will soon be submitted for publication in *Limnology and Oceanography* (Chapter 2). Therefore, there is some redundancy in the text, and results from one chapter are often cited in other chapters. The chapters are not organized by chronology of publication date, but rather are arranged by the order that the scientific questions that drove the research presented here were asked.

**Chapter 2: Bottom-up controls of the phytoplankton
spring bloom in biological hotspots in the West Antarctic
Peninsula**

2.1 Abstract

The West Antarctic Peninsula (WAP) shows overall high productivity, yet highly variable in space and time. The depth of the mixed layer and upwelling of warm, nutrient-enriched modified Upper Circumpolar Deep Water (mUCDW) have been identified as potential drivers of phytoplankton bloom development in the WAP canyons. Using shipboard trace-metal clean incubation experiments in three different WAP canyon systems, we tested both factors for enhanced phytoplankton growth. Diatoms dominated the southern region of the Peninsula while the northern region was co-dominated by diatoms and cryptophytes. With ample concentrations of macronutrients at the surface and no iron limitation recorded in any incubation, the addition of deep, nutrient-enriched water to surface waters showed no enhancement in phytoplankton growth. Irradiance levels tested were, in most experiments, relatively high compared to the light levels phytoplankton cells were initially acclimated to, resulting in declines in chlorophyll in some cases, but over the 4 day experiments, significant increases in phytoplankton biomass were recorded in most experiments. Magnitude of the concurrent production of photoprotective pigments was consistent with the light levels tested, suggesting that given a stable light environment, provided by a shallow mixed layer (ML) depth and a well-stratified water column, phytoplankton in the WAP canyons are able to photoacclimate to higher irradiances in a matter of a few days. In a region with a rapid changing climate forecasting decreased sea ice and increased winds, photoacclimation mechanisms are crucial to the bloom development that supports the highly productive regional food web.

2.2 Introduction

Coastal waters of the WAP are a highly productive ecosystem and have been historically associated with large diatom-dominated phytoplankton blooms [*Nelson and Smith, 1991; Prézelin et al., 2004; Smith et al., 2008*], however changes in climate over the past six decades have impacted the WAP ecosystem. Summer chlorophyll concentrations are reported to have declined 12% over the past 3 decades [*Montes-Hugo et al., 2009*]. These declining populations are also shifting from communities dominated by larger diatoms to smaller celled (<20 µm) cryptophyte blooms [*Moline et al., 2004; Montes-Hugo et al., 2009*].

Seasonal dynamics of phytoplankton have been strongly linked to the timing of sea ice retreat [*Ducklow et al., 2012; Rozema et al., 2017*]. Increased phytoplankton production is often observed in the spring along the retreating ice edge, where ample supply of nutrients at the surface together with increased water column stability and shallower mixed layer depth (MLD) provide ideal conditions for phytoplankton to grow. However, changes in the sea ice coverage have not always resulted in the expected response of primary production to decreased seasonal sea ice coverage, and increased light. In the northern WAP (and as far south as Palmer Deep canyon), reduced sea ice cover, increased winds and cloud formation have been accompanied by a deepening of the MLD and consequent reduction in the phytoplankton biomass [*Montes-Hugo et al., 2009*]. Sea ice used to cover most of the Mid WAP, where Margarite Trough is located. This region now shows increased primary production as the decrease in sea ice coverage allows light to penetrate deeper into the water column.

Cross-shelf submarine canyon systems in the WAP are considered biological “hotspots” [Schofield *et al.*, 2013] by providing predictable food resource and driving penguin foraging locations [Erdmann *et al.*, 2011; Fraser and Trivelpiece, 1996]. The association of penguin colonies and increased phytoplankton biomass with submarine canyon heads has led to the hypothesis that primary production is enhanced at those locations as a result of water column dynamics, reduced sea ice coverage and an ample reservoir of macro- and micronutrients [Kavanaugh *et al.*, 2015].

Macronutrients are generally abundant in the WAP shelf [Ducklow *et al.*, 2012; Kim *et al.*, 2016; Serebrennikova and Fanning, 2004] as deep winter mixing resupplies surface layer following biological drawdown. Although they show marked seasonality [Clarke *et al.*, 2008], in most cases it doesn’t seem to limit primary production [Holm-Hansen and Mitchell, 1991] except during very large phytoplankton blooms [Ducklow *et al.*, 2007]. Previous studies have implicated intrusions of modified Upper Circumpolar Deep Water (mUCDW) onto the WAP shelf as a source of nutrients fueling primary production over the shelf [Prézelin *et al.*, 2000; Prézelin *et al.*, 2004] , which supports a productive regional food web [Schofield *et al.*, 2010]. This topographically forced flow of warm, nutrient enriched deep water interacts with bathymetry promoting mixing across the shelf [Martinson and McKee, 2012; Martinson *et al.*, 2008]. The iron concentrations found offshore are lower than the ones found on the shelf and specifically near the canyon heads [Annett *et al.*, submitted]. In addition, previous studies in coastal waters of the WAP have shown that inshore regions do not show iron limited primary production [Annett *et al.*, 2015; Carvalho *et al.*, 2016b; Hopkinson *et al.*, 2007].

Light is an important factor controlling primary production in the WAP shelf. Both the mixed layer depth (MLD) and water column stability have been widely link to phytoplankton dynamics [Carvalho *et al.*, 2016b; Holm-Hansen and Mitchell, 1991; Moline and Prezelin, 1996; Sakshaug *et al.*, 1991] by controlling the amount of light available to the phytoplankton community. Phytoplankton live in a dynamic light environment which is driven by a combination of MLD and the rate of turbulent mixing [Cullen and Lewis, 1988; Lewis *et al.*, 1984]. Since these fluctuations in the light environment vary over a wide range of timescales from second to hours, phytoplankton have different physiological adaptations that span across the different scales. Under high light, phytoplankton undergo the xanthophyll cycle, a mechanism of nonradiative energy dissipation, to prevent photo-oxidative damage to the photosynthetic apparatus [Falkowski and Raven, 2007]. This cycle involves a light-driven, reversible de-epoxidation. In diatoms, dinoflagellates and prymnesiophytes, the carotenoids responsible for this photoprotection are diatoxanthin (DT) and diadinoxanthin (DD) [Demers *et al.*, 1991]. High light induces the conversion of diadinoxanthin into its epoxy-free form, diatoxanthin. Hence, evaluating changes in DT and DD provides an indication on the ecological past of the cells in terms of light exposure [Brunet *et al.*, 1993]. On shorter timescales (seconds to minutes), there is only conversion of DD to DT as there is no time for new pigment production to occur, and therefore DD+DT remains constant. Thus, the ratio $DT/(DT+DD)$ is a good indicator for light exposure on shorter timescales, while the photoprotective pigment concentration (DT+DD) normalized to Chl *a*,

$(DT+DD)/T_{chl}$ is helpful in evaluating phytoplankton light history in timescales of days [Fujiki *et al.*, 2003].

Understanding the links between some of the physical drivers and the biological responses are of high importance as the higher trophic levels are heavily dependent on phytoplankton to survive. Here, we present results from shipboard incubation experiments conducted to evaluate the drivers (light or nutrients) of phytoplankton at the heads of submarine canyons in the WAP. We test two main hypotheses: 1) the upwelling of mUCDW is driving this system by supplying both macro- and micronutrients to the surface waters; 2) this system is driven by light, where the MLD, and therefore the amount of light available for the phytoplankton community, is limiting primary production. We show that phytoplankton in these coastal canyon systems are not nutrient limited, but show efficient use of photoacclimation mechanisms to high light which allows them to thrive under highly variable light environment settings.

2.3 Materials and Methods:

2.3.1 Experimental approach and water collection

Several shipboard incubation experiments were conducted during the annual PAL-LTER (Palmer Long-Term Ecological Research) cruise in January 2015 along the West Antarctic Peninsula, onboard the ARSV Laurence M. Gould (cruise LMG15-01). Water was collected at the canyon heads of three different submarine canyon systems (Figure 2.1a) that are major breeding colonies for the Adelie penguins in the WAP [Schofield *et al.*, 2013]. Additionally, there is evidence of increased phytoplankton biomass which

has been inferred from satellite observations [Kavanaugh *et al.*, 2015]. The northernmost site was located at Palmer Deep Canyon near Anvers Island (64.91° N, 64.58° W), followed by mid location down the peninsula at Margarite Trough near Avian Island (68.03° N, 69.28° W) and the southernmost reachable point we were able to reach at the ice edge near Charcot Island (69.11° N, 76.45° W).

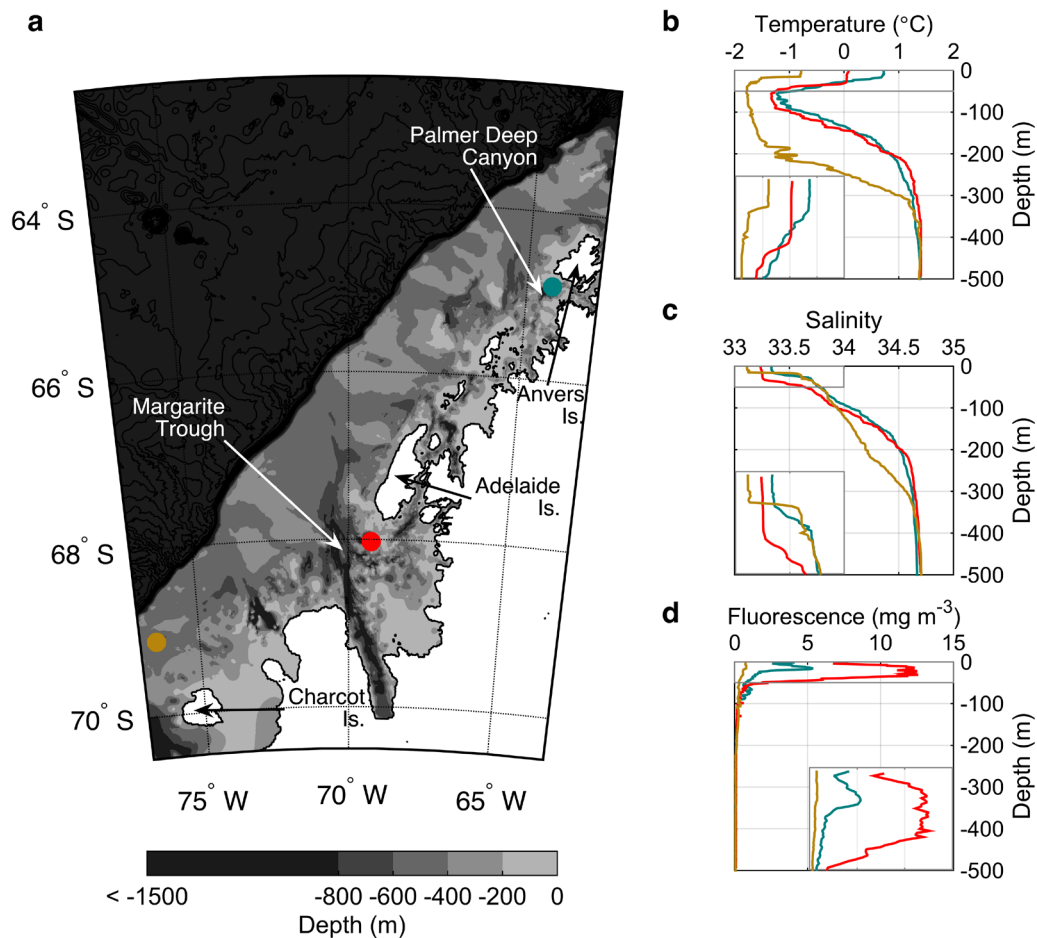


Figure 2.1: (a) Bathymetry maps overlaid with the location of the water collection for the incubation experiments conducted along submarine canyons in the West Antarctic Peninsula: Palmer Deep Canyon (blue), Margarite Trough (red) and Charcot (purple). (b) Temperature, (c) salinity and (d) chlorophyll fluorescence depth profiles from CTD casts of source waters at the three incubation sites. Top 50 m of the water are zoomed in on the grey box for each depth profile. Colors denote cast location.

Source waters (Table 2.1) were collected using a trace metal-clean rosette composed of twelve Niskin-X bottles mounted onto an epoxy-coated frame free of metal anodes and a CTD sensor to obtain physical measurements down the water column. Detailed methodology for trace-metal clean water collection and sampling is described in section 2.3.7. Acid washed trace-metal clean clear polycarbonate 1-L incubation bottles were filled with source waters in the ratios described below. Macrozooplankton were cleanly removed from unfiltered water using an acidwashed 350 μm Nitex mesh.

Table 2.1: Incubation source waters parameters for all three sites (PD: Palmer Deep Canyon, MT: Margarite Trough, C: Charcot Is). Relevant initial parameters from the incubation water collection casts, including water source (S: near surface, D: deep), depth of sampling for incubation setup, chlorophyll a concentration (Chl *a*). Initial F_v/F_m measured on water collected for incubation are reported. For each cast, we report mixed layer depth (MLD) and corresponding Quality index (QI, following *Carvalho et al.* [2017]) as well as 1% light level. Macronutrients and iron (Fe) concentrations for the source waters are also presented.

Site	Water source	Depth, m	Chl <i>a</i> , $\mu\text{g L}^{-1}$	F_v/F_m	[N+N], $\mu\text{mol L}^{-1}$	[PO ₄], $\mu\text{mol L}^{-1}$	[SiO ₄], $\mu\text{mol L}^{-1}$	[Fe], nmol L^{-1}	MLD, m (QI)	1% light level, m
PD	S	10	4.24	0.35	20.68	1.57	60.37	0.49	26 (0.52)	19.8
	D	1200	0	-	27.13	1.96	73.11	1.49		
MT	S	10	12.9	0.40	8.34	0.70	40.66	0.18	44 (0.56)	15.8
	D	490	0	-	29.02	2.06	76.86	0.61		
CI	S	15	0.67	0.39	23.11	1.64	48.50	0.12	15 (0.89)	47.5
	D	440	0	-	27.25	1.97	67.08	0.31		

Two sets of shipboard incubation experiments were conducted at each location to individually evaluate the importance of the depth of the mixed layer (light experiments) and the upwelling of mUCDW (nutrient addition experiments) for driving phytoplankton bloom in submarine canyons in the West Antarctic Peninsula. “Deep”

water was collected at the depth of T_{max} , one of the signatures of mUCDW on the shelf and “surface” water was collected from 10-15 m depth and in the upstream direction of the dominant current flow to minimize any influence from the ship.

In both experiments, parameters were collected at setup (T_i) and the full bottle sacrificed after 4 days of incubation (T_f) to prevent bottle effect. Standard measurements at both timepoints included collecting samples for chlorophyll-a (Chl a) and accessory pigment analysis for community composition classification, nutrient concentration determination and photosynthetic efficiency evaluation using in vivo chlorophyll-a fluorescence kinetics [Gorbunov and Falkowski, 2004].

2.3.2 Physical measurements

Mixed layer depth (MLD) was calculated using the method described in *Carvalho et al.* [2017]. A Quality index was also determined to quantify the uncertainty of the MLD computation, where 0.5 sets the threshold between MLD not determined (<0.5) or determined (>0.5), respectively. Changes in light intensity from clouds were detected using a mast-mounted Photosynthetically Available Radiance (PAR) sensor (Figure 2.2).

As the Trace Metal Clean (TMC) rosette did not have a PAR sensor, the 1% light level was calculated by modeling PAR (Figure 2.3) using the chlorophyll fluorescence profile setting in HydroLight [Mobley, 1994]. Standard default settings were for the HydroLight simulations. This modeled PAR was then used to evaluate the phytoplankton light history (Figure 2.2) by averaging PAR over the ML from the 2 days prior to collection casts (MLD_{ave} PAR, Table 2.2).

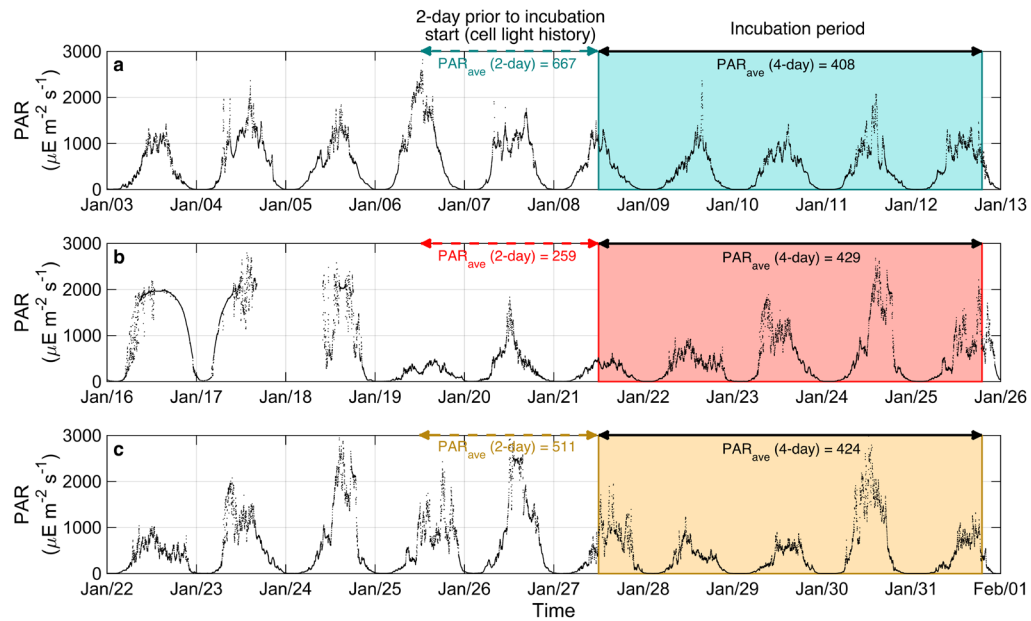


Figure 2.2: Surface Photosynthetically Available Radiation (PAR, $\mu\text{E m}^{-2} \text{s}^{-1}$) for the period preceding and during each experiment: (a) Palmer Deep Canyon, (b) Margarite Trough and (c) Charcot. Incubation periods indicated by the colored box. Average PAR corresponding to the 2 day period prior to incubation casts (dashed colored arrow) sets the phytoplankton light history and the 4-day average incident PAR (solid black arrow), used to calculate the light levels at each light treatment (Table 2.2), are also reported.

2.3.3 Nutrient addition experiments

In the first set of experiments, we tested the “canyon hypothesis” by evaluating whether the upwelling of warm, nutrient enriched, deep mUCDW enhanced phytoplankton growth. Two different treatments were set, one surface (S) with “surface” water only and one mix (M) where equal amounts of “surface” water was mixed with “deep” water totaling 1 L. Given that no phytoplankton were present in the “deep” water, half of the “surface” water in the S treatments was filtered, so all treatments started with similar phytoplankton biomass. For each treatment, three

replicates were spiked with $2 \text{ nmol L}^{-1} \text{ FeCl}_3$ from an acidified stock solution ('+' treatments), and three bottles were left unaltered as controls. Bottles were sealed and transferred to a seawater flow-through incubator shaded with a screen to provide an irradiance of 50% of the incident sea surface level inside the incubator. At T_f , samples were collected for metal concentrations before any other measurements were made to limit contamination.

2.3.4 Light experiments

The importance of light was evaluated by incubating bottles at different light levels, stimulating different mixed layer depths. Using the same mix treatment setup as the iron addition experiment (equal amounts of "surface" and "deep" water), each light treatment was incubated at 75%, 50% and 25% of the incident sea surface irradiance. To prevent any potential iron limitation, $2 \text{ nmol L}^{-1} \text{ FeCl}_3$ was added to all treatments. Each treatment had three replicates.

Table 2.2: Average incident Photosynthetic Available Radiation (PAR, $\mu\text{Ein m}^{-2} \text{ s}^{-1}$) for the 2-day period prior to incubation start and for the 4-day incubation duration for all 2 sites (PD: Palmer Deep Canyon, MT: Margarite Trough, C: Charcot Is). Modeled mixed layer depth averaged PAR (MLD_{ave}) indicates phytoplankton light acclimation history. Average light for each screening used (75%, 50%, 25%) is also shown, considering the 4-day average incident PAR during incubation.

Site	2-day average prior to incubation		4-day average during incubation			
	Incident PAR_i	MLD_{ave}	Incident PAR (PAR_{inc})	75% PAR_{inc}	50% PAR_{inc}	25% PAR_{inc}
PD	667	109	408	305	204	102
MT	259	20	429	322	215	107
CI	511	198	424	318	212	106

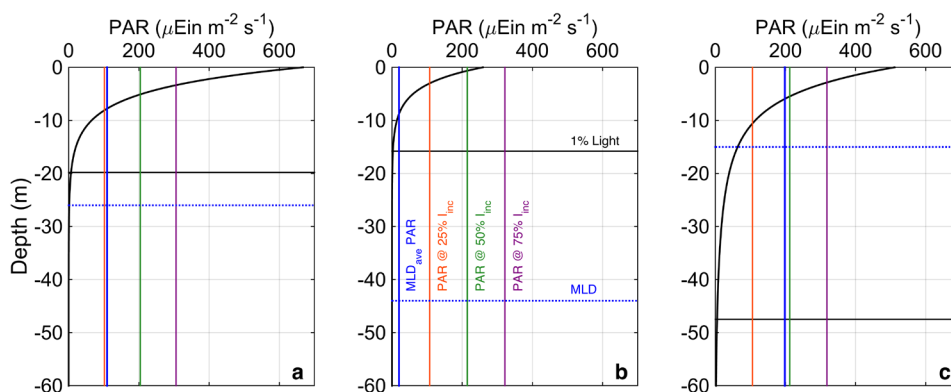


Figure 2.3: Photosynthetically Available Radiation (PAR, black line) profiles from collection casts for all three regions modeled using HydroLight: (a) Palmer Deep Canyon, (b) Margarite Trough and (c) Charcot Is. Vertical lines indicate average light level when screened to 75% (purple), 50% (green) and 25% (orange) of the incident radiation during the incubation experiment, where incident radiation is the average surface PAR during the 4-day incubation. Blue dotted and black solid horizontal lines indicate MLD and 1% light level for each region, respectively. The blue vertical line represents the average PAR within the mixed layer (from Table 2.2).

2.3.5 Chlorophyll *a* and accessory pigments

Samples were filtered onto GF/F filters, then wrapped in foil, flash frozen in liquid nitrogen and stored at -80°C for high-performance liquid chromatography (HPLC) analysis for phytoplankton accessory pigments (mg pigment m^{-3}). The taxonomic composition of the phytoplankton assemblages was derived from HPLC pigment data analysis with CHEMTAX (V195) using initial pigment ratios previously derived from WAP phytoplankton [Kozłowski *et al.*, 2011]. While diatoms, cryptophytes, prasinophytes and haptophytes have distinctive marker pigments, “mixed flagellates” represent a range of taxa that includes both dinoflagellates and unidentified phytoflagellates.

2.3.6 Macro- and micro-nutrient analysis

Water samples from all experiments were collected at T_i and T_f for macronutrient determination, nitrate + nitrite (N+N), phosphate (PO_4^{3-}) and silicate (SiO_2). Samples were filtered through a 0.45 μm pore size Whatman GF/F filter and stored frozen at -20°C in 15 mL acid rinsed FalconTM centrifuge tubes until analysis at Lamont Doherty Earth Observatory (Columbia University, NY) using a SEAL Analytical AutoAnalyzer AA3 HR, Software version 6.10 (Mequon, WI), G-297-03 Rev 4 (Multitest MT19 for PO_4^{3-}), G-172-96 Rev 16 (Multitest MT 19 for NO_3^- and NO_2^-) and G-177-96 Rev 11 (Multitest MT19 for SiO_2). Standards used for the phosphate, nitrate + nitrite, and silicate analyses were potassium dihydrogen phosphate, potassium nitrate and sodium nitrite, and sodium meta-silicate nonahydrate, respectively. The Joint Global Ocean Flux Study (JGOFS) Methods (1994) was used as a reference for all macronutrient analysis methods. Although initial concentrations varied within region, no macronutrient limitation was recorded at the end of any of the incubation experiments.

2.3.7 Trace-metal clean methodology

Seawater samples for iron analysis were collected using a trace metal-clean rosette composed of twelve Niskin-X bottles mounted onto an epoxy-coated frame free of metal anodes. The rosette was deployed using a Kevlar conducting cable through a non-rusted aluminum block. Niskin-X bottles were stored and prepped in a metal-free “bubble” composed of plastic sheeting and inflated using HEPA-filtered air to avoid any

metal contamination. Immediately before each cast, each bottle was individually carried and mounted on the rosette, and bottles were opened on deck for as short a time as possible to prevent deck contamination. Bottles were tripped on ascent at <10 m/min to ensure that the seawater sample was collected as the rosette moved into newly refreshed (uncontaminated) seawater. Filled Niskins bottles were returned to the trace metal bubble as soon as possible after recovery in order to prevent deck contamination.

Once in the bubble, each Niskin-X bottle was pressurized to ~4 psi using an air manifold fed by HEPA-filtered air. An acid-cleaned piece of Bev-A-Line tubing was placed in the spigot and rinsed with sample seawater before an Acropak-200 (0.2 μm) capsule filter was added onto the line. After the filter was flushed with ~1 L of seawater, acid-cleaned LDPE bottles were filled with filtered seawater after three ~10%-volume bottle rinses. Samples were acidified to pH 2 with concentrated hydrochloric acid (Optima grade, Fisher Scientific) for storage.

More than a year after acidification, filtered seawater samples were analyzed for their Fe concentration using a modification of the isotope dilution-inductively coupled plasma mass spectrometry (ICP-MS) method published by *Lagerström et al.* [2013]. In short, samples were weighed into 30 mL bottles and spiked with a mixed isotope spike containing a known concentration of ^{57}Fe . Spiked seawater samples were automatically extracted using the commercially available SeaFAST pico system (Elemental Scientific, Inc.) after online buffering to pH ~6.5 using ammonium acetate and a 25-fold pre-concentration into 10% v/v nitric acid (Optima grade, Fisher Scientific). Within a few days, these samples were analyzed for ^{56}Fe and ^{57}Fe on an Element 1 (Thermo Fisher)

high-resolution ICP-MS in medium resolution. Analysis of SAFe standard seawater solutions was found to be within error of consensus values, indicating the high accuracy of this analytical method.

2.3.8 In vivo Chlorophyll a Fluorescence Kinetics

Photosynthetic efficiency of Photosystem II (F_v/F_m , or $[F_m - F_o]/F_m$) was measured using a Satlantic Fluorescence Induction and Relaxation (FIRE) system [Gorbunov and Falkowski, 2004], where F_o and F_m are minimum and maximum yields of chlorophyll fluorescence and F_v is variable fluorescence. All samples were kept at *in situ* temperatures for > 30 min and under dim light conditions (ca. $5 \mu\text{mol quantam}^{-2} \text{s}^{-1}$) to minimize the effects of fluorescence quenching [Ohad *et al.*, 1990]. We applied a 100- μs single-turnover flash (STF) given by a blue light-emitting diode. Fluorescence response was analyzed using FPRO Software with both STF and Multiple Turnover Flash (MTF) protocols set to off. For all samples, a 0.45 μm filtered sample was analyzed to deduce the blank which was subsequently subtracted from the fluorescence signals (F_o and F_m) to remove background signal. We quantified the response to nutrient-enrichment or irradiance exposure in each experiment by comparing control and treatment at the final time (T_f) using the following index by Olson *et al.* [2000]:

$$\Delta F_v/F_m = [(F_v/F_m)_{\text{treatment}} - (F_v/F_m)_{\text{control}}]/[0.65 - (F_v/F_m)_{\text{control}}] \times 100, \quad (4.1)$$

where $\Delta F_v/F_m$ is relative change (%) in photosynthetic efficiency and 0.65 represents the maximum potential value of F_v/F_m . For the iron experiments control was the no iron

addition treatment and for the light, normalization was done relative to the lowest irradiance, 25%.

Table 2.3: Physiological parameters collected during light incubation experiments for the three canyon systems (PD: Palmer Deep Canyon, MT: Margarite Trough, C: Charcot Is). F_v/F_m is presented for the starting population (T_i). Changes in F_v/F_m and the functional absorption cross-section of PSII ($\Delta\sigma_{PSII}$) are reported in percentage as the difference between T_i and T_f , normalized by T_i .

Site	F_v/F_m @ T_i	75 % light		50 % light		25 % light	
		$\Delta F_v/F_m$	$\Delta\sigma_{PSII}$	$\Delta F_v/F_m$	$\Delta\sigma_{PSII}$	$\Delta F_v/F_m$	$\Delta\sigma_{PSII}$
PD	0.40	-65%	-7%	-62%	-28%	-28%	-34%
MT	0.39	-59%	-20%	-35%	-31%	-16%	-30%
CI	0.31	+22%	+25%	+32%	-8%	+64%	-8%

2.3.9 Statistical analyses

Analysis of variance (ANOVA) was used to evaluate whether the mean values of total chlorophyll, photosynthetic efficiency and photoprotective pigment ratios changed with time and treatments. A post-hoc Tukey's honest significance test (Tukey test) was used to assess which treatment means were significantly different from each other.

2.4 Results and Discussion

A total of six incubation experiments were conducted during the cruise, with one light experiment and one nutrient experiment at each canyon system (PD: Palmer Deep Canyon, MT: Margarite Trough, CI: Charcot Island). A synthesis of experimental results for each canyon is illustrated in Figure 2.4-2.6 and discussed below.

2.4.1 Palmer Deep Canyon

Palmer Deep (PD), the northernmost canyon tested, showed a clear dissimilarity both in the phytoplankton community composition and the responses to the different incubation irradiance levels when compared to the other two regions in the south. Phytoplankton assemblages collected at PD showed a community composition consistent with previous studies [Montes-Hugo *et al.*, 2009; Schofield *et al.*, in review] with waters co-dominated by diatoms and cryptophytes (Figure 2.4L3, 2.4N3). Increasing records in the northern regions of the WAP show a change from diatom-dominated communities [Garibotti *et al.*, 2003a] to smaller celled phytoplankton assemblages such as cryptophytes [Moline *et al.*, 2004; Moline and Prezelin, 1996; Montes-Hugo *et al.*, 2009]. Water was collected with phytoplankton biomass at $4.24 \mu\text{g Chl } a \text{ L}^{-1}$. Biomass decreased significantly ($p < 0.001$) in all light treatments as recorded by T_{chl} (Figure 2.4L1). Two potential explanations for the decrease in chlorophyll are presented below, where a combination of the two could be responsible for the decreasing trend. Since the biomass gradient is controlled by cell size [Garibotti *et al.*, 2003b], the change in community composition from big cell diatoms to small cell cryptophytes, as seen in most treatments, can explain part of the observed decrease in biomass. The decreases in T_{chl} were accompanied by matching increases in photoprotective pigments (Figure 2.4L4-5), as evident by the ratios $(Dt+Dd)/T_{\text{chl}}$ and $Dt/(Dt+Dd)$, indicating that these phytoplankton assemblages were low-light adapted [Brunet *et al.*, 1993], compared to the light levels exposed to during the experiments. The photoadaptation response observed by the increase in photoprotective carotenoid

(DT and DD) concentration indicated cells focused directing metabolism energy to photoprotection and not increasing light-harvesting pigments ones, such as chlorophyll a . However, since decreases in T_{chl} were only recorded in PD where there was an abundance of small phytoplankton, it is likely that the increase in cryptophytes (and therefore decrease in the overall community cell size) is the major reason for the observed decrease in T_{chl} . The lowest light tested (25%) yielded significantly lower T_{chl} ($p < 0.001$) than the other 2 light treatments with a significant change in community composition that promoted growth of mixed flagellates instead of cryptophytes, consistent with results from *Schofield et al.* [in review], where mixed flagellates were associated with deeper MLD. The magnitude of photoprotective carotenoid normalized to chlorophyll ratio is indicative of the degree of low light adaptation, with phytoplankton at Margarite Trough (Figure 2.5L2, N2) showing a ratio up to 5 times higher than the ones at PD (Figure 2.4L2, N2), indicating a much lower light adaptation than the latter region.

In surface waters, macronutrients and iron (0.49 nmol L^{-1}) concentrations were high (Table 2.1), making nutrient limitation unlikely. In incubations testing the effect of nutrient enrichment, neither the addition of deep, nutrient enriched mUCDW (M treatment), nor iron addition ('+' treatments) resulted in significant differences in phytoplankton growth (Figure 2.4N1) or community composition (Figure 2.4N3).

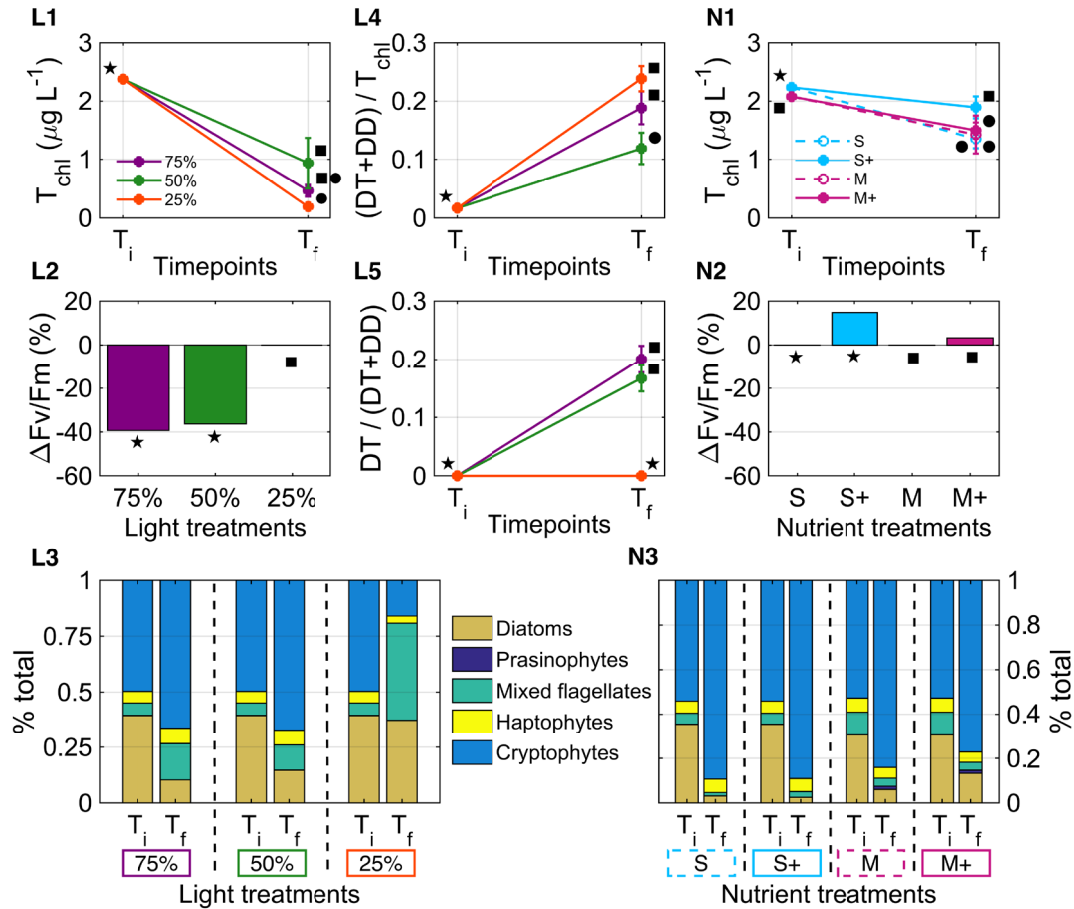


Figure 2.4: Light (L1-5) and nutrient (N1-3) manipulation experiments at Palmer Deep Canyon. Total chlorophyll (T_{chl} , L1 and N1), relative change (%) in photosynthetic efficiency ($\Delta F_v/F_m$) at T_{final} (L2 and N2) and community composition from CHEMTAX (L3 and N3) are presented for the light and nutrient experiments, respectively. Light treatments are shown as the percentage of light screened from surface irradiance (75%, 50% and 25%). Nutrient controls are shown as surface (S) and mix (M) with the correspondent iron addition treatments (S+ and M+). Photoprotective pigment ratios, $DD+DT/T_{chl}$ and $DT/(DT+DD)$, are shown for light experiment only. Different symbols (top 2 rows) denote treatments and timepoints that were found to be significantly different ($p < 0.05$).

Photosynthetic efficiency of Photosystem II (F_v/F_m) was also evaluated for both the light (Figure 2.4L2) and nutrient (Figure 2.4N2) experiments. F_v/F_m for the initial population was relatively low (0.4) compared to 0.65, the F_v/F_m for phytoplankton cultures growing under optimal conditions [Kolber et al., 1988], indicating that the population in the source water was possibly already under some environmental stress.

Also, changes in community composition are known to affect the photosynthetic efficiency of a phytoplankton population, but data is not available to evaluate this. While no significant increases in F_v/F_m between T_i and T_f were found for the nutrient treatments, a significant decrease was found in all light treatments, with declines recorded between 0.1 (-28%) and 0.25 (-65%) for irradiances 25% and 75% respectively (Table 2.3). At the end of the incubation, when comparing F_v/F_m between light treatments relative to the lowest irradiance (25%), both higher irradiances resulted in a marked and significant decrease, affecting photosynthetic efficiency between 35-40%. In the nutrient experiment, slight increases in F_v/F_m were recorded for iron addition treatments, however these differences were not significant ($p>0.05$).

2.4.2 Margarite Trough

Margarite Trough (MT) showed the highest initial phytoplankton biomass, with constant $13 \mu\text{g L}^{-1}$ in the upper 35 m (Figure 2.1d). Diatoms were clearly the dominant phytoplankton group present in the surface source waters with over 95% occurrence within the five major taxonomic groups in the WAP. This result is in accordance with *Kavanaugh et al.* [2015] who detected higher chlorophyll-a and diatom abundance in this region comparatively to the other canyon systems. It also matches observations by *Rozema et al.* [2017], where heavier ice years were associated with increased diatom concentration.

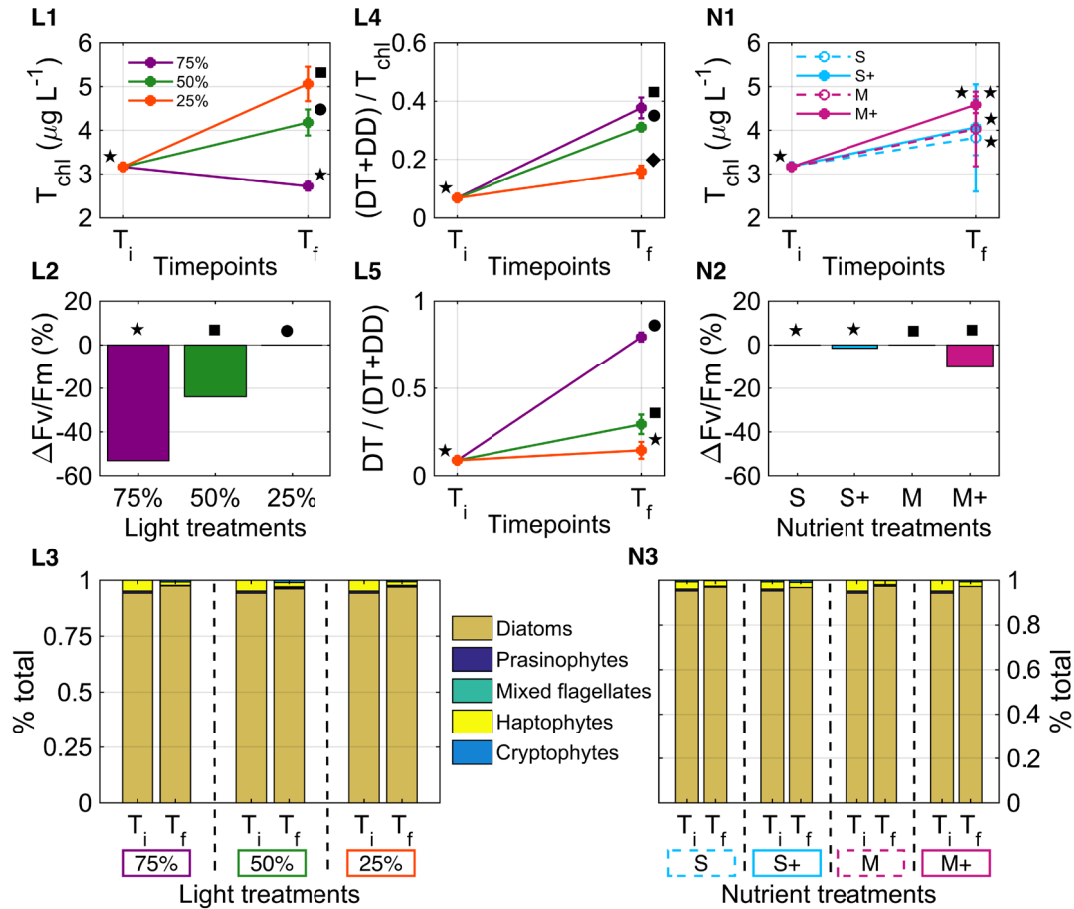


Figure 2.5: Light (L1-5) and nutrient (N1-3) manipulation experiments at Margarite Trough. Total chlorophyll (T_{chl} , L1 and N1), relative change (%) in photosynthetic efficiency ($\Delta F_v/F_m$) at T_{final} (L2 and N2) and community composition from CHEMTAX (L3 and N3) are presented for the light and nutrient experiments, respectively. Light treatments are shown as the percentage of light screened from surface irradiance (75%, 50% and 25%). Nutrient controls are shown as surface (S) and mix (M) with the correspondent iron addition treatments (S+ and M+). Photoprotective pigment ratios, $DD+DT/T_{chl}$ and $DT/(DT+DD)$, are shown for light experiment only. Different symbols (top 2 rows) denote treatments and timepoints that were found to be significantly different ($p < 0.05$).

Phytoplankton population found at MT was adapted to the lowest light levels of the three canyons tested. The light history analysis (Table 2.2) revealed that the light levels in the 2-days prior to incubation were at least half (average $259 \mu E m^{-2} s^{-1}$) those at PD and CI, mostly due to increased cloud cover. Using the MLD during the water collection cast and the average incident radiation from the previous 2 days, we can

establish the light history of the incubated phytoplankton cells, by calculating the average PAR phytoplankton in the MLD were exposed to during the 2 days prior to collection ($MLD_{ave} PAR = 20 \mu\text{Ein m}^{-2} \text{ s}^{-1}$, Table 2.2). With a MLD (44 m) deeper than the euphotic depth (15.8 m) (Figure 2.3b, Table 2.1), the diatom population was clearly low light adapted. Except for the highest irradiance tested (75%), growth was significant ($p < 0.001$), as seen by increases in T_{chl} (Figure 2.5L1), suggesting phytoplankton were able to acclimate to those irradiances. When exposed to a significant higher light level during the 4-day incubation experiments (average surface irradiance was $429 \mu\text{Ein m}^{-2} \text{ s}^{-1}$), photoprotective pigment concentration normalized by chlorophyll showed the highest ratio of the three regions (Figure 2.5L4-5).

Waters at MT are more exposed to wind events than neighboring Ryder Bay, where most studies occur and report shallower MLD, which could explain the deep MLD recorded. However, sustained 30-knot winds over the 24 hours prior to water collection could have deepened the MLD and influenced our light history analysis by determining a much lower light adaptation than was in fact true. However, results still support a very low light adapted population at MT. Assessment of photosynthetic health by variable fluorescence indicated, just like at PD, a significant reduction in photochemical efficiency of PSII (F_v/F_m) in all irradiance levels tested. Comparatively to the lowest irradiance, the 75% irradiance yielded a reduction of over 50% in F_v/F_m . No significant differences were found for the nutrient addition treatments, although a decrease was found, likely due to the relatively high light (50% screening) bottles were exposed to. Chlorophyll increases were found in all nutrient treatments, although neither the added

“deep” water (M treatment) nor the iron addition treatments (+) showed increased growth comparatively to the surface water only (S) treatment. This growth is thus consistent with a photoacclimation response to higher-light than to any nutrient addition, further suggesting no nutrient limitation.

2.4.3 Charcot Island

The region near Charcot Island (CI) showed the shallowest MLD, likely from the increased sea ice melting in the region as seen from the low salinity at the surface (purple, Figure 2.1d). Community composition in the source water was more varied than the other two regions, with diatoms comprising only half the phytoplankton community and haptophytes and mixed flagellates the other half (Figure 2.6L3, 6N3. Cryptophytes were seen in very low numbers in the water around CI. Low phytoplankton concentrations were seen in the source waters and no significant growth ($p > 0.05$) was seen in the incubation experiments probably due to the low ($0.25 \mu\text{g L}^{-1}$) starting Chl a concentration, likely a consequence of more persistent sea ice cover all year round at that location [Kavanaugh *et al.*, 2015].

Evidence collected from both the PAR profile (Figure 2.3c) and the responses to varying irradiances show that the phytoplankton population at CI was relatively higher-light acclimated comparatively to the other regions. This region shows the 1% light level (47.5 m) well below the MLD (15 m). No long-term increases in the photoprotective pigment pool ($[\text{DT}+\text{DD}]/T_{\text{chl}}$, Figure 2.6L4) were recorded for the lowest irradiance tested, showing that the MLD averaged light level (Figure 2.3a; Table 2.2)

phytoplankton were acclimated to was higher than the 25% irradiance tested ($106 \mu\text{Ein m}^{-2} \text{s}^{-1}$), consistent with our MLD_{ave} PAR determined ($198 \mu\text{Ein m}^{-2} \text{s}^{-1}$).

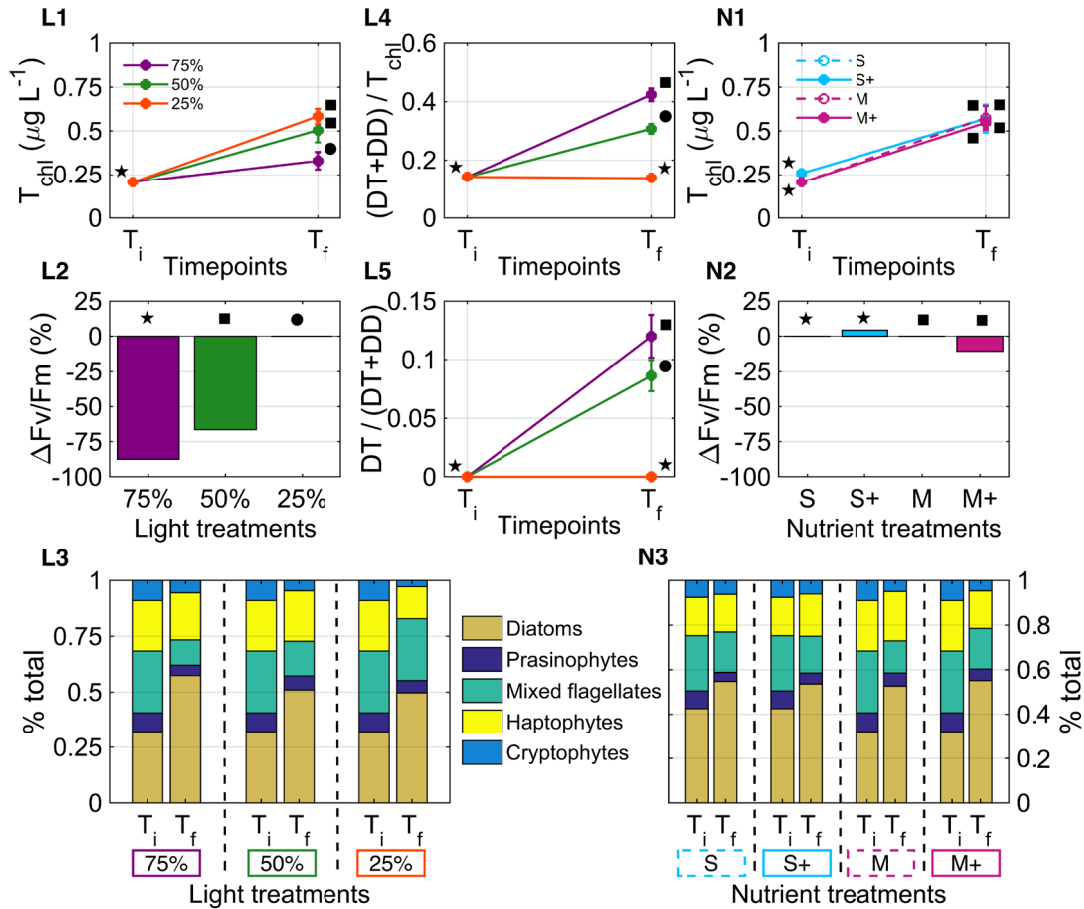


Figure 2.6: Light (L1-5) and nutrient (N1-3) manipulation experiments at Charcot Is. Total chlorophyll (T_{chl} , L1 and N1), relative change (%) in photosynthetic efficiency ($\Delta F_v/F_m$) at T_{final} (L2 and N2) and community composition from CHEMTAX (L3 and N3) are presented for the light and nutrient experiments, respectively. Light treatments are shown as the percentage of light screened from surface irradiance (75%, 50% and 25%). Nutrient controls are shown as surface (S) and mix (M) with the correspondent iron addition treatments (S+ and M+). Photoprotective pigment ratios, $\text{DD}+\text{DT}/T_{\text{chl}}$ and $\text{DT}/(\text{DT}+\text{DD})$, are shown for light experiment only. Different symbols (top 2 rows) denote treatments and timepoints that were found to be significantly different ($p < 0.05$).

Contrary to the other two regions, CI showed increases in photosynthetic efficiency in all light treatments, ranging from 22% to 64% increases in F_v/F_m (Table 2.3),

suggesting phytoplankton were able to easily photoacclimate within the timescale of the incubation experiment, even at the highest irradiance. While phytoplankton dynamic studies regarding the region around Charcot Island are scarce as it is a newly accessible canyon, it is thought that the dynamics seen in the Margarite Trough region are yet still representative of the southernmost region [*Kavanaugh et al.*, 2015; *Montes-Hugo et al.*, 2009]. As the wet and warm subpolar environment moves southward, Charcot will likely show increased production (similarly to MT) as a wider area will be ice free creating a better light environment for local primary production.

2.4.4 Canyon dynamics and ecosystem implications

Major penguin breeding colonies around Anvers, Avian and Charcot Islands are associated with cross-shelf submarine canyon systems where increased chlorophyll has been recorded [*Ducklow et al.*, 2012; *Kavanaugh et al.*, 2015; *Oliver et al.*, 2013; *Prézelin et al.*, 2000]. These underwater depressions act as conduits for warm, nutrient enriched deep mUCDW to the near shore regions [*Martinson et al.*, 2008; *Prézelin et al.*, 2004]. Relatively high water temperatures at the surface concurrent with earlier sea ice retreat, increased melting and shallower MLD and increase chlorophyll [*Kavanaugh et al.*, 2015] have been linked to the intrusion of this warm deep water mass. While the concept of mUCDW replenishing surface waters with significant amounts of macro- and micronutrients required to fuel primary production [*Prézelin et al.*, 2000; *Prézelin et al.*, 2004] is plausible, results from this and previous studies [*Annett et al.*, submitted; *Annett et al.*, 2015; *Bown et al.*, 2016; *Carvalho et al.*, 2016b] conducted at the head of

these canyons suggests it is unlikely. In this study, neither mixing deep water with surface water (simulating upwelling of mUCDW) nor iron enrichments yielded increased chlorophyll, as nutrients were widely abundant in the near shore surface waters. Also, glider-based surveys at the head of PD show that although there is intrusion and mixing of mUCDW occurring at that location [*Carvalho et al.*, 2016b], the timing of it is important as winter water was present throughout the duration of the spring and summer phytoplankton blooms. Though this water mass was slowly eroded both from above and below, it acted as a physical barrier preventing the warm deep (and nutrient enriched) water from mixing with surface waters throughout the bloom season.

Increased sea ice melting at canyon heads leads to shallower MLD and increased stratification, both linked to increased phytoplankton concentrations [*Carvalho et al.*, 2016b; *Mitchell and Holm-Hansen*, 1991; *Moline and Prezelin*, 1996]. A shallow MLD and increased water column stratification resulting from freshwater input from glacial and sea ice melt [*Meredith et al.*, 2008], low wind speeds over weekly timescales [*Moline*, 1998; *Moline and Prezelin*, 1996] and surface warming from incoming solar radiation, provide a stable light environment for phytoplankton to thrive.

Canyons also facilitate the reduction of the sea ice concentration earlier in the season, increasing the light penetration into the water column in ice free zones. This is beneficial in regions with persistent winter sea ice (southern region), where the clearing of the ice opens up regions where phytoplankton can thrive [*Montes-Hugo et al.*, 2009]. However, in the northern region (Palmer Deep), earlier ice retreat has little to no advantages. Warmer temperatures and decreased salinities can cause earlier shifts in

the phytoplankton population from diatoms to cryptophytes [*Moline et al.*, 2004; *Rozema et al.*, 2017; *Schofield et al.*, in review], resulting in repercussions through the entire food web [*Schofield et al.*, 2010]. Open water over longer periods of time together with increased winds can result in deeper MLD, which will limit primary production. Warmer surface waters and less persistent sea ice will result in a less pronounced winter water layer which influences water column stratification [*Carvalho et al.*, 2016b; *Venables et al.*, 2013]. Increased winds deepen the ML, resulting in further decreases in primary production. Meteoric water (glacial melt and precipitation) may be the most significant source of iron to the surface water [*Annett et al.*, submitted], with the likelihood of increasing iron supply to surface water with the current WAP warming trend. However, the increased winds and consequent deepening of the ML will likely dilute this increased iron supply over a larger volume of water that may not translate in increased primary production and phytoplankton biomass.

The latitudinal observations in terms of primary productivity and phytoplankton community composition are heavily associated with geographic and temporal differences in receding sea ice, wind patterns and incident radiation at the surface [*Montes-Hugo et al.*, 2009]. With a southward migration of the wet and warm sub-polar climate, it is anticipated that Margarite Trough will soon resemble the conditions seen now at Palmer Deep Canyon and in the future Charcot will resemble MT today, with increased chlorophyll due to more open ocean areas where light is not limiting primary productivity.

Phytoplankton are continuously exposed to variations in light due to changes in atmospheric light and vertical mixing within the water column [Sakshaug and Slagstad, 1991]. Thus, both the depth of the mixed layer and the rate of mixing are crucial in controlling the light available to the phytoplankton [Mitchell and Holm-Hansen, 1991]. Phytoplankton respond to these variations in the light field by photoadaptive mechanisms [Sakshaug and Holm-Hansen, 1986] which minimize changes in the growth rates under light-limiting conditions. Under high-light conditions, phytoplankton were able to prevent photo-oxidative damage to the reaction centers (xanthophyll cycle) and invest in the production of photoprotective pigments, as evaluated by the photoprotective pigment to light harvesting pigment ratio ($([DT+DD])/T_{chl}$), allowing them to thrive under shallow MLDs. Light experiments have shown that given a relatively stable light environment (just like a shallow MLD), phytoplankton are able to acclimate on the timescales of a few days [Schofield *et al.*, 1995], consistent with previous work linking increased chlorophyll to a stable and shallow MLD [Carvalho *et al.*, 2016b; Moline and Prezelin, 1996; Venables *et al.*, 2013]. Differences in the photoacclimation response at Palmer Deep comparatively to the southern canyons, where the 50% light showed chlorophyll increases despite the initial lower-light acclimation, could be explained by the dominance of diatoms in the latter region, as diatoms are better suited for adapting to higher irradiance levels [Arrigo *et al.*, 2010; Mills *et al.*, 2010].

2.5 Conclusions

In conclusion, this study supports the hypothesis that light, not nutrient intrusions of the mUCDW, is the main contributing factor influencing phytoplankton biomass and physiology in the canyon hotspots of the WAP. While all the light exposures tested (75%, 50% and 25% of incident radiation) turned out to be too high to fully evaluate the best light conditions for phytoplankton to thrive, it showed that phytoplankton in these canyon systems succeeded in employing photoadaptation mechanisms that allowed them to quickly overcome the variability in the light fields (due to varying incident radiation, MLD and vertical mixing rates) they are constantly exposed, with diatoms showing a higher success under high-light conditions.

Incubation results do not support the canyon hypothesis initially postulated, that the nutrient enrichment [Prézelin *et al.*, 2000; Prézelin *et al.*, 2004] from the upwelling of warm, deep modified Upper Circumpolar Deep Water (mUCDW) was responsible for the increased phytoplankton biomass observed over submarine canyons. This is also supported by previous studies looking at the temporal evolution of the water masses at the canyon head at Palmer Deep [Carvalho *et al.*, 2016b] where, although there is evidence of mUCDW at the canyon heads, this water mass consistently does not reach the upper 100 m until after the spring bloom ends. However, the uplift of this water mass can potentially influence the depth of the winter water layer which sets up the water column stratification and the depth of the surface ML.

2.6 Acknowledgements

The authors thank Nicole Couto, Mansha Pasricha and Cheryl Zubrick for help with incubation setup; Nicole Waite, Lora McGuinness, Naomi Shelton and Joe Roccanova for help analyzing HPLC pigments, nutrients and trace metal concentrations. We also thank the crew and support staff of ARSV Laurence M. Gould during LMG15-01. The research was supported by the National Science Foundation grant ANT- 0823101 (Palmer-LTER). Filipa Carvalho was funded by a Portuguese doctoral fellowship from Fundação para a Ciência e Tecnologia (DFRH - SFRH/BD/72705/2010) and a Teledyne Marine Graduate Fellowship.

Chapter 3: Defining the ecologically relevant mixed layer depth for Antarctica's Coastal Seas

3.1 Abstract

Mixed Layer Depth (MLD) has been widely linked to phytoplankton dynamics in Antarctica's coastal regions, however inconsistent definitions have made inter-comparisons among region specific studies difficult. Using a dataset with over 20,000 water column profiles corresponding to 32 Slocum glider deployments in three coastal Antarctic regions (Ross Sea, Amundsen Sea and West Antarctic Peninsula), we evaluated the relationship between MLD and phytoplankton vertical distribution. Comparisons of these MLD estimates to an applied definition of phytoplankton bloom depth, as defined by the deepest inflection point in the chlorophyll profile, show that the maximum of buoyancy frequency is a good proxy for an ecologically relevant MLD. A Quality index is used to filter profiles where MLD is not determined. Despite the different regional physical settings we found that the MLD definition based of the maximum of buoyancy frequency best describes the depth to which phytoplankton can be mixed in Antarctica's coastal seas.

3.2 Introduction

The surface mixed layer is a portion of the upper ocean where turbulent mixing processes form an upper density layer distinct from the layer below. The depth of these layers varies greatly across the world's ocean in time and space and plays an important role in interpreting the environmental factors driving phytoplankton blooms [Behrenfeld and Boss, 2014]. Mixed Layer Depth (MLD) is therefore a central metric for understanding phytoplankton dynamics [Sverdrup, 1953] especially in Antarctica's

coastal seas [Fragoso and Smith, 2012; Venables *et al.*, 2013]. The depth of the surface mixed layer can regulate the amount of solar radiation available to the phytoplankton community [Denman and Gargett, 1983; Mitchell *et al.*, 1991]. From below, water column stability at the base of the ML has been linked to the flux of nutrients to the surface layer [Ducklow *et al.*, 2007; Prézelin *et al.*, 2000; Prézelin *et al.*, 2004]. A recent study by Smith and Jones [2015] showed that vertical mixing and phytoplankton biomass in the Ross Sea are consistent with the critical depth concept formalized by Sverdrup [1953]. This critical depth is a function of incoming radiation, which in the poles shows a marked seasonality, and is an important factor controlling phytoplankton dynamics in polar seas [Smith and Sakshaug, 2013]. Similar conclusions relating the critical depth hypothesis with phytoplankton growth were found for the West Antarctic Peninsula [Carvalho *et al.*, 2016b; Cimino *et al.*, 2016; Vernet *et al.*, 2008].

While seasonal mixed layers have been widely used to better understand the critical links between the physical structure of the water column and primary production, there are a wide range of methods and metrics used to estimate this important parameter. MLD calculations are based on temperature, salinity or density. Common methods used in MLD calculations in Antarctic waters are based on either a difference or gradient in the target variable, and every study justifies their specific method. Estimates of MLD from a difference measured at two depths use a range of values. Temperature thresholds vary from 0.8°C [Kara *et al.*, 2000] to 0.2°C [de Boyer Montégut *et al.*, 2004; Dong *et al.*, 2008] while potential density thresholds vary from 0.01 kg m⁻³ [Smith and Jones, 2015], 0.03 kg m⁻³ [Sallée *et al.*, 2010] and 0.05 kg m⁻³

[Venables *et al.*, 2013]. The reference depths over which these differences are estimated can vary from the near surface [Venables *et al.*, 2013] to as deep as 10 meters [Smith and Jones, 2015]. All these differences in criteria and method can potentially yield different estimates of MLD. This is especially troublesome when trying to compare results between studies and distributed seas within which local physical conditions lead to different optimal methods to estimate local MLD. In this study, we use concurrent profiles of hydrography and chlorophyll-*a* (chl-*a*) fluorescence during the austral spring/summer season in three coastal regions around Antarctica and propose a standard and ecologically relevant metric of MLD as it consistently captures the lower vertical limit of phytoplankton distribution across the Amundsen Sea (AS), the Ross Sea (RS), and the shelf along the Western Antarctic Peninsula (WAP) that facilitate comparisons between studies.

3.3 Data and Methods

3.3.1 Slocum gliders

Slocum electric gliders are 1.5 m torpedo-shaped buoyancy driven autonomous underwater vehicles that provide high-resolution surveys of the physical and bio-optical properties of the upper water column [Schofield *et al.*, 2007]. All gliders used in this analysis were equipped with a Seabird Conductivity-Temperature-Depth (CTD) sensor and carried WET Labs Inc Environmental Characterization Optics (ECO) pucks, which measured chl-*a* fluorescence. Glider based conductivity, temperature and depth measurements were compared with a calibrated ship CTD sensor on deployment and

recovery to ensure data quality, as well as with a calibrated laboratory CTD prior to deployment (as described in *Kohut et al.* [2014b]). Each glider profile was averaged into 1-meter bins and assigned a mid-point latitude and longitude. Only profiles with 50 bins or more were considered for the analysis. Glider profiles start at 2-4m depth.

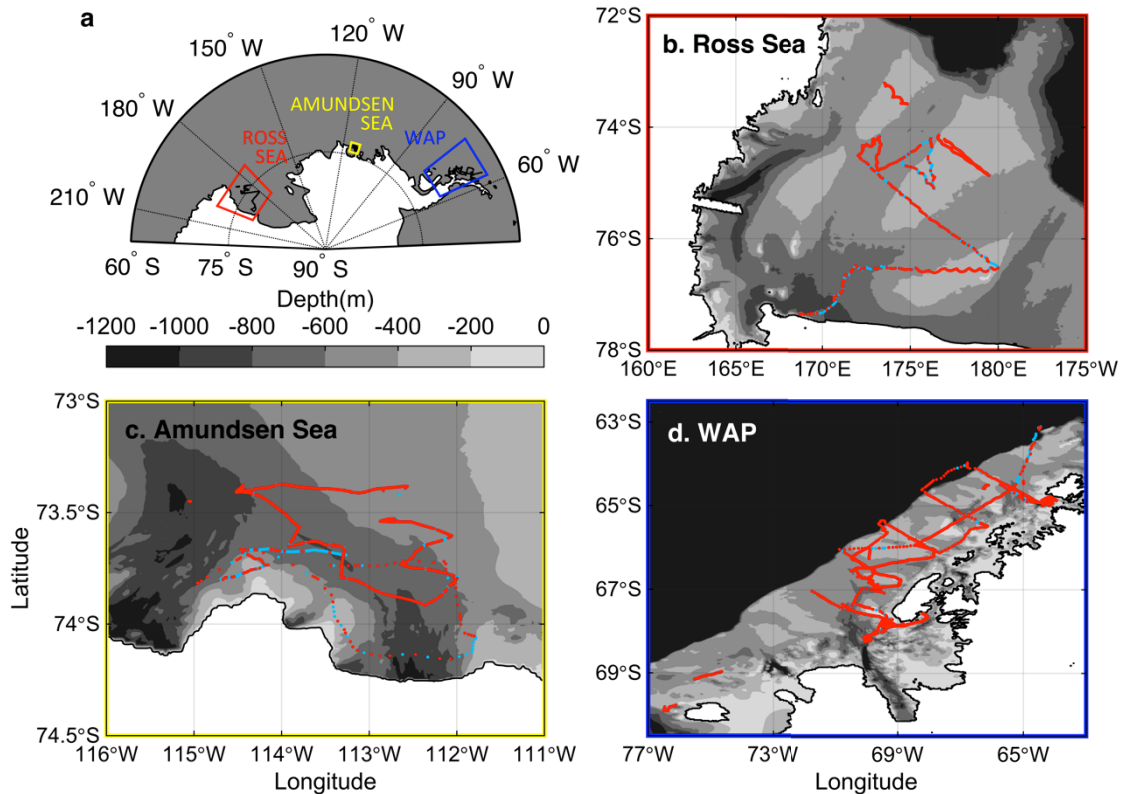


Figure 3.1: Location of glider data used in the analysis: (a) glider tracks in the three main regions. Panels 1b-d show bathymetry maps overlaid with the detailed location of each individual glider profile (dots) for the regions shown in the first panel: (b) Ross Sea, (c) Amundsen Sea and (d) WAP. Red dots – MLD Quality index (QI) > 0.5 (see Section 2.2 for details); blue dots, remaining profiles not considered for the MLD analysis (QI < 0.5).

In the AS, 3 missions collected 2,247 profiles (December 2010 - February 2011 and Jan 2015). In the RS, 3 missions collected 2,212 profiles (December 2010 - January 2011). Along the WAP, 26 missions collected 16,673 profiles (December - March, 2009

through 2015). Overall, these data include 21,132 profiles, 465 days at sea and 9,836 km flown during the austral spring/summer (Figure 3.1).

3.3.2 Mixed layer depth

We evaluated an ecologically relevant MLD definition based on comparisons with concurrent chl-*a* fluorescence profiles (described below). We show a detailed analysis on the MLD estimated based on the maximum of buoyancy frequency ($\max(N^2)$, or stability frequency). For each profile (a, b), MLD was determined by finding the depth of the maximum water column buoyancy frequency. The same analysis was conducted for the most commonly used estimates of MLD in Antarctica's coastal seas and presented in the supplemental information as a comparison against our proposed MLD definition.

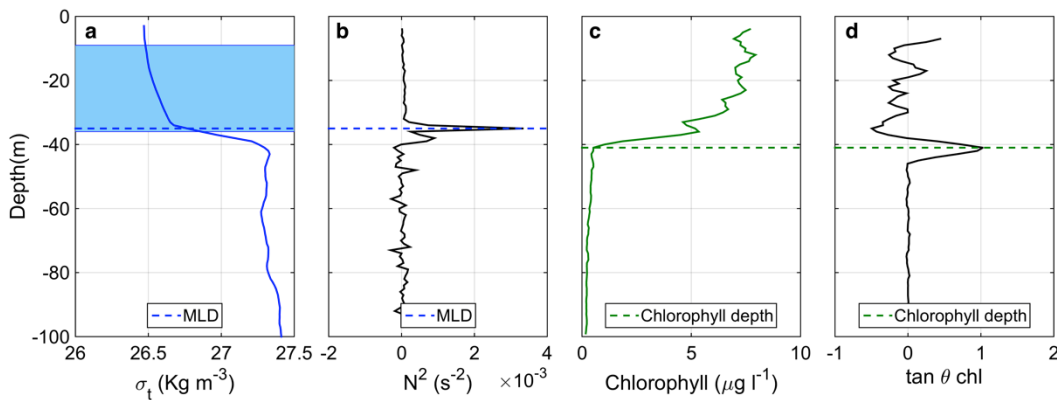


Figure 3.2: Determination of mixed layer depth (MLD) and chl-*a* depth (Z_{chl}) from a glider profile (located at 64.827°S, 64.286°W at GMT 4:29 on January 6th, 2014). (a) density profile (solid blue line) with MLD (dashed blue) calculated by $\max(N^2)$ and range of MLD (shaded blue) calculated using methods described in Table 3.2; (b) calculated buoyancy frequency (N^2) profile and MLD; (c) chl-*a* profile (solid green line) with Z_{chl} (dotted line) defined by the maximum angle method [Chu and Fan, 2011], or the $\max(\tan \theta_{chl})$, and (d) calculated $\tan \theta_{chl}$ and Z_{chl} .

The determination of MLD is based on the principle that there is a near-surface layer characterized by quasi-homogeneous properties with a standard deviation of the property within this layer close to zero. Below the MLD, the variance of the property should increase rapidly. To clarify the relationship between MLD and chl- a in such a high-resolution dataset, a Quality Index (QI, Equation 3.1) by Lorbacher et al. (2006) was used to evaluate our MLD calculations and filter out profiles where MLD could not be resolved:

$$QI = 1 - \frac{rmsd(\rho_k - \bar{\rho})|_{(Z_1, Z_{MLD})}}{rmsd(\rho_k - \bar{\rho})|_{(Z_1, 1.5 \times Z_{MLD})}} \quad (3.1)$$

where ρ_k is the density at a given depth (k), Z_1 is the first layer near the surface and $rmsd()$ denotes the standard deviation from the vertical mean $\bar{\rho}$ from Z_1 either to the MLD or $1.5 \times MLD$. This index evaluates the quality of the MLD computation.

Using this, MLDs can be characterized into estimates determined with certainty ($QI > 0.8$), determined but with some uncertainty ($0.5 < QI < 0.8$) or not determined ($QI < 0.5$). Example of profiles for data removed from the analysis ($QI < 0.5$) can be found in Figure 3.6.

This QI metric does not consider the strength of stratification, just homogeneity of the surface layer above the defined MLD. Therefore, by definition the MLD estimate is close to the lower boundary of that vertically uniform layer. Following the thresholds set by Lorbacher et al. [2006], for the analyses presented in this study, a quality index of 0.5 was used to reasonably warrant a calculation of MLD. The quality index threshold of

0.5 was determined based on the insensitivity of the slope of the trend lines using higher QI values (0.8).

Apart from the depth of the ML, stratification also plays an important role in phytoplankton dynamics [Holm-Hansen and Mitchell, 1991; Mitchell *et al.*, 1991]. The differences in the vertical physical structure setting seen in the TS plots (Figure 3.3) result in differences in stratification. To identify the profiles with the highest stability at the base of the MLD in each region, stability was normalized independently for each region by dividing the buoyancy frequency at the base of MLD of that profile by the regional average of buoyancy frequency at the base of the MLD. The normalized stability was calculated to find the magnitude of each point as it relates to the overall stability in each region. This allows the regional differences due to the vertical structure of the water column to be removed.

3.3.3 Chlorophyll-a Fluorescence

Chl-*a* fluorescence, as measured by the glider ECO pucks, is our indicator of phytoplankton biomass. Discrete *in situ* water samples were collected from several depths from casts during each glider deployment and recovery. Water samples were filtered onto 25 mm Whatman GF/F filters and extracted using 90% acetone and chl-*a* concentration was then measured using a fluorometer. For each deployment, the structure and magnitude of chl-*a* measured by the glider puck was verified against both the independent discrete measurements and an independent calibrated fluorometer deployed from a collocated ship station. While the complex relation between

fluorescence vs. biomass was not fully evaluated, we provide an accurate characterization of the observed fluorescence, fully realizing that our measurements may not accurately represent phytoplankton biomass. Also, since our analysis focuses on the bottom of the phytoplankton biomass layer, daily non-photochemical quenching of chl-*a* fluorescence is not a factor in our analysis.

Following a method adapted from the maximum angle principle used to calculate MLD [Chu and Fan, 2011], the depth of lower boundary of chl-*a* was estimated, referred to as chlorophyll depth (Z_{chl}) in the analysis. This method is based on three main steps: 1) fitting the profile data with a vector (pointing downward and with n points) from shallower depths to a certain depth k and a second vector from that depth to deeper depth ($k+1+n$); 2) identifying the tangent angle ($\tan\theta$) between the 2 vectors for each depth k ; and 3) defining the MLD by determining the maximum angle in each profile. Here we apply the same principle using the maximum angle, as we are interested in calculating the depth of the deepest inflection point in the chl-*a* profile. Using a vector of $n=7$ data points, the depth of the $\max(\tan\theta)$ of the chl-*a* profile was determined and used as the Z_{chl} (Figure 3.2c, d). A quality index (QC, Equation 3.2) was also applied to the chlorophyll data to evaluate the Z_{chl} computation. A modification to Equation 3.1 was made to account for the homogeneity occurring below the Z_{chl} and not above:

$$QC = 1 - \frac{rmsd(CHL_k - \overline{CHL})|_{(Z_{chl}, Z_D)}}{rmsd(CHL_k - \overline{CHL})|_{(Z_D - 1.5(Z_D - Z_{chl}), Z_D)}} \quad (3.2)$$

As both variables have errors in them and linear relationships are expected between both variables [Holm-Hansen and Mitchell, 1991; Mitchell *et al.*, 1991], model-2 regressions were applied to concurrent MLD and Z_{chl} calculations to evaluate the MLD determination of the definitions chosen by comparing it to a 1:1 line.

3.4 Results and Discussion

Each region had a different distribution of water masses as indicated in temperature (T) and salinity (S) space (Figure 3.3). Surface water in the RS and AS were similar, but quite different from the WAP while at depth, AS and WAP showed similarities.

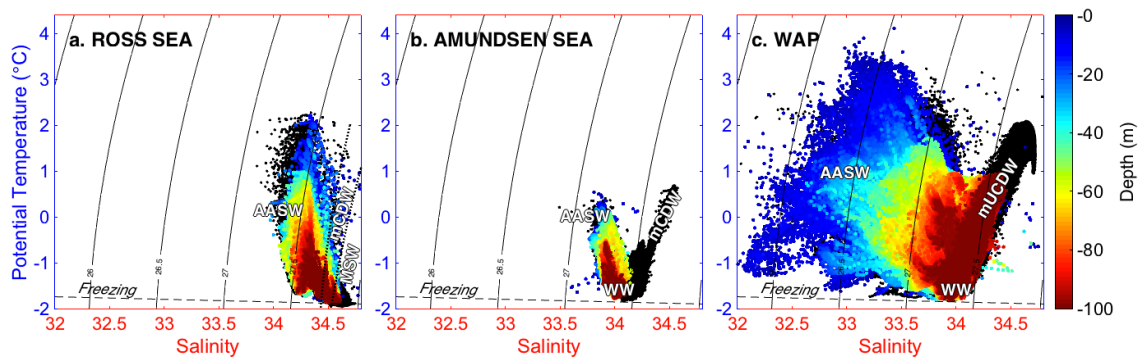


Figure 3.3: θ -S scatters plots for all 3 areas shown in Figure 1: (a) Ross Sea, (b) Amundsen Sea and (c) WAP. Color indicates depth of the water column measurement in the upper 100 m of the water column. All data between 100-1000 meters are plotted in black. Primary water masses sampled are indicated and labeled (WW = Winter Water; MSW = Modified Shelf Water; AASW = Antarctic (summer) Surface Water; m(U)CDW = modified (Upper) Circumpolar Deep Water.

Compared to the WAP, both Ross and Amundsen Seas showed overall colder and saltier waters with the latter being on average saltier. The warmer, saltier and deep mUCDW found in shallower depths in the WAP was not seen in the upper 100 m (colored dots in Figure 3.3) in RS and AS. In both the latter regions, T_{min} was found

generally in the deepest sampled waters (red). The WAP (Figure 3.3c), with the widest range of T-S properties as it is located at lower latitudes, spans entire seasonal cycles due to more sustained sampling and is more influenced by coastal inputs.

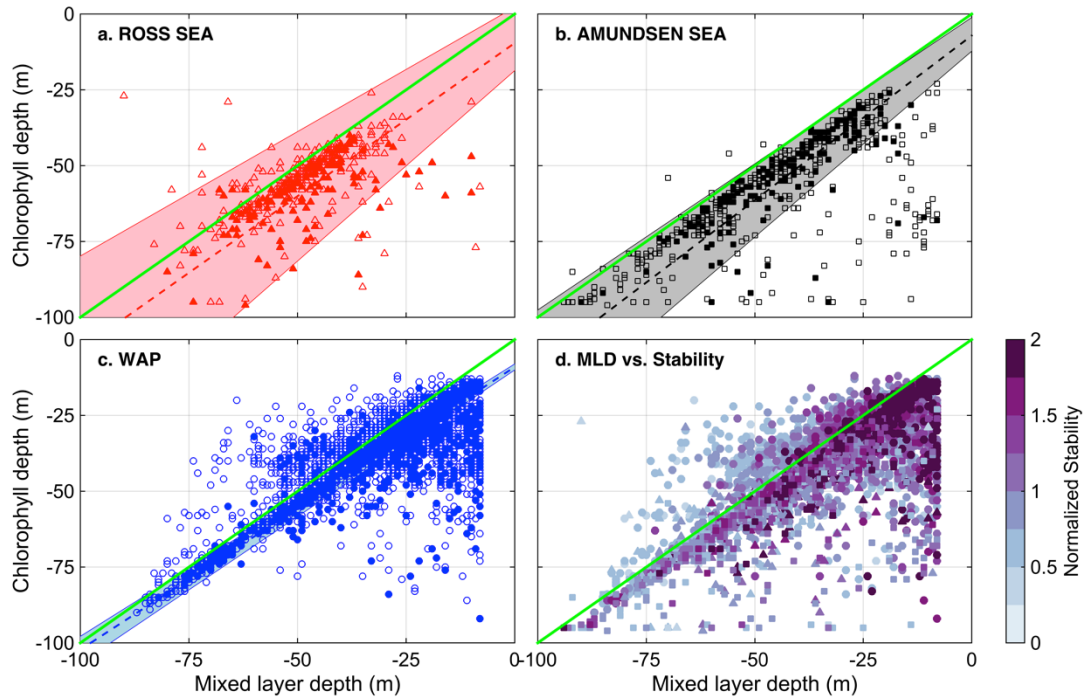


Figure 3.4: Correlation between MLD and Z_{chl} for all glider profiles with Quality Index (QI) over 0.5 (open marker) and over 0.8 (filled marker) for all 3 regions: (a) Ross Sea (triangle); (b) Amundsen Sea (square); (c) WAP (circle); (d) comparison between all three Antarctic regions (QI>0.5) with normalized stability frequency colored and markers representing region. 95% confidence intervals (shaded area) and model-2 regression line are shown for QI>0.8 (dashed line). A quality index (QC) was also applied to chl-*a* profiles and only profiles with QC>0.8 are shown above. Line 1:1 is shown in green.

We compared our MLD estimation based on N^2 and chlorophyll depth, described in section 3.3.2, across each of the coastal regions. Profiles with QI and QC values less than 0.5 [Lorbacher *et al.*, 2006] were removed as MLD and Z_{chl} was not clearly defined. The remaining profiles were characterized as 'estimated with uncertainty' ($0.5 < QI < 0.8$; Figure 4, open markers) and 'estimated with certainty' ($QI > 0.8$; Figure 4, filled markers).

A linear, model-2 regression was applied to each regional dataset (Table 3.1). Although some regional differences were found in the MLD ranges, all three regions showed a MLD-chl- α relationship close to 1:1 with 95% confidence (compare dashed trend lines with green), i.e., the deeper the MLD, the deeper the lower boundary of the chl- α profile. The observed differences in the depth of the ML across regions (Figure 3.4) were mostly influenced by the timing of the measurements, i.e. uneven sampling in time in different regions. Nevertheless, the MLD calculations are within range of those reported for each region [Schofield *et al.*, 2015b; Smith *et al.*, 2014; Vernet *et al.*, 2008].

Given the disproportionately greater number of profiles collected in the WAP, (Figure 3.4c) the region showed the widest range of MLDs estimated with certainty ($QI > 0.8$) of all three regions, ranging from 8 to 65 meters of depth. This region showed, on average, the shallowest MLD ($\overline{MLD} = -33\text{m} \pm 13$) and a trend line ($y = 0.93175x - 9.0415$; $R^2 = 0.82$; $p < 0.0001$) close to the 1:1 line (green line). The RS (Figure 3.4a) showed the deepest MLD ($\overline{MLD} = -49\text{m} \pm 9$) but regardless, the relationship between MLD and chl- α ($y = 1.0098x - 9.5745$; $R^2 = 0.60$; $p < 0.0001$) was similar to those seen in the other two regions. The AS exhibited the smallest number of data points, however showed a high R^2 ($y = 1.0849x - 7.125$; $R^2 = 0.78$; $p < 0.0001$) for both quality indices used. This region shows again a wider range of MLD comparatively to the Ross Sea, but has also, in average, deeper MLDs ($\overline{MLD} = -41\text{m} \pm 13$) than the WAP. All three regions showed slopes not significantly different than the 1:1 line (Table 3.1).

Table 3.1: Model-2 regressions between MLD as determined by the $\max(N^2)$ method and chlorophyll depth for the three regions. Statistics show regression coefficients for both MLD quality indices thresholds (QI>0.8, QI>0.5) determined by *Lorbacher et al.* [2006] tested as well as for all the data points (no QI filtering). Results are shown for a chlorophyll quality index (QC) of QC>0.8, QC>0.5 and no QC filtering.

Area	Chl Quality Index (QC)	MLD Quality Index (QI)	N	Slope (95% CI)	Intercept (95% CI)	R ²	p-value
Ross Sea	0.8	0.8	165	1.0098 (0.82031; 1.256)	-9.5745 (2.23; -18.6574)	0.59488	p<0.0001
		0.5	487	0.99608 (0.86834; 1.146)	-7.359 (-0.038756; -13.5968)	0.5461	p<0.0001
		N/A	563	0.9138 (0.78004; 1.0752)	-10.6651 (-2.6039; -17.345)	0.46469	p<0.0001
	0.5	0.8	481	1.0823 (0.93326; 1.2542)	-7.3749 (0.45007; -14.1622)	0.52906	p<0.0001
		0.5	1302	1.0461 (0.93792; 1.1674)	-5.317 (0.58982; -10.5855)	0.45084	p<0.0001
		N/A	1630	0.99502 (0.90476; 1.0953)	-6.4361 (-1.4365; -10.9373)	0.45854	p<0.0001
	N/A	N/A	2194	1.1844 (1.0753; 1.307)	2.3384 (8.4211; -3.0719)	0.40251	p<0.0001
Amundsen Sea	0.8	0.8	188	1.0849 (0.96433; 1.225)	-7.125 (-1.1499; -12.2705)	0.77585	p<0.0001
		0.5	578	0.95271 (0.87439; 1.0389)	-14.579 (-10.658; -18.1405)	0.69412	p<0.0001
		N/A	671	0.89311 (0.8221; 0.97076)	-17.1111 (-13.4214; -20.4857)	0.67937	p<0.0001
	0.5	0.8	330	1.1981 (1.0494; 1.3741)	-4.6835 (2.6865; -10.9094)	0.6448	p<0.0001
		0.5	1044	1.0111 (0.93064; 1.0993)	-12.297 (-8.318; -15.9213)	0.59817	p<0.0001
		N/A	1289	0.85954 (0.7917; 0.93315)	-17.5785 (-13.9995; -20.877)	0.56149	p<0.0001
	N/A	N/A	2238	0.97282 (0.87089; 1.0865)	-5.0872 (0.95163; -10.5035)	0.35838	p<0.0001
WAP	0.8	0.8	1594	0.93175 (0.89798; 0.96663)	-9.0415 (-8.0353; -10.0157)	0.82221	p<0.0001
		0.5	4355	0.86901 (0.8465; 0.89199)	-9.7637 (-9.0476; -10.4641)	0.76798	p<0.0001
		N/A	5142	0.72911 (0.7048; 0.75403)	-12.4623 (-11.6235; -13.2791)	0.648	p<0.0001
	0.5	0.8	2804	0.95158 (0.9145; 0.98986)	-9.0115 (-7.9997; -9.9908)	0.73033	p<0.0001
		0.5	8249	0.8212 (0.7986; 0.84427)	-10.0579 (-9.3747; -10.7262)	0.64446	p<0.0001
		N/A	10238	0.59648 (0.5760; 0.61735)	-14.2683 (-13.5637; -14.9587)	0.51431	p<0.0001
	N/A	N/A	16637	0.6789 (0.6519; 0.70671)	-10.7427 (-9.8179; -11.6421)	0.42085	p<0.0001

Comparing the trends obtained using both indices ($QI > 0.8$ compared to $QI > 0.5$, corresponding to 26-31% and 80-87% of the profiles, respectively) showed little differences (Table 3.1). Higher QIs are observed during summer and fall, where sharp gradients at the base of the seasonal mixed layer are present [Lorbacher *et al.*, 2006]. A maximum MLD difference of 3 m for the AS was observed when using $QI > 0.5$ compared to a higher MLD quality index, $QI > 0.8$; and overall this difference was much smaller for the remaining 2 regions. This ensures that even though we are using a lower quality index to include more data in the analysis ($QI > 0.5$, the minimum threshold set by Lorbacher *et al.* [2006] for determining MLD), we are capturing the same patterns. Points that are closer to the trend line, show, on average, much higher water stability (Figure 3.4d), with the shallowest MLD showing the highest water stability due to freshwater input from meltwater [Martinson and Iannuzzi, 1998]. Since our gliders measurements start at a minimum of 2 m depth and our Z_{chl} computation relies on a 7-point vector, it was not possible to evaluate the biophysical relationship in this study within the upper 7 m. This is a constraint on our method of evaluating the correlation between MLD and chlorophyll depth and not on the actual MLD determination. Studies in the region have also shown that most Z_{chl} occur deeper than 7 m [Moline *et al.*, 1997; Smith *et al.*, 2013]. Note that, as this method captures the maximum stability frequency of the water column profile, its accuracy depends both on the vertical resolution and the vertical extent of the measurements. This is especially important in the presence of meltwater lenses in the surface layer, which our gliders were not able to capture. This method relies on the implicit assumption of a two-layer ocean. Cases where the surface

ocean has a well defined (and deeper) ML and a surface active mixing layer [Brainerd and Gregg, 1995], this method will capture the depth of the strongest water column stability and therefore a lower QI may be determined based on this 2-step surface ML if the base of the ML has a stronger N^2 value.

Table 3.2: Examples of criteria used to define MLD in waters around Antarctica

Author	Area studied	MLD threshold criterion
Kara et al. [2000]	Global ocean	$\Delta T = 0.8^\circ\text{C}$ $\Delta\sigma_\theta = \sigma_\theta(T+\Delta T, S) - \sigma_\theta(T, S)$ with $\Delta T=0.8^\circ\text{C}$
de Boyer Montégut et al. [2004]	Global ocean	$\Delta T = 0.2^\circ\text{C}$ $\Delta\sigma_\theta = 0.03 \text{ Kg m}^{-3}$
Dong et al. [2008]	Southern Ocean (open ocean)	$\Delta\rho = 0.03 \text{ Kg m}^{-3}$ $ \Delta T = 0.2^\circ\text{C}$
Sallée et al. [2010]	Southern Ocean (open ocean)	$\Delta\sigma_\theta = 0.03 \text{ Kg m}^{-3}$
Long et al. [2012]	Ross Sea	$\Delta\sigma_\theta = 0.05 \text{ Kg m}^{-3}$
Smith and Jones [2015]	Ross Sea	$\Delta\sigma_\theta = 0.01 \text{ Kg m}^{-3}$
Fragoso and Smith [2012]	Ross and Amundsen Seas	$\Delta\sigma_\theta = 0.01 \text{ Kg m}^{-3}$
Schofield et al. [2015b]	Amundsen Sea	$\max(N^2)$
Vernet et al. [2008], Prézelin et al. [2004]	WAP	not specified
Venables et al. [2013]	Margarite Trough (WAP)	$\Delta\sigma_\theta = 0.05 \text{ Kg m}^{-3}$
Moline et al. [1997], Cimino et al. [2016]	Anvers Island (WAP)	$\max(\partial\rho/\partial z)$
Walsh et al. [2001]	Northern WAP	not specified
Mitchell and Holm-Hansen [1991]	SW Bransfield Strait (WAP) and Drake Passage	$\Delta\sigma_\theta = 0.05 \text{ Kg m}^{-3}$ (in 5m window)

To determine the value of our combined method linking physical MLD with chl- α depth, we evaluated several MLD methodologies. The most commonly used MLD criteria in polar waters (Table 3.2) were tested for each individual profile and matched against the Z_{chl} . The range of MLD calculated using the different criteria are presented for a representative profile as the shaded area in Figure 3.2a.

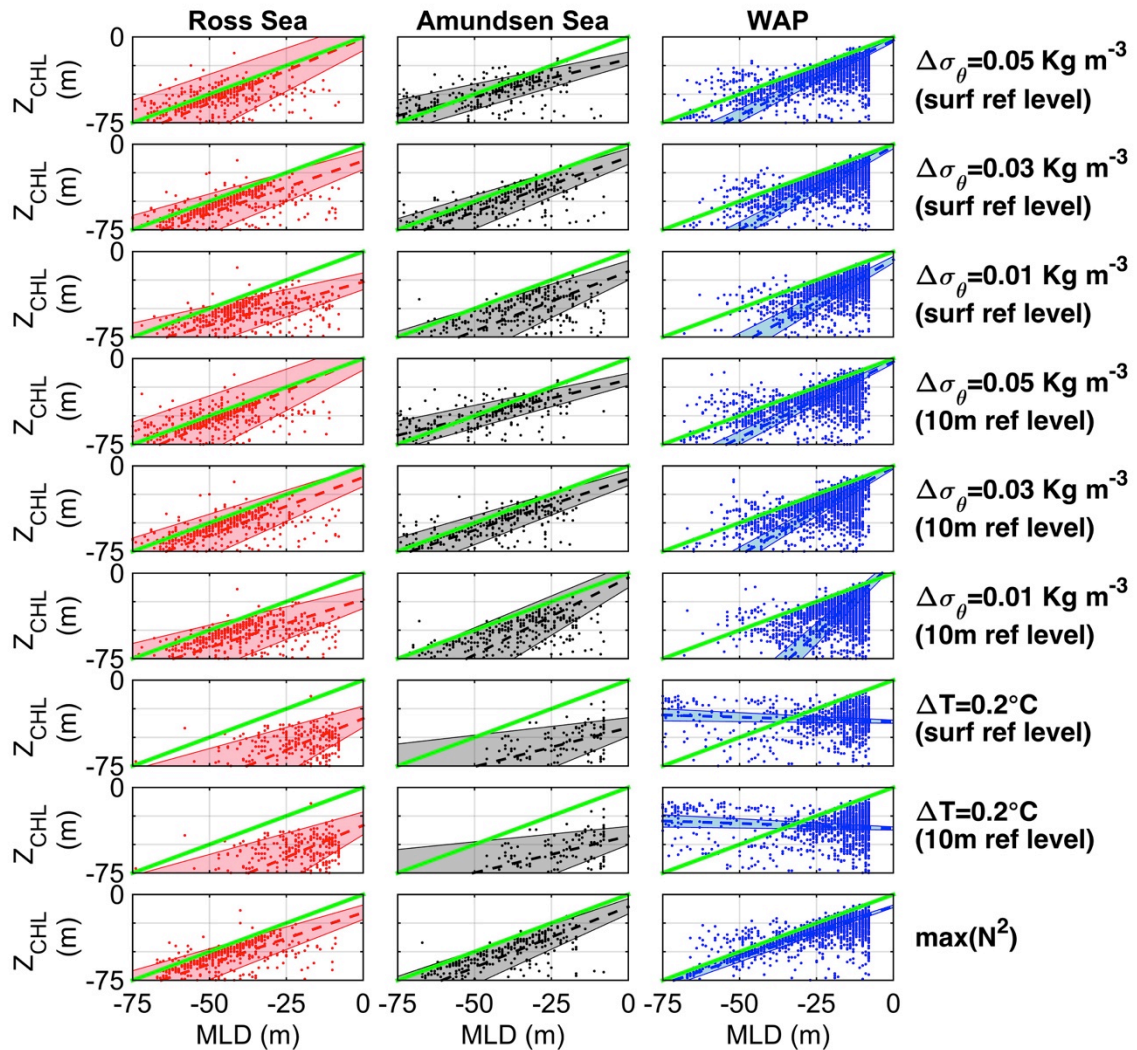


Figure 3.5: Model-2 regression comparison between most commonly used MLD calculations and Chlorophyll depth for all 3 regions: Ross Sea (left, red); Amundsen Sea (middle, black) and WAP (right, blue). Each row indicates one method. 95% confidence intervals (shaded area) and regression line are shown for quality index (QI)>0.8 (dashed line). Statistics summary presented in Table 3.3. Line 1:1 is shown in green.

Using a model-2 linear regression we were able to evaluate the various MLD definitions (Table 3.3; Figure 3.5) and concluded that the most ecological relevant MLD determination method across all regions based on the strength of the correlation with the lower boundary of the chl-*a* profile was the maximum of buoyancy frequency.

Table 3.3: Comparison between the most commonly used MLD calculations ($QI > 0.8$) and chlorophyll depth ($QC > 0.5$) for all three regions. Statistics presented include regression coefficients (slope and intercept) in the linear Model II, 95% confidence intervals, R^2 and p-value.

Area	Reference level	MLD definition	Slope (95% CI)	Intercept (95% CI)	R^2	p-value
Ross Sea	surface	$\Delta\sigma_t = 0.05 \text{ Kg m}^{-3}$	1.1315 (0.91162; 1.4223)	-1.2501 (12.9705; -12.0039)	0.38331	<0.0001
	surface	$\Delta\sigma_t = 0.03 \text{ Kg m}^{-3}$	0.9236 (0.75683; 1.1199)	-14.6279 (-5.7293; -22.1882)	0.42873	<0.0001
	surface	$\Delta\sigma_t = 0.01 \text{ Kg m}^{-3}$	0.75883 (0.5858; 0.95946)	-26.6302 (-18.7633; -33.4153)	0.36077	<0.0001
	10 m	$\Delta\sigma_t = 0.05 \text{ Kg m}^{-3}$	1.1409 (0.93085; 1.4152)	0.3619 (14.0309; -10.106)	0.40284	<0.0001
	10 m	$\Delta\sigma_t = 0.03 \text{ Kg m}^{-3}$	1.0136 (0.83915; 1.225)	-10.097 (-0.40501; -18.0979)	0.43893	<0.0001
	10 m	$\Delta\sigma_t = 0.01 \text{ Kg m}^{-3}$	0.84269 (0.64345; 1.0846)	-23.0492 (-13.388; -31.0078)	0.33713	<0.0001
	surface	$\Delta T = 0.2^\circ\text{C}$	1.0964 (0.74109; 1.5924)	-33.5223 (-22.7087; -41.2677)	0.30514	<0.0001
	10 m	$\Delta T = 0.2^\circ\text{C}$	1.1218 (0.74434; 1.6628)	-33.2245 (-21.5044; -41.4021)	0.29097	<0.0001
	N/A	$\max(N^2)$	0.90187 (0.76634; 1.0503)	-15.7886 (-9.1416; -21.8578)	0.51018	<0.0001
Amundsen Sea	surface	$\Delta\sigma_t = 0.05 \text{ Kg m}^{-3}$	0.65963 (0.55834; 0.77402)	-19.3709 (-13.257; -24.7847)	0.56261	<0.0001
	surface	$\Delta\sigma_t = 0.03 \text{ Kg m}^{-3}$	0.96196 (0.81993; 1.1307)	-11.3562 (-3.7911; -17.7242)	0.57117	<0.0001
	surface	$\Delta\sigma_t = 0.01 \text{ Kg m}^{-3}$	1.0438 (0.82773; 1.3155)	-17.5556 (-7.9942; -25.1627)	0.4492	<0.0001
	10 m	$\Delta\sigma_t = 0.05 \text{ Kg m}^{-3}$	0.64711 (0.55836; 0.74662)	-18.532 (-12.9901; -23.4746)	0.60654	<0.0001
	10 m	$\Delta\sigma_t = 0.03 \text{ Kg m}^{-3}$	0.89772 (0.77734; 1.0373)	-11.4868 (-4.7832; -17.2684)	0.60916	<0.0001
	10 m	$\Delta\sigma_t = 0.01 \text{ Kg m}^{-3}$	1.3512 (1.116; 1.6665)	-3.9644 (7.8925; -12.8122)	0.48795	0.0008
	surface	$\Delta T = 0.2^\circ\text{C}$	0.67979 (0.30621; 1.1027)	-41.5799 (-32.7969; -49.3392)	0.3112	0.0119
	10 m	$\Delta T = 0.2^\circ\text{C}$	0.64084 (0.27056; 1.057)	-42.6756 (-34.1247; -50.2841)	0.2958	0.0013
	N/A	$\max(N^2)$	1.0596 (0.90613; 1.2333)	-10.7674 (-3.6717; -17.0337)	0.59985	<0.0001
WAP	surface	$\Delta\sigma_t = 0.05 \text{ Kg m}^{-3}$	1.3143 (1.2388; 1.3963)	-2.8101 (-0.88221; -4.5856)	0.58075	<0.0001
	surface	$\Delta\sigma_t = 0.03 \text{ Kg m}^{-3}$	1.4596 (1.3677; 1.5605)	-1.9897 (0.22594; -4.0087)	0.55859	<0.0001
	surface	$\Delta\sigma_t = 0.01 \text{ Kg m}^{-3}$	1.4859 (1.343; 1.645)	-7.2379 (-4.2724; -9.9011)	0.44174	<0.0001
	10 m	$\Delta\sigma_t = 0.05 \text{ Kg m}^{-3}$	1.3344 (1.2583; 1.4163)	-2.581 (-0.66811; -4.3578)	0.54337	<0.0001
	10 m	$\Delta\sigma_t = 0.03 \text{ Kg m}^{-3}$	1.5534 (1.4555; 1.6602)	-0.7396 (1.5334; -2.8253)	0.50735	<0.0001
	10 m	$\Delta\sigma_t = 0.01 \text{ Kg m}^{-3}$	2.4802 (2.2766; 2.7156)	9.0207 (13.0761; 5.5137)	0.4085	<0.0001
	surface	$\Delta T = 0.2^\circ\text{C}$	-0.0789 (-0.1302; -0.02810)	-36.2913 (-34.907; -37.6905)	-0.088436	0.0024
	10 m	$\Delta T = 0.2^\circ\text{C}$	-0.0873 (-0.1409; -0.03424)	-35.91 (-34.5426; -37.2933)	-0.083361	0.0013
	N/A	$\max(N^2)$	0.9063 (0.8642; 0.94952)	-10.337 (-9.2471; -11.3978)	0.67345	<0.0001

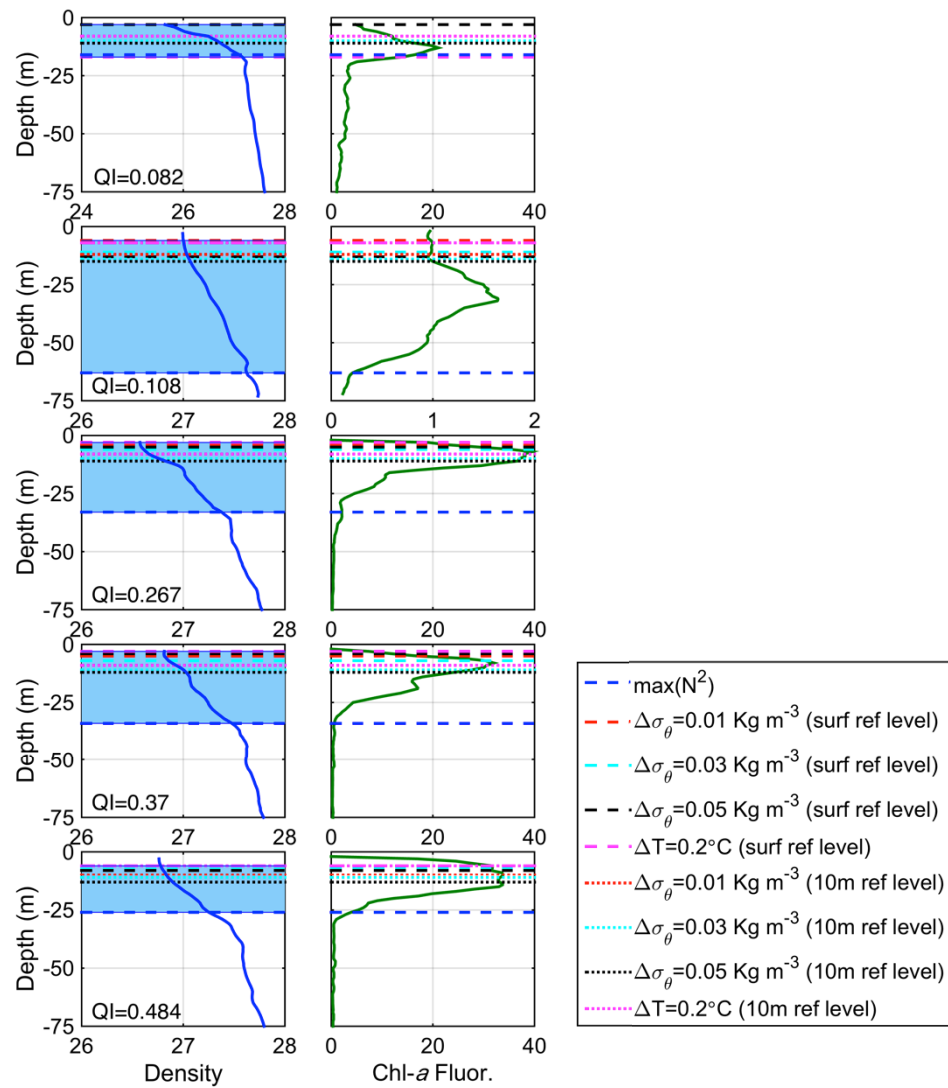


Figure 3.6: Example of profiles when MLD was not determined ($QI < 0.5$). Left: Density (Kg m^{-3}). Right: Chlorophyll-a fluorescence ($\mu\text{g L}^{-1}$). Horizontal lines indicate MLD for the most commonly used definitions in Antarctica's coastal seas. Shaded area denotes range of calculated MLD.

Independent of the different water mass compositions and dynamics present in each region, the biophysical relationship between MLD and chl-*a* remains the same in all three regions. With slopes not significantly different from the 1:1 line (within the 95% confidence intervals of the model-2 regression fit) in all three regions suggests that the MLD definition we are using is a good predictor of the depth of the inflexion point in the

chl-*a* profile (lower boundary of the chl-*a* patch in the water column), and is therefore an important parameter in phytoplankton dynamics studies.

3.5 Conclusions

Understanding the spatial and temporal variability of phytoplankton is important, especially to assess ecological dynamics of marine foodwebs. Historically different MLD calculations have been applied in Antarctic continental shelves and linked to phytoplankton dynamics [Mitchell and Holm-Hansen, 1991; Smith and Jones, 2015; Vernet *et al.*, 2008]. These calculations were based on different subjective thresholds (sometimes linked to local hydrography) for the same regions. This leads to significant variability in MLD estimations, making comparisons between studies and regions problematic. MLDs calculated from buoyancy frequency were similarly correlated with our adapted estimate of Z_{chl} across all three coastal regions. Given the variability in water mass distribution and volume between the RS, AS and along the WAP, this bio-physical relationship was similar in all regions, which suggests that the maximum of stability frequency (or $\max[N^2]$) is an appropriate and robust metric to compare and contrast bio-physical processes across all three Antarctic regions.

3.6 Acknowledgements

We thank the crews of R/V Nathaniel B. Palmer, ARSV Laurence M. Gould, R/V Araon, Palmer Station support staff and the Rutgers glider team for facilitating our long-term data collection efforts. We also wish to thank five anonymous reviewers for their

suggestions regarding the analysis in this paper. The research was supported by the National Science Foundation grants ANT- 0823101 (Palmer-LTER), ANT-1327248 and ANT-1326541 (CONVERGE), ANT-0839039 (SEAFAReRS), ANT-0838995 (ASPIRE) and the Korean Polar Research Institute grant PP1502 (KOPRI). Filipa Carvalho was funded by a Portuguese doctoral fellowship from Fundação para a Ciência e Tecnologia (DFRH - SFRH/BD/72705/2010). Glider data can be accessed at ERDDAP server at <http://erddap.marine.rutgers.edu/erddap/info/>.

**Chapter 4: Mixing and phytoplankton dynamics in a
submarine canyon in the West Antarctic Peninsula**

4.1 Abstract

Bathymetric depressions (canyons) exist along the West Antarctic Peninsula shelf and have been linked with increased phytoplankton biomass and sustained penguin colonies. However, the physical mechanisms driving this enhanced biomass are not well understood. Using a Slocum glider dataset with over 30,000 water column profiles, we evaluate the relationship between mixed layer depth (MLD, estimated using the depth of maximum buoyancy frequency) and phytoplankton vertical distribution. We use the glider deployments in the Palmer Deep region to examine seasonal and across canyon variability. Throughout the season, the ML becomes warmer and saltier, as a result of vertical mixing and advection. Shallow ML and increased stratification due to sea ice melt are linked to higher chlorophyll concentrations. Deeper mixed layers, resulting from increased wind forcing, show decreased chlorophyll, suggesting the importance of light in regulating phytoplankton productivity. Spatial variations were found in the canyon head region where local physical water column properties were associated with different biological responses, reinforcing the importance of local canyon circulation in regulating phytoplankton distribution in the region. Observations show that the intrusion of warm, nutrient enriched modified Upper Circumpolar Deep Water (mUCDW) plays a smaller role in explaining the elevated productivity observed over the canyon than was initially hypothesized.

4.2 Introduction

The cross-shelf canyon systems in the West Antarctic Peninsula (WAP) are considered biological “hotspots” because they are associated with penguin chick rearing locations [Erdmann *et al.*, 2011; Fraser and Trivelpiece, 1996]. The association of penguin colonies with deep submarine canyons has led to the hypothesis that phytoplankton productivity is enhanced as a result of water column dynamics in the canyon heads [Schofield *et al.*, 2013]. The presence of the UCDW has been linked to increased phytoplankton productivity [Kavanaugh *et al.*, 2015; Prézelin *et al.*, 2000; Prézelin *et al.*, 2004] which supports a productive regional food web [Schofield *et al.*, 2010], yet the physical mechanisms driving phytoplankton blooms in these canyons are not well understood.

The canyons in the WAP are shelf-incising [Harris and Whiteway, 2011], and often connect the off-shelf region to the coast. Heat transport facilitated by cross-shelf canyons/troughs is enhanced by mixing particularly due to tides [Allen and de Madron, 2009]. Small-scale roughness in canyons can be responsible for much of the internal tidal energy [Kunze *et al.*, 2002], which tends to be enhanced in canyons. Additionally these regions have enhanced internal waves with periods shorter than that of tides, and has been associated with the vertical mixing over the slope and shelf waters [Bruno *et al.*, 2006]. Tides in these canyons also appear to be important for penguin foraging behavior [Oliver *et al.*, 2013] and krill swarms [Bernard and Steinberg, 2013].

These canyons allow UCDW to penetrate across the shelf, providing warmer [Martinson and McKee, 2012; Martinson *et al.*, 2008] and nutrient enriched water to

mix with coastal surface waters [Arrigo *et al.*, 2015; Prézelin *et al.*, 2000; Prézelin *et al.*, 2004]. The presence of these canyons has been connected to locally increased sea surface temperature (SST), reduced sea ice coverage and increased diatom biomass [Kavanaugh *et al.*, 2015]. Using a model, Allen *et al.* [2001] showed that the formation of an eddy over the head of a canyon trapped passive particles such as phytoplankton and small zooplankton in that location.

Globally, light and nutrients are key drivers of a bloom, but their relative importance in primary production depends on the region and the role of local stratification. Light is a key factor regulating phytoplankton growth in polar regions, including the WAP. Several studies have linked shallower mixed layer depths (MLD), which increases the overall light available to phytoplankton [Holm-Hansen and Mitchell, 1991; Mitchell and Holm-Hansen, 1991; Moline and Prézelin, 1996; Sakshaug *et al.*, 1991], with increased phytoplankton biomass, especially diatoms [Fragoso and Smith, 2012]. Increased irradiance and vertical stratification have also been positively correlated with increased diatom biomass [Mitchell and Holm-Hansen, 1991; Nelson and Smith, 1991], especially during early spring season [Fragoso and Smith, 2012]. Macronutrients are generally abundant throughout the WAP [Ducklow *et al.*, 2012; Serebrennikova and Fanning, 2004] and although they show marked seasonality [Clarke *et al.*, 2008], in most cases they don't seem to limit phytoplankton growth [Holm-Hansen and Mitchell, 1991]. Micronutrients such as iron do not seem to limit primary production in the coastal waters of the WAP where canyon heads are located either

[Annett *et al.*, 2015; Helbling *et al.*, 1991; Martin *et al.*, 1990], but available data are limited.

It is important to understand the link between some of the physical drivers, like stratification and MLD, and phytoplankton dynamics as the higher trophic levels are dependent on primary producers [Schofield *et al.*, 2010]. In this work we characterize the phytoplankton dynamics in submarine canyons in the WAP using Palmer Deep Canyon (PD) as a focused study area. Here we describe, both temporally and spatially, the phytoplankton spring bloom at PD, using a 6-year Slocum glider dataset. The high spatial and temporal resolution sampling provides a detailed analysis of the phytoplankton and physical dynamics at the head of a submarine canyon in the WAP. While the mechanism initially hypothesized to produce the observed increases in phytoplankton over the canyons was the intrusion of warm, nutrient enriched mUCDW [Prézelin *et al.*, 2000; Prézelin *et al.*, 2004; Schofield *et al.*, 2013], our analysis suggests that ML dynamics are key to increased primary production over submarine canyons in the WAP.

4.3 Materials and Methods:

4.3.1 Slocum gliders

Slocum electric gliders are a robust tool to map in high resolution the upper water column properties in different environments [Schofield *et al.*, 2007] including polar regions [Kohut *et al.*, 2013; Oliver *et al.*, 2013; Schofield *et al.*, 2013]. These 1.5 m torpedo-shaped buoyancy driven autonomous underwater vehicles provide high-

resolution surveys of the physical and bio-optical properties of the water column [Schofield *et al.*, 2007]. Data were collected using both shallow (100-meter depth range) and deep (1000-meter) gliders. However, only data above 100 meters depth were considered for this analysis as we are focusing on processes happening within the euphotic zone. All gliders were equipped with a Seabird Conductivity-Temperature-Depth (CTD) sensor and WET Labs Inc. Environmental Characterization Optics (ECO) pucks, which measured chlorophyll-*a* fluorescence, and optical backscatter at 470, 532, 660 and 700 nm. Glider based conductivity, temperature and depth measurements were compared with a calibrated ship CTD sensor on deployment and recovery to ensure data quality, as well as with a calibrated laboratory CTD prior to deployment. Glider profiles were binned into 1-meter bins and assigned a mid-point latitude and longitude.

4.3.2 Sampling overview

Our analysis includes all available concurrent glider physical and biological profiles in the WAP region (Figure 4.1) where bathymetric depressions have been linked to deep-water intrusion onto the shelf, with a focus on the dynamics at PD. Overall, the data include 26,455 profiles, 265 days deployed and 3,937 km flown. For comparison purposes, the WAP-shelf analysis excluded all the points in PD region (purple rectangle in Figure 4.1).

The deployments on the shelf along the WAP were part of the NSF Palmer - Long Term Ecological Research Project (PAL-LTER; Ducklow *et al.* [2007]) effort, with the goal

of understanding changes 1) in the entire WAP ecosystem with 26 deployments conducted throughout the peninsula from Anvers Island to Charcot Island (-64° to -69° latitude) and 2) with a focus on the PD region where Palmer Station is located. In the PD region (Figure 4.1, right), data were collected during 6 field seasons (2010-2015) over the austral summer as part of the NSF PAL-LTER and one field season (2014-2015) as part of the NSF CONVERGE Project [Kohut *et al.*, 2014a]. Gliders were deployed from Palmer Station (Anvers Island) with the goal of characterizing PD, focusing on the head of the canyon.

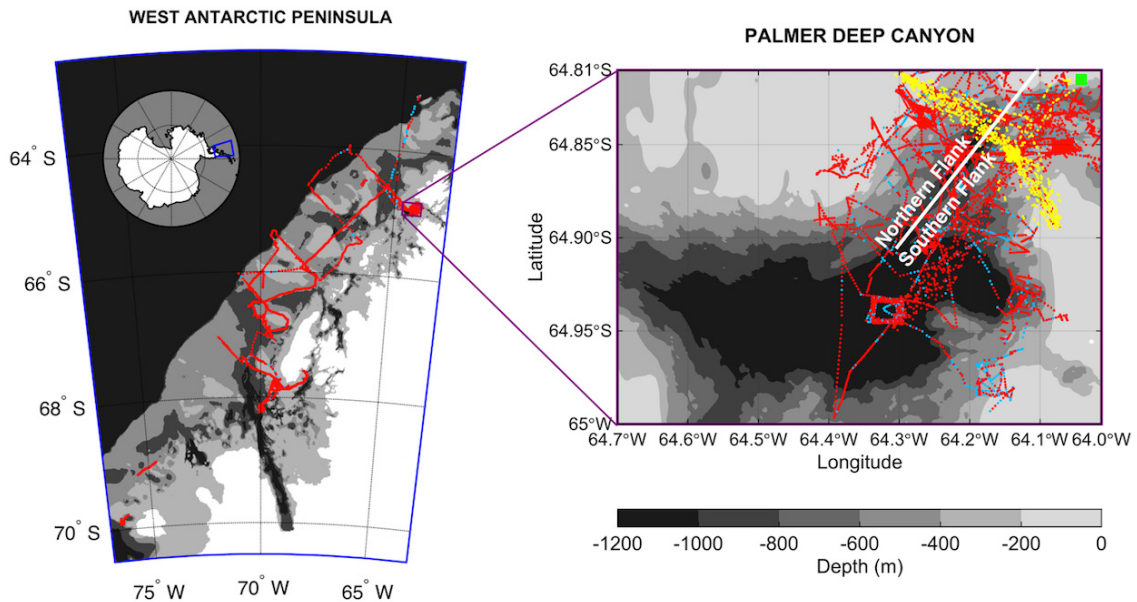


Figure 4.1: Bathymetry maps overlaid with location of the glider profiles (red – MLD Quality index (QI) > 0.5; blue dots, remaining profiles where MLD was not determined and therefore not included in the analysis, i.e., QI < 0.5) for the regions, WAP (left) and PD (right). Cross-canyon transects highlighted in yellow from the 2015 mission (gliders ru05 and ud134). White line separates the head of the canyon into northern and southern flanks. Green square indicates location of Station E where dissolved iron data were collected.

PD (Figure 4.1, right), a cross-shelf canyon bathymetrically similar to others in the WAP, is associated with large penguin colonies [Fraser and Trivelpiece, 1996; Schofield *et al.*, 2013]. PD extends approximately 22 km in length and 10 km across with a maximum depth of 1420 m. Over the head of the canyon there is evidence of increased primary production [Kavanaugh *et al.*, 2015] and localized penguin foraging [Oliver *et al.*, 2013]. Our study will describe glider data collected over varying spatial scales from the WAP shelf, to PD, and, at the smallest scale, the head of PD.

4.3.3 Mixed layer depth estimation

For each profile, MLD was determined by finding the depth of the maximum water column buoyancy frequency, $\max(N^2)$. A quality index (Equation 3.1) following Lorbacher *et al.* (2006) was used to quantify the uncertainty in the MLD estimate, and to filter out profiles where MLD was not resolved. Using

$$QI = 1 - \frac{rmsd(\rho_k - \bar{\rho})|_{(H_1, H_{MLD})}}{rmsd(\rho_k - \bar{\rho})|_{(H_1, 1.5 \times H_{MLD})}} \quad (4.1)$$

where ρ_k is the density at a given depth (k) and $rmsd()$ denotes the standard deviation of from the vertical mean $\bar{\rho}$ from H_1 , the first layer near the surface, to the MLD or $1.5 \times MLD$. This index evaluates the quality of the MLD computation, where MLD was determined with certainty ($QI > 0.8$), determined but with some uncertainty ($0.5 < QI < 0.8$) or not determined ($QI < 0.5$). This index does not take into account the strength of stratification, rather it indicates that there is a homogeneous layer present and the MLD calculated is close to the lower boundary of that vertically uniform surface

layer. Higher QI are observed during summer and fall, where sharp gradients at the base of the seasonal mixed layer are present [Lorbacher *et al.*, 2006].

MLD criteria were tested and matched against the chlorophyll fluorescence data to evaluate whether the MLD definition chosen was capturing the biological observations (Figure 4.2). ML-averaged temperature and salinity were calculated by averaging all 1-meter binned data points from the surface to the base of the ML.

4.3.4 Optical Measurements

4.3.4.1 ML averaged and integrated chlorophyll

Chlorophyll-*a* (chl-*a*) fluorescence, as measured by the glider ECO pucks, is our indicator of phytoplankton biomass. Discrete in situ water samples were collected from eight depths (0, 5, 10, 20, 35, 50 and 60 m) from CTD casts during each glider deployment and recovery. Water samples were filtered onto 25 mm Whatman GF/F filters and extracted using 90% acetone. Chl-*a* concentration was then measured using a fluorometer and compared to its correspondent glider profiles. QA/QC methods were applied to the data to ensure data quality. Concurrent measurements of optical backscatter and chl-*a* fluorescence were used to correct for light dependent effects. Given the high linear correlation found between backscatter and chlorophyll-*a* fluorescence (R^2 between 0.76 to 0.95 for all deployments), a correction was applied to the latter to account for non- photochemical quenching [Behrenfeld *et al.*, 2005]. Linear regressions were calculated by deployment using all the measurements taken between 20 and 40 m, below the light influenced chl-*a* values and above the possible

sedimentary (deep) sources of backscatter. Slope and intercept were calculated and used to correct chlorophyll from the surface to the chlorophyll maximum in each profile. No chlorophyll maxima were found shallower than 15 m.

Integrated and averaged chlorophyll from our defined MLD to the surface were determined using the trapezoid method. Chl-*a* concentration was calculated for each 1-meter bin and a cumulative value from the surface down to the MLD was calculated to determine the ML integrated chlorophyll. The ML averaged chlorophyll was determined by dividing the ML integrated chlorophyll by the depth of the mixed layer.

4.3.4.2 Chlorophyll Depth

A model-2 regression was used to compare the MLD with the lower boundary of the surface chlorophyll fluorescence layer. Following a method adapted from the maximum angle principle [Chu and Fan, 2011], the depth of lower boundary of chlorophyll was estimated (referred to as chlorophyll depth in Figure 4.2). Here we apply the same principle using the maximum angle, as we are interested in calculating the depth at which the chlorophyll profile starts decreasing. Using a vector of $n=7$ data points, the depth of the max ($\tan \theta$) of the chlorophyll profile was determined and used as the chlorophyll depth.

4.3.5 Climatology

One of the main goals of this study is to characterize the physical setting and to map the seasonal phytoplankton dynamics at the head of the PD by taking advantage of

the high spatial and temporal glider coverage. Using a six-year dataset of glider deployments (13,972 profiles after all filters applied), MLDs were calculated for each individual profile and daily MLD averages were calculated for temperature, salinity and chlorophyll by averaging all the values between the surface and the base of the MLD.

Wind and Photosynthetic Available Radiation (PAR) data were collected from an automated weather station (AWS) at Palmer Station, on Anvers Island. Daily averages were calculated by averaging 2-minute data.

4.3.6 Seawater iron methods

Surface water was collected at LTER Station E (6.5 km NE of the head of PD), at 8 time points between January 5 and March 9, 2015. Samples were cleanly collected in duplicate from a Zodiac inflatable boat using all-polypropylene syringes and filtered directly into 60mL LDPE bottles (Nalge®) using 25mm Acrodisc (Pall®) 0.45 μm pore size syringe filters, within minutes of sample collection. The resulting samples were stored at 4°C until arrival at Rutgers University, where they were acidified to pH~2.0 with ultrapure HCl (Fisher Optima®, concentration in seawater 0.012 M). The mean of the duplicates is reported if they agree within 15% (difference about the mean), otherwise the lower of the two values is reported.

Seawater samples were prepared for analysis of dissolved Fe and other trace metals at Rutgers University using the commercially available version of an automated pre-concentration and matrix elimination system (SeaFAST pico®, ESI, Omaha, NB) which operates on the same principle as reported in *Lagerström et al.* [2013] , and

employs the method of isotope dilution, but collects eluates offline rather than directly analyzing online.

The eluate solutions, 25-fold concentrates of the trace metals in the sample but with greatly reduced major ion concentrations, were analyzed in medium resolution on a Thermo Element-1 HR-ICP-MS. Determined process blanks for Fe typically averaged 0.040 nM and precision was 1–3% standard deviation about the mean. Accuracy was verified by repeated analysis of reference seawater materials (SAFe S and D2, GEOTRACES S and D), which showed agreement within one standard deviation of the consensus values.

4.3.7 Cross-canyon analysis

To better understand the across canyon spatial variability in MLD and chlorophyll, we conducted a 1-month long glider mission was designed with a repeated transect (yellow, Figure 4.1) that crossed the head of the canyon perpendicularly to its deep channel axis (64°48.7'S and 64°17.9'W to 64°53.7'S and 64°4.2'W, corresponding to the northern and southernmost extreme of the transect, respectively). Gliders used for this temporal/spatial study were both shallow gliders (ru05 and ud134) rated to 100 meters. The first glider (ud134) was deployed January 6th, 2015 and performed 6 full transects before ru05 took over its mission of surveying the head of the canyon. The second glider was recovered, brought back to Palmer Station and redeployed twice more during its mission to replace batteries and resume the cross-canyon mission. Final recovery took place on February 8th, 2015. Gliders repeated transects across the head of

the canyon 39 times throughout their missions, taking an average of 16 hours to complete each cross-section. The orientation of PD was used to divide (Figure 4.1, white line) the head of the canyon into two regions, the northern and the southern flanks.

4.4 Results

4.4.1 Physical properties around the Palmer Deep Canyon

Gliders were able to map many of the key water masses during the austral summer in the WAP shelf and PD region (top panels of Figure 4.2). The glider profiles over six field seasons identified the Antarctic Surface Water (AASW), Winter Water (WW) and modified Upper Circumpolar Deep Water (mUCDW). The core-UCDW seen immediately offshore of the WAP shelf ($1.7 \leq T \leq 2.13$; $34.54 \leq S \leq 34.7$, following *Martinson et al.* [2008]) was not present in the canyon; instead the canyon was characterized by a modified colder and fresher mUCDW water mass. This mUCDW extended to depths below 100m. A second water mass present in PD was the WW (or T_{\min} , minimum temperature), defined by $T \leq -1.2^{\circ}\text{C}$ and $33.85 \leq S \leq 34.13$. The WW represents the remnants of the mixed-layer water from the previous winter [*Martinson et al.*, 2008] and was found over a range of depths. Above the WW was the AASW (seen in the blue colors of Figure 4.2). In the canyon, AASW showed a wider range of temperature, salinity and depth. In both the WAP and PD, this water mass was freshest of all the water masses present. The main differences between the PD and the WAP shelf (PD profiles were excluded from the latter) were the absence of core-UCDW and

fresh surface waters at PD. WW was found at greater depths in the WAP compared to the canyon.

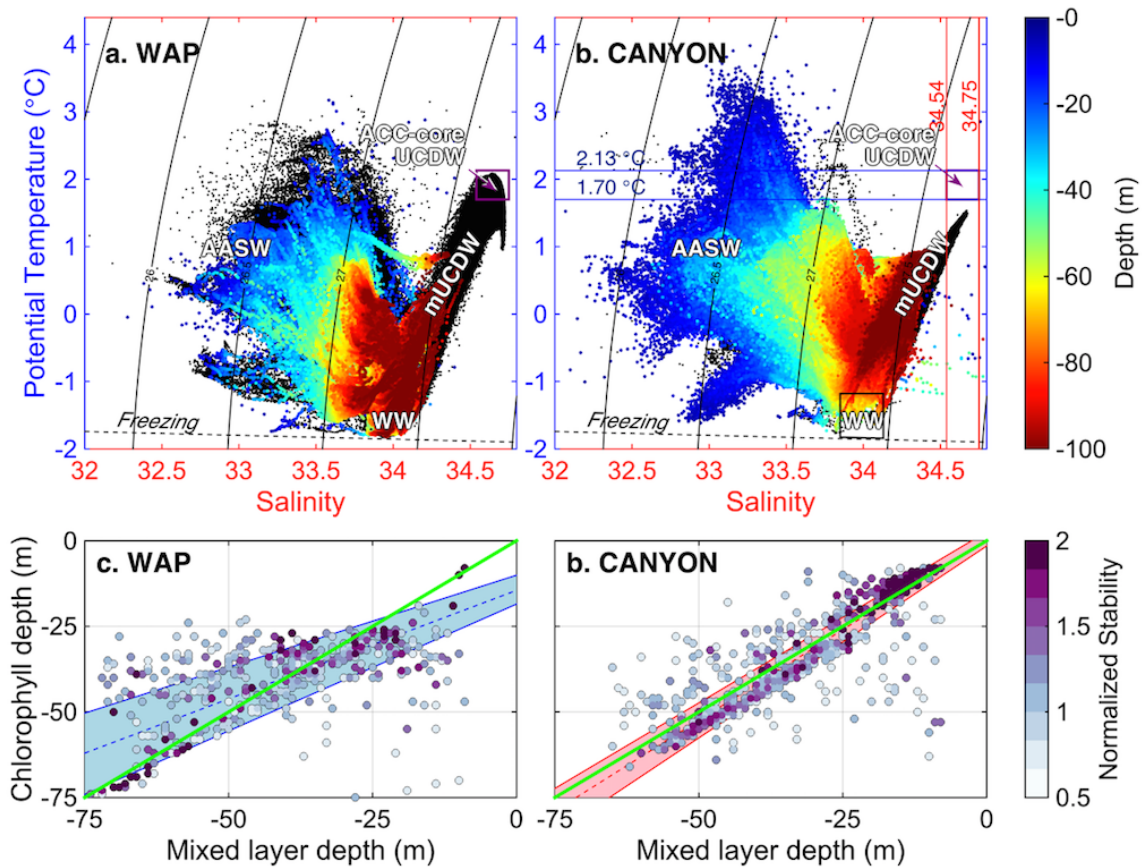


Figure 4.2: Top row: θ -S for the two areas shown in Figure 1: (a, c) WAP, and (b, d) Palmer Deep Canyon. All data collected below 100 meters are plotted in black. Color indicates depth of the water column measurement (upper 100 m of the water column). Primary water masses sampled are indicated and labeled (WW = Winter Water; AASW = Antarctic (summer) Surface Water; mUCDW = modified Upper Circumpolar Deep Water; and the regional ACC-core UCDW). Bottom row: Scatter plots comparing depth of the mixed layer (MLD) with the depth of the lower boundary of the chlorophyll profile for all glider profiles with Quality Index (QI) over 0.5. Shaded region represents 95% confidence intervals (CI) for each region. Trend lines are shown for each area and each quality index. Line 1:1 shown in green. A quality index of 0.5 was also applied to chlorophyll (QI_{chl}) profiles and only profiles with $QI_{chl} > 0.5$ are shown above. Color of the dots represents normalized stability, i.e., the stability frequency at that the depth of the ML ($\max(N^2)$) divided by the median stability of that region.

We evaluated the relationship between the MLD and chlorophyll depth with a model-2 linear regression (Figure 4.2c,d). In the canyon, the MLD-chlorophyll

relationship was close to a 1:1 line with 95% confidence levels with the tightest regression associated with the profiles with the highest stability. Generally the PD had shallower MLD than the WAP. Although more profiles in the WAP fell away from the 1:1 line, there were no significant differences (with a 95% CI) from that line for MLDs below 23 m.

4.4.2 Coupled dynamics at Palmer Deep Canyon

4.4.2.1 Seasonal climatology of MLD and chlorophyll

A seasonal climatological analysis of the MLD properties (Figure 4.3) was conducted by averaging the data between the surface and the corresponding ML for temperature, salinity and chlorophyll-*a* fluorescence. Generally, MLD shoaled in December, reaching its shallowest depth ($\overline{MLD} = -11 \pm 0.76$ m) in the beginning of January. MLD remained fairly constant (above 20 meters) throughout most of January, then started to deepen at the end of this month. The ML in January was generally fresher and colder and as it deepened it became warmer and saltier. Wind speed was fairly constant and low until late January. From then there was increasing wind speed until the end of the growing season. The summer MLD reached its maximum depth ($\overline{MLD} = -52 \pm 0.66$ m) during the first week of February and then started shoaling again in early March. Both the temperature (Figure 4.3a) and salinity (Figure 4.3c) showed a very clear temporal signal. A secondary shoaling of the ML in mid-February was accompanied by a freshening and slight cooling of the ML. The MLD chlorophyll (Figure 4.3b) concentration was highest when MLD was shallowest, i.e. throughout January.

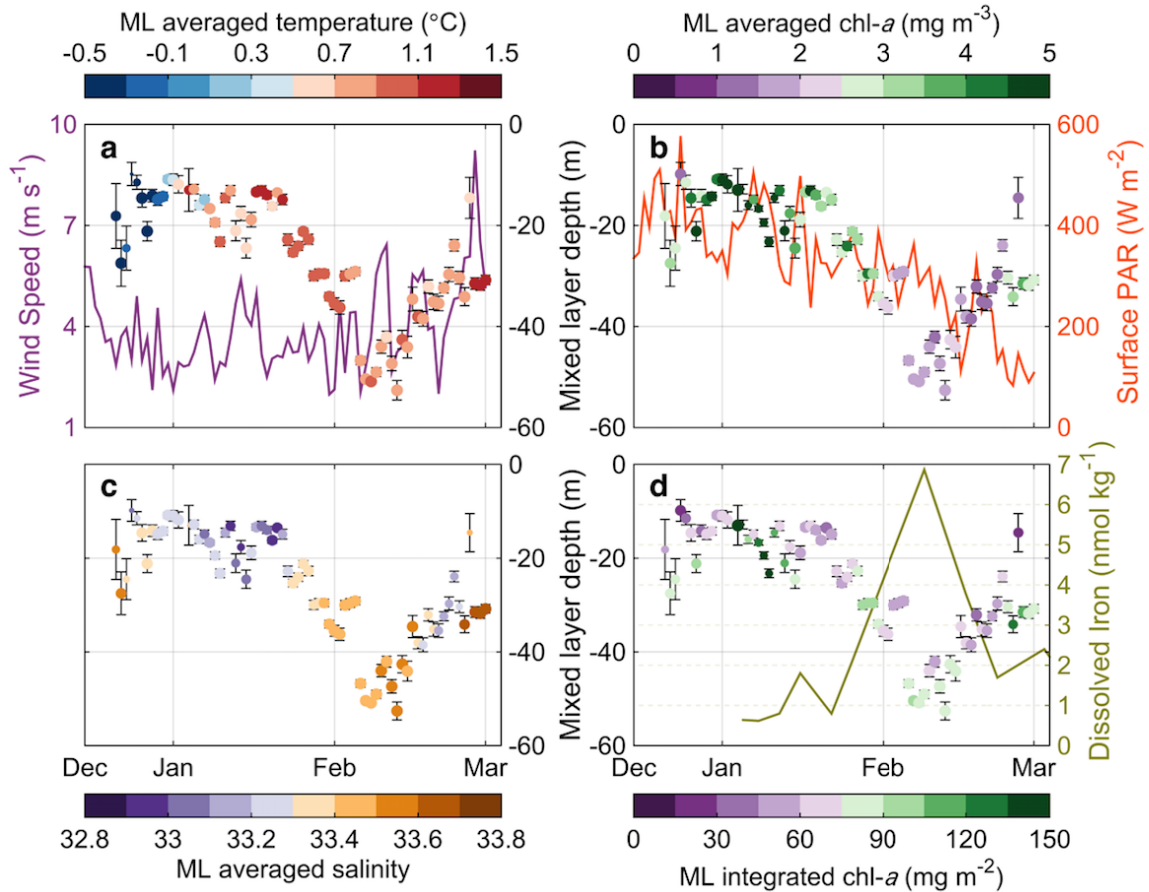


Figure 4.3: Mixed Layer Depth (MLD) in the Palmer Deep region showing evolution on MLD throughout the spring/summer season. Color denotes ML averaged: (a) temperature, (b) chlorophyll, (c), salinity and (d) ML integrated chlorophyll. Marker size represents the standard error of the variable in color (larger marker represents lower standard error, and vice-versa). Standard error of depth MLD is shown in the vertical bars. Averages were calculated using 13,972 individual glider profiles collected during 2010-2015 deployments. Daily averages of wind and surface PAR are shown in panels (a) and (b), respectively. Surface iron measurements at Station E are shown in panel (d) from 2014-2015 season.

Going into February, when MLD was deepest, chlorophyll concentrations were low. ML averaged chlorophyll showed a direct relationship with MLD ($y=0.136x + 7.03$; $r^2=0.42$; $p<0.0002$), with higher chl-*a* when MLD is shallow and lower chl-*a* when deeper. An increase in chlorophyll was observed when MLD shoaled again later in the season. Surface dissolved iron (Fe) concentrations (Figure 4.3d) at a station 6.5 km from the canyon head, exhibited an inverse relationship with chlorophyll, reaching maximum

values when MLD was deepest. Throughout the season, Fe concentrations at this station never fell below 0.6 nmol kg^{-1} .

The strength of water column stratification ($\max N^2$) was seen to vary through the season. In January, when chlorophyll concentrations were high, the water column was more stable (Figure 4.4b) and over the season the water column stability decreased. Stability was inversely correlated with salinity ($R^2=-0.77$, $p<0.0001$), with higher stability associated with shallower MLD and lower salinities (Figure 4.4a) suggesting the importance of sea ice melt and potentially glacial melt in phytoplankton primary productivity.

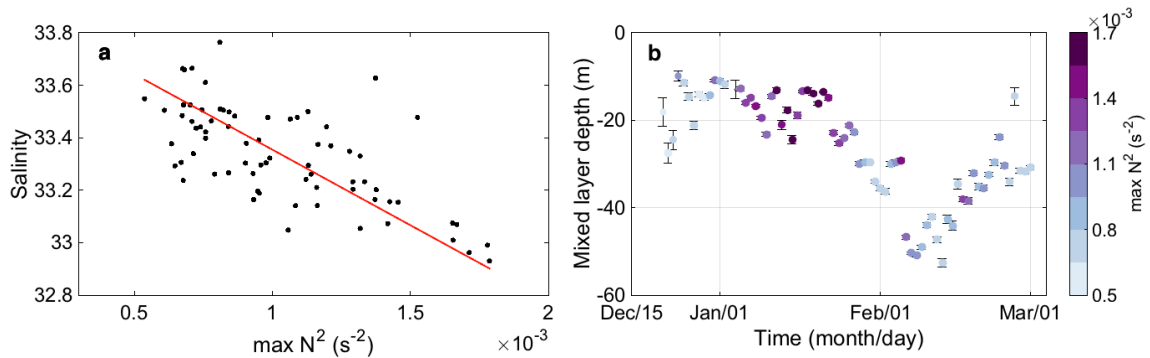


Figure 4.4: Water stability in the Palmer Deep region using daily averages: (a) salinity and maximum of stability frequency ($\max N^2$); (b) seasonal climatology of MLD with $\max(N^2)$. Averages were calculated using 13,972 individual glider profiles collected during 2010-2015 deployments.

4.4.2.2 Cross-canyon variability

Four glider deployments, conducted over one month, collected high-resolution data across the head of the canyon in PD with the goal of understanding the dynamics of the water masses in the canyon over the summer season. The mission characterized the spatial variability between the northern and southern regions of PD (Figure 4.1). A

temporal and spatial analysis of the TS plot is shown in Figure 4.5. The AASW, represented by the shallowest depths (blue), was cold and fresh in the beginning of January. As the month progressed, surface water became warmer and saltier. Winter water ($T < -1.2^{\circ}\text{C}$), was present in the beginning of January and was found in deeper waters as time progressed. Deeper water (reds) was warmer and saltier in the beginning of January. The AASW was warmer at the beginning of February (Figure 4.5, last column).

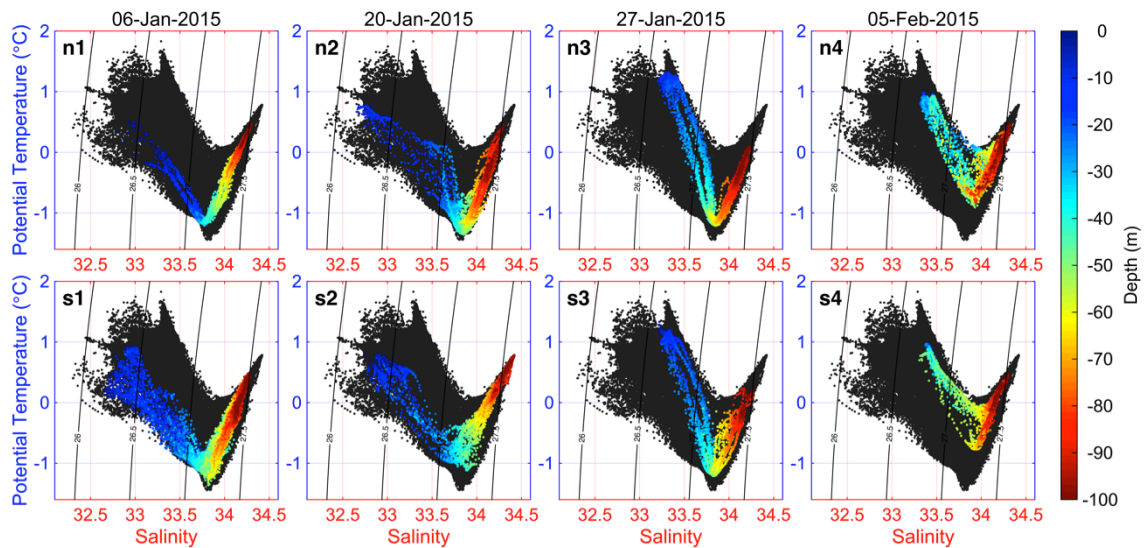


Figure 4.5: θ -S scatter plots from ru05/ud134 gliders, comparing the water masses of Northern (N, top) and Southern (S, bottom) flanks of the head of the Palmer Deep canyon through time (panels left to right). Black dots represent all glider measurements (both areas) for the entire deployment. Color denotes depth of the water column measurement.

Given the importance of ML structure in driving the chlorophyll, the θ -S plots in Figure 4.5 were decomposed into average depth profiles (Figure 4.6). The average temperature (b plots, middle row) and salinity (c plots, bottom row) depth profiles for each time point, were calculated and then compared between the 2 regions (blue and

red) at the head of the PD canyon. The top row in Figure 6 is for the average distribution and respective standard deviation for the temperature and salinity for each depth and different time periods over the month. The southern region (blue, Figure 4.6a1) showed overall a wider range in temperature and salinity in the beginning of January.

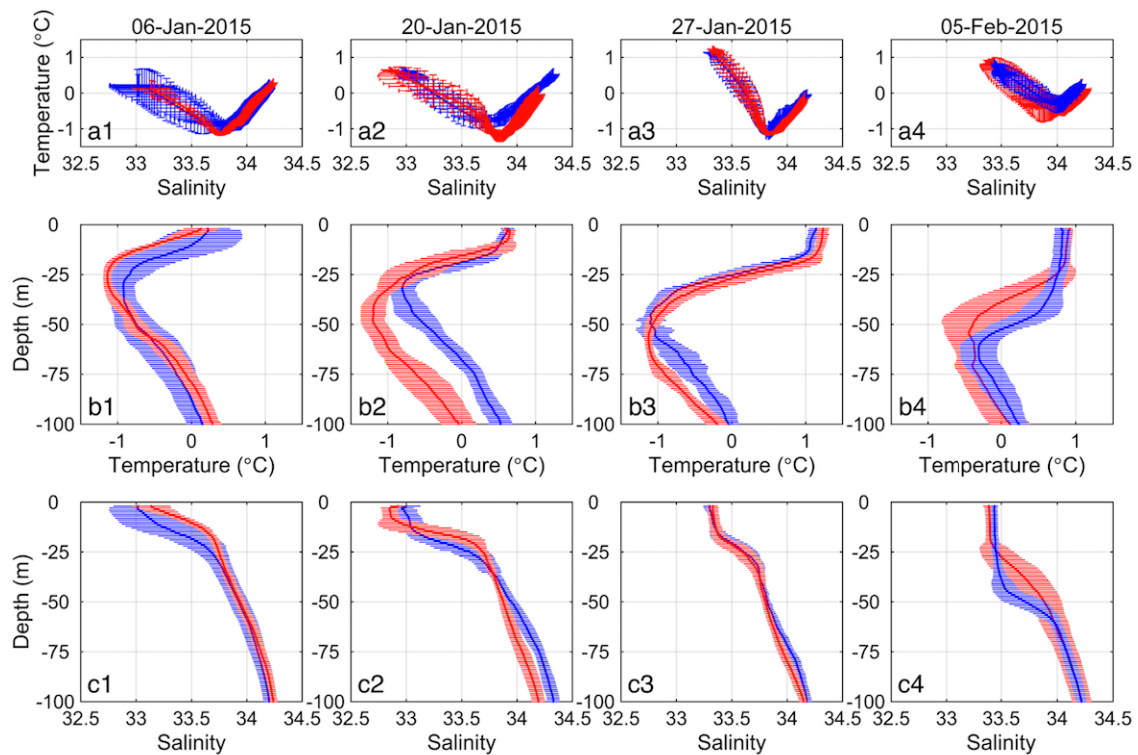


Figure 4.6: Decomposition of the θ -S diagrams from Figure 4.5, for Northern (red) and Southern (blue) flanks of the head of the Palmer Deep canyon: (a1-4) average θ -S diagram with average (center points) and standard deviation (horizontal bars for salinity; vertical bars for temperature), (b1-4) average temperature profile, (c1-4) average salinity profile, with standard deviation (shaded area), per depth for each time point.

This increased variance was especially marked in AASW, which was characterized by lower salinities. This trend reversed over the month with the northern region of the canyon (red) showing a wider variance in surface water properties (both temperature and salinity). Observed differences were more influenced by temperature (Figure 4.6b1-

4) than by salinity (Figure 4.6c1-4). Although surface temperatures were similar between regions, below the MLD, the northern region (red) had consistently lower temperatures (Figure 4.6b1-4) compared to the southern region. Differences of over 0.5°C, sometimes almost up to 1°C, were found at depth on January 20th (Figure 4.6b2). Both areas showed similar salinity profiles in January. The only salinity differences found were in February and were mostly due to deeper MLDs in the southern region.

The ML averaged and integrated chlorophyll were calculated for each profile and plotted against its corresponding MLD (Figure 4.7). Here we define the end of the bloom (January 21/22) by evaluating the evolution of individual profiles of chlorophyll and the change of the trends between MLD and chl-*a* through time. This date separated two time periods, one during bloom conditions (blue, from January 5-21) and the second during post-bloom conditions (red, from January 22-February 9). Bloom conditions were characterized by a clear progression from a moderately shallow (30 m) and highly productive MLD (dark blue) to an even shallower (8m) and less productive ML (light blue). Both ML integrated (Figure 4.7a) and averaged chlorophyll (Figure 4.7b) showed similar trends. While ML averaged chlorophyll decreased with the deepening of the ML and consequent ending of the bloom, ML integrated chlorophyll increased during this post-bloom condition (Figure 4.7, Figure 4.9e). When comparing the two regions (northern - solid line; southern – dashed line), few differences were found.

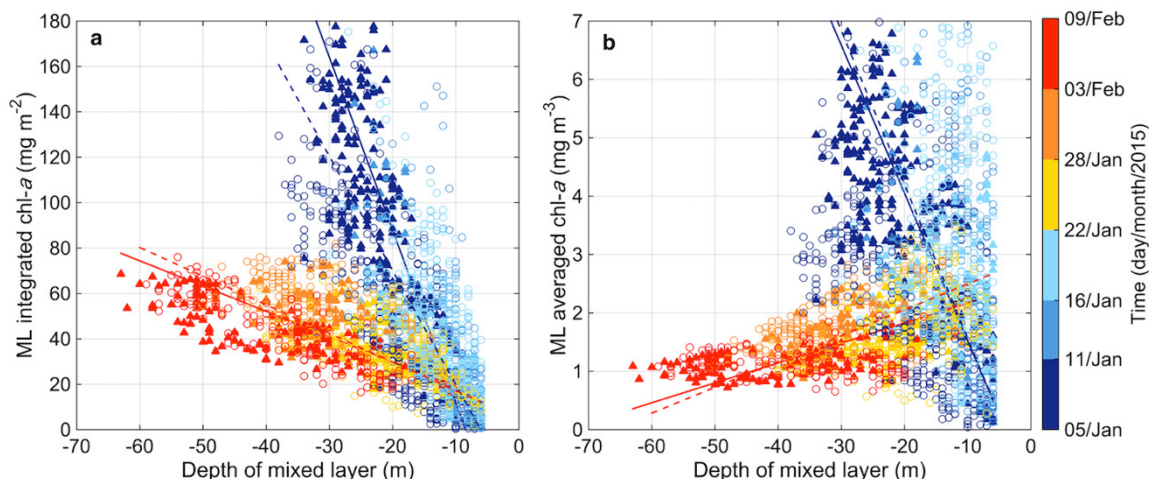


Figure 4.7. Relationship between the depth of the mixed layer (defined by the maximum water column buoyancy frequency, N^2) and: (a) ML integrated and (b) ML averaged chlorophyll concentrations. Comparison between the northern (filled marker, solid line) and southern (open marker, dashed line) flanks. The colors indicate time. Lines represent the trends seen between Jan 6 – Jan 21 (blue) and Jan 22 – Feb 9 (red).

Sustained across canyon sampling in 2015 allowed for an analysis for the spatial differences within the canyon. The time-averaged transect (Jan 6 –Jan 28, 2015) for temperature and salinity is shown in Figure 4.8a-b. While the warm surface layer appears uniform in both regions, a thicker and colder layer (light blue), with a tongue of colder ($T < -1$ °C; dark blue) water at mid depths of 45-70 m was evident in the northern region. The southern region showed warmer and saltier water at depths below the colder layer. A fresher layer was evident in the surface few meters in the northern region. The bottom panel of Figure 8 shows a time averaged mixed layer depth (blue dotted line) and upper 100 m integrated chlorophyll (solid green line) for each 1 km along the transect line. Northern region was characterized by shallower MLD and increased integrated chlorophyll in the upper 100 m of the water column while the

southern region showed overall deeper MLD and slightly lower integrated chlorophyll concentrations.

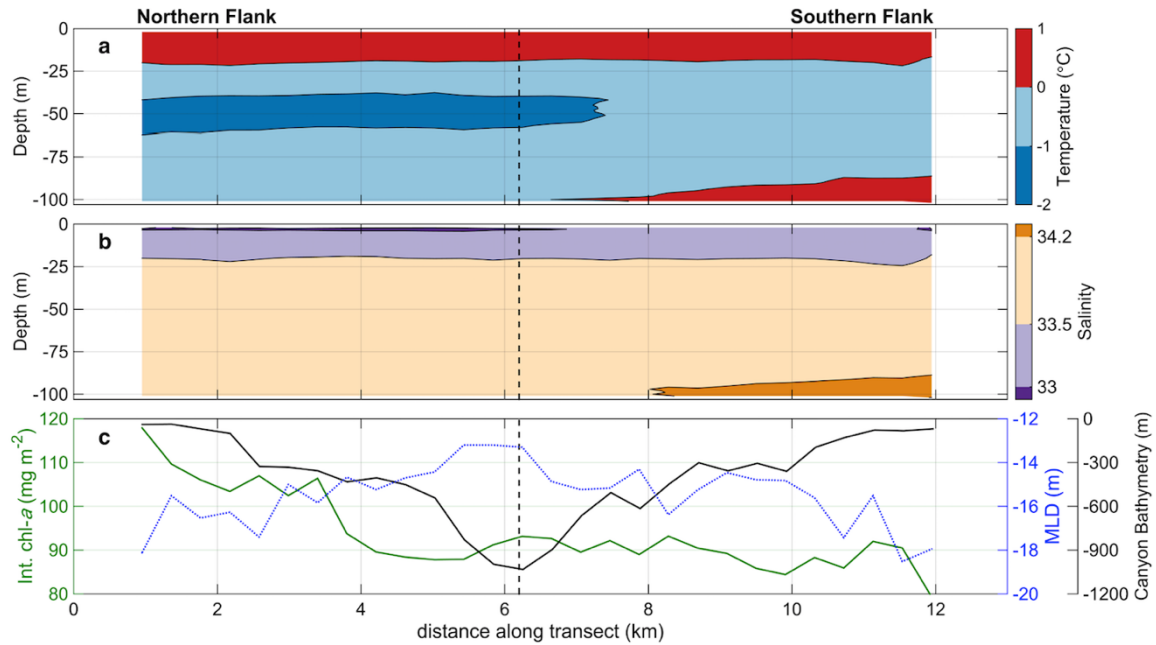


Figure 4.8. Time averaged transect (Jan 6 - Jan 28, 2015) Northern and Southern regions are separated by the dashed vertical line at km 6.2 in the along-track distance. Variables plotted are time averaged transect of: (a) temperature, where warm layer at the surface represents AASW, dark blue denotes WW, bottom layer in red indicates possibly mUCDW intrusion; (b) salinity and (c) mixed layer depth (MLD; blue dotted line) with integrated chlorophyll (upper 100m; green solid line) and canyon bathymetry (black solid line).

A repeated glider section across the head of the canyon captured the temporal and spatial variability of the phytoplankton dynamics (Figure 4.9). Each glider cross-section was interpolated through space and time with a resolution of 500 m and 16 hours, respectively. Temporal gaps in Figure 4.9 correspond to glider recovery and redeployment after battery exchange. The top panel shows bathymetry of the two regions (northern and southern) being fairly symmetrical, going from deeper (~1000 m)

depths at the center to shallower depths (~100 m) when moving away from the deep trough.

Again, the temporal signal is the most evident across all 5 panels. Early in January, the MLD was shallow, colder and fresher. This period was also characterized by increased chlorophyll (both ML integrated and averaged chlorophyll). As January progressed, the MLD (Figure 4.9a) deepened, accompanied by warming (Figure 4.9b) and increased salinity (Figure 4.9c) in the upper ML with a decrease in the chlorophyll concentration (Figure 4.9d, e). An increase in ML integrated chlorophyll (Figure 4.9e) late in the mission is also present in the climatology (Figure 4.3).

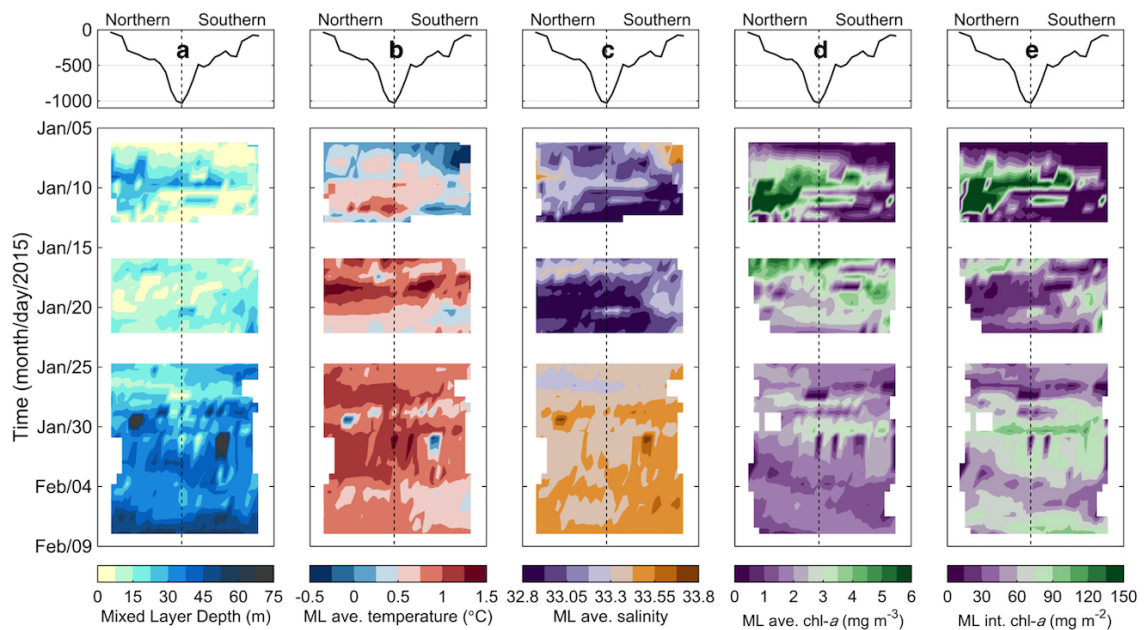


Figure 4.9. Top panels: Bathymetry of the cross-canyon transect performed by ru05 (yellow, Figure 4.1). Bottom panels: Hovmöller diagram of the temporal evolution of each transect by ru05 regarding: (a) mixed layer depth, (b-d) ML averaged (b) temperature, (c) salinity, (d) chlorophyll and (e) ML integrated chlorophyll. Dashed line separates northern and southern flanks of the head of the Palmer Deep canyon.

The magnitude of the spatial variability was less than the temporal variability observed over the entire summer season, yet differences were observed, particularly in the physical properties of the water. The MLD was overall shallower in the northern region. This is especially true for the second and fourth deployments. Warmer temperatures and lower salinities also characterized this region. This pattern was also clear when looking at the homogeneous surface ML later in the season (Figure 4.6b4, c4).

4.5 Discussion

The WAP ecosystem is characterized by high interannual phytoplankton variability [Smith *et al.*, 2008], with chlorophyll-*a* showing a wide range in both time and space [Moline *et al.*, 1997; Montes-Hugo *et al.*, 2008; Smith *et al.*, 1998]. Chlorophyll concentrations are highest near shore with a decreasing gradient moving offshore [Vernet *et al.*, 2008]. The canyons are known hotspots for penguin foraging [Kahl *et al.*, 2010; Oliver *et al.*, 2012; Schofield *et al.*, 2013] with increased chlorophyll compared to coastal regions with shallow bathymetry [Kavanaugh *et al.*, 2015]. While previous studies have focused on the primary productivity over the entire WAP [Moline and Prézelin, 1996; Montes - Hugo *et al.*, 2010; Prézelin *et al.*, 2004], the high-resolution sampling capabilities introduced with gliders, allowed us to conduct a detailed analysis of the canyon primary production focusing on the physical forcing of the increased production observed over submarine canyons.

4.5.1 The seasonal cycle at Palmer Deep canyon

4.5.1.1 Primary water masses

A fundamental question regarding phytoplankton dynamics in the region [Schofield *et al.*, 2013] involves the supply of heat and nutrients from the warm, deep water (UCDW) found at depth off the shelf. Canyons provide a conduit for this water to move across the shelf [Martinson *et al.*, 2008]. No direct pathways have been found of ACC-core UCDW onto the Palmer Deep Canyon, so no ACC-core UCDW is present in the canyon, but by looking at T_{\max} at depth, we find a modified-UCDW (relatively colder and fresher than pure UCDW) at depth. Because the bulk of the mUCDW is found at deeper depths and the gliders are usually only sampling the upper 100 m of the water column, we are only partially capturing this intrusion onto the canyon. This intrusion however is not observed to reach the euphotic zone until after the growing season. Therefore it is unlikely that it plays an important role in supplying nutrients to primary producers over the canyon during the growing season.

The WW, identified by T_{\min} in the profile, was found above mUCDW. This water mass is the remnant surface water from the preceding winter season and is typically found at 50-60 m. WW has a very clear seasonal pattern (Figure 4.5), showing a well-defined and strong presence early in the season, followed by erosion by mixing with warmer water from above and below as the season progresses. The increase in solar radiation and winds, typical of the late summer season in the region, deepens the MLD, further mixing AASW with the WW below. As the latter, saltier water mass is slowly eroded, together with the decrease in freshwater input later in the season due to the

reduction in sea ice meltwater, a marked increase in the overall salinity of surface water is observed.

4.5.1.2 Phytoplankton seasonal dynamics

In the WAP, chlorophyll-*a* variability has been correlated with local physical forcing such as wind, water column stability and sea ice [Saba *et al.*, 2014]. The relationship between sea ice dynamics and biological productivity is complex. While decreasing sea ice cover can remove the shading effect of ice resulting in higher productivity, as seen in the southern region of the WAP [Montes-Hugo *et al.*, 2009; Saba *et al.*, 2014]. At the same time the decrease in fresh water input from melting sea ice will result in lower stratification and likely deeper MLDs, which should result in decreased primary production resulting from decreasing average light levels [Vernet *et al.*, 2008].

The high variability in the timing of the sea ice retreat [Stammerjohn *et al.*, 2008] matches the high variability seen in the MLD (y-axis, Figure 4.3) in late December. Shallower MLDs in the early growing season show both increased stability (Figure 4.4) and decreased salinity (Figure 4.3d). They have been associated with low wind speeds over weekly timescales [Moline, 1998; Moline and Prezelin, 1996], freshwater input from glacial and sea ice melt [Meredith *et al.*, 2008] and surface warming from incoming solar energy. The input of fresh water from glacial and sea ice melting shoals the MLD, increases the stability of the water column [Garibotti *et al.*, 2003a] and restricts deep mixing. This creates a stable upper water column in which phytoplankton cells are

allowed to remain in a favorable light regime [Garibotti *et al.*, 2003a; Vernet *et al.*, 2008]. In addition, the canyon's proximity to land shelters the canyon head from storms and strong winds seen offshore [Hofmann *et al.*, 1996], helping to maintain the observed shallow and stable MLD. Modeling work by Mitchell and Holm-Hansen [1991] concluded that intense phytoplankton blooms develop when MLD is shallower than 25 m, there is no limitation by nutrients and specific loss rate is $\sim 0.3\text{--}0.35\text{ day}^{-1}$, with grazing and respiration comprising over 2/3 of this loss. Although we do not have direct measurements of nutrients or loss rates at the same time as the glider profiles, our MLD and chlorophyll data match this model, with high concentrations of chlorophyll observed in MLD of 25-30 m or shallower and declining when the MLD is deeper. Note that there was a decrease in ML averaged chlorophyll when MLD shoals to values close to 10 m (Figure 4.7), suggesting some photoinhibition processes due to high light or light limitation by self-shading [Moline *et al.*, 1996].

The mechanisms driving the chlorophyll decrease later in the growing season remain an open question. Data show that decreases in ML averaged chl-*a* are accompanied by a deepening of the ML (Figure 4.3 and Figure 4.7). Decrease in freshwater input together with increased vertical mixing from wind forcing causes MLD to deepen and water stability to decrease. Another contributor to this decreased water column stability is the warming of WW by vertical mixing with intruding mUCDW from below. The deepening of the ML can decrease the ML averaged chl-*a* concentrations by diluting a high concentration of phytoplankton over a larger depth interval; this idea is also supported by the increase in ML integrated chl-*a* as MLD deepens (red line; Figure

4.7a), indicating there are phytoplankton below the MLD. While the deepening of the ML alone could drive down the ML averaged chl-*a* concentrations as it also decreases the mean light levels required for phytoplankton photosynthesis [Mitchell and Holm-Hansen, 1991], other factors, such as nutrient limitation and grazing, can also play a role in this decrease and must be discussed. Although gliders do not provide *in situ* measurements of the nutrient concentrations in the water column, an inspection of historical nutrient data from the LTER Station E (6.5 km NE of the sampled area) shows that no macronutrient limitation is observed throughout the season [Ducklow *et al.*, 2012]. The scarce micronutrient (trace metal) studies in the region make it difficult to evaluate the micronutrient limitation question, especially regarding iron deficiency after a bloom. Iron is known to be a limiting factor controlling primary productivity in the Southern Ocean, mainly due to the lack of efficient supply mechanisms [Boyd *et al.*, 2012]. However recent studies have shown that regions in close proximity to the coast in Antarctica, such as canyon heads, are not iron limited, and that in certain parts of the WAP there is enough iron to allow the potential utilization of all macronutrients available [Annett *et al.*, 2015]. Surface dissolved Fe:PO₄ ratios measured at Station E were always above 1.1 mmol mol⁻¹, much higher than cellular Fe:P ~0.2 mmol mol⁻¹ measured in Fe-limited Southern Ocean waters [Twining and Baines, 2013]. In addition, dissolved Fe was always >0.5 nmol/kg (Fig. 3), higher than dissolved Fe concentrations ~0.1 nmol kg⁻¹ typical of Fe-limited waters [Sedwick *et al.*, 2008], further supporting our inference that Fe is not limiting phytoplankton production at the head of Palmer Canyon. Increases in surface dissolved Fe concentrations at Station E (Figure 4.3) are

concurrent with the deepening of the ML, indicating a potential source of iron to the surface waters. The presence of WW, acting as a physical barrier between the AASW and mUCDW implies that this Fe source is likely related to vertical mixing from shallow sediments or lateral advection of surface inputs such as glacial meltwater. Losses by grazing are likely a contributing cause of chl-*a* decline as canyons are known to aggregate zooplankton prey for the apex predators [Bernard and Steinberg, 2013], however, we do not have concurrent zooplankton data to address this question.

The timing of a secondary shoaling of the MLD in late February/early March is matched with a freshening of the ML and a small increase in water column stability. The rising air temperatures in the summer months drive the increased fresh, glacial meltwater input onto the surface coastal waters. Concurrent with this, a secondary peak in chl-*a* is observed, consistent with previous work by Moline and Prezelin [1996], and a reduction of dissolved Fe to intermediate values, presumably a result of decreased supply from below and increased Fe removal in association with the chl-*a* increase, balancing the increased supply of Fe from glacial meltwater.

4.5.2 Palmer Deep cross-canyon spatial analysis

While most phytoplankton studies in the WAP canyons have focused on the temporal (seasonal and inter-annual) variability [Kavanaugh *et al.*, 2015; Moline and Prezelin, 1996], little is known about what is driving the high small-scale spatial variability observed in the foraging behavior of penguins [Oliver *et al.*, 2013]. Spatial differences in phytoplankton are also likely to occur as a cyclonic eddy feature is

expected to dominate the upper water column circulation over the canyon and to aggregate small non-migratory species at the head of canyons, particularly at the downstream side of the canyon [Allen *et al.*, 2001].

Preliminary analysis of CODAR High Frequency Radar (HFR) data at PD [Kohut *et al.*, 2014a], which provides surface maps of ocean currents, shows on average for the months of January and February, a strong Northeastward (onshore) current towards the Bismarck Strait that crosses the southern region of this study, with average speeds an order of magnitude faster than in the flow that crosses the northern region. On the other hand, although a less prominent feature, a weaker Southeastward (offshore) coastal current crosses the northern flank of the transect. Initial analysis of the mean current standard deviation shows higher variability in the flow that crosses the southern region [Todoroff *et al.*, 2015]. This highly energetic and variable flow can explain the increased variability in the water properties in that region as seen in Figure 4.5 and Figure 4.6. This variability decreases with the temporal evolution of the water masses, with surface water becoming warmer and saltier and with WW being warmed both from above and below. Main spatial differences in water properties can be found at depth, with the northern region showing overall colder temperatures, as evident by the presence of WW until later in the season. The southern flank shows intrusions of warm, salty, deep water likely from the onshore current forcing the mUCDW onto the shelf that then mixes upward, weakening the signal of WW from below (Figure 4.8). The northern flank shows a strong presence of winter water and a fresh water lens that comes from glacial and sea ice melt brought by the coastal current. The differences in

magnitude and the variability of the currents between the two regions are likely to contribute to the stability of the MLD dynamics on local scales. With less energetic currents, the water in the northern region is likely to show higher residence times, ideal for local primary production to occur. On the other hand, southern region mean currents show higher variability and magnitude that can potentially impede local production to fully thrive as the timescales of the mean currents are shorter than the doubling time of Antarctic phytoplankton.

Another factor known to control primary production is the availability of iron [Twining and Baines, 2013]. Although there are several potential sources of iron to surface waters (glacial melt, sea-ice melt, seawater interaction with shallow sediments, atmospheric input and deep water upwelling), glacial meltwater has been identified as one of the most important [Dierssen *et al.*, 2002; Hawkings *et al.*, 2014], by its volume flux and because of the continuous yet variable supply during the growing season [Meredith *et al.*, 2008]. The close proximity of canyon head systems on the WAP to the coast where glaciers are prominent features, may also contribute favorably to the increased production seen in the canyon as the increased glacial meltwater input (and pushed by the coastal current) contributes to increased water column stability and is a potential source of iron to the system [Alderkamp *et al.*, 2015; Annett *et al.*, 2015; Arrigo *et al.*, 2015]. While mUCDW upwelling enriched with iron from sediments has been proposed as a potential source of iron to coastal WAP regions [Annett *et al.*, 2015], at Ryder Bay (340 km south of Palmer Deep) it was found to account for very little of the iron input due to the highly stratified waters during the growth season. It is however

identified as an important source of iron over annual or longer time-scales. The same seems true for the overall nutrient budget. Glider observations during the austral spring and summer show no evidence of this mUCDW upwelling reaching surface waters during the growth season as there is a clear layer of WW physically separating surface waters from the deep waters below while the bloom is present. However, this water mass is slowly warming throughout the season due to vertical mixing from above and below, contributing to the decreased water column stability. While there is no evidence of the surface waters at PD being limited by macro- or micronutrients at any point, a drawdown in the nutrient pool is apparent while the bloom is thriving [Ducklow *et al.*, 2012]. After the growth season, as the stratification weakens, mUCDW intrusions from below will replenish the surface water with both micro- and macronutrients required for the following year's spring phytoplankton bloom.

4.6 Conclusions

Understanding the spatial and temporal variability of phytoplankton is important, especially to assess the dynamics of higher trophic levels as they are dependent on primary producers for food source. The high-resolution capabilities of gliders allow sampling and coverage at appropriate scales to evaluate phytoplankton dynamics. Using the 6-year glider observations over PD we were able to describe the fine temporal and spatial variability of the phytoplankton seasonal cycle and relate it to its main physical drivers, namely MLD and water stability. Although interannual variability was observed in the data, the shoaling of the MLD in late spring matching

increased chlorophyll concentration was a pattern observed in all years sampled, (2010-2015), as more light becomes available to the phytoplankton community. Following this period, a summer (February) deepening of the MLD was accompanied by decreased chlorophyll.

Observations showed that MLD dynamics and chlorophyll variability were tightly coupled in both time and space. Spatial variability was evaluated by glider transects across the head of the canyon. While MLD dynamics was similar in the northern and southern canyon regions, the physical setting observed in different regions of the canyon, such as water column stratification and water masses present, explain some of the observed chlorophyll variability. Preliminary analysis of surface currents provides an insight on what could be driving some of the observed differences in water column structure that are key for phytoplankton development. The northern region with increased chlorophyll showed a more coastal influence, with increased freshwater input, slower currents and increased stratification, while the southern region with lower chlorophyll showed more influence from offshore with faster currents and more intrusions of mUCDW from below. However, further sampling and analysis is necessary to evaluate whether water column physics is driving the spatial differences in chlorophyll concentrations alone or if iron supply plays a role in the system at any point in the growth season.

4.7 Acknowledgements

We thank the two anonymous reviewers whose suggestions helped improve and clarify this manuscript. The research was supported by the National Science Foundation grants ANT- 0823101 (Palmer-LTER), ANT-1327248 and ANT-1326541 (CONVERGE) and ANT-1142250 (iron WAP). Filipa Carvalho was funded by a Portuguese doctoral fellowship from Fundação para a Ciência e Tecnologia (DFRH - SFRH/BD/72705/2010).

**Chapter 5: Mapping *in situ* chlorophyll variable
fluorescence using autonomous underwater gliders**

5.1 Abstract

Environmental factors, nutrient and light availability, regulate phytoplankton physiology and photosynthesis in the ocean. These processes are poorly sampled using traditional shipboard techniques over relevant scales. The integration of a Fluorescence Induction and Relaxation (FIRe) sensor in a Slocum glider allows autonomous high-resolution and vertically-resolved measurements of physiological variables together with physical oceanographic data. Evaluating *in situ* variable fluorescence measurements under ambient light allows a better understanding of the physical controls of primary production (PP) used in PP models. The approach allows the evaluation of light stress, nutrient limitation or a combination of both as well as the role of vertical mixing in phytoplankton dynamics and the underlying physiology.

5.2 Introduction

Phytoplankton are the basal component of all aquatic ecosystems and their photosynthetic activity and production of organic carbon not only supports highly productive ocean/lake ecosystems but also plays a significant role in shaping the chemistry of the Earth. Phytoplankton populations are highly dynamic with high turnover rates driven by a suite of environmental factors (light, macronutrients, micronutrients, grazing, temperature, etc.) [Falkowski and Raven, 2007]. Given the remote/harsh locations where phytoplankton thrive, their small size and the rapid changes in the environmental conditions in the ocean, it has been difficult to evaluate spatial distributions of phytoplankton biomass and their physiological state for

sustained periods of time using traditional sampling approaches. Chlorophyll fluorometers have been widely adopted by the oceanographic community and are used for sensitive non-intrusive estimates of phytoplankton biomass [Lorenzen, 1966]. However, conventional fluorometers do not provide insight into the physiological state of phytoplankton or photosynthetic rates.

Phytoplankton photophysiology can be assessed using variable fluorescence techniques [Falkowski *et al.*, 2004]. The pump-and-probe technique [Kolber *et al.*, 1988], the Fast Repetition Rate (FRR) fluorometers [Kolber *et al.*, 1998], the Fluorescence Induction and Relaxation (FIRe) sensors [Gorbunov and Falkowski, 2004] are some of the traditional sampling methods used to study phytoplankton physiology and evaluate potential controls on ocean primary production. Variable fluorescence signals provide a sensitive tool to measure the optical cross-sections for photosynthesis, the quantum yields and rates of photosynthetic electron transfer in phytoplankton [Falkowski *et al.*, 2004]. As the photophysiology of phytoplankton is highly sensitive to changes in the environment, variable fluorescence measurements have allowed the oceanographic community to study the underlying mechanisms and factors regulating the physiological state and growth of phytoplankton [Suggett *et al.*, 2010]. Variable fluorescence is rapidly becoming a fundamental method used in oceanography; however the application of this technology has been largely limited to when humans are present (on ships or diving), which limits when, where and how much data is collected.

Recent years have seen the rapid development of autonomous underwater vehicles (AUV) for conducting oceanographic research [Griffiths *et al.*, 2007]. Some

classes of the AUVs (buoyancy vehicles) can conduct sustained missions (weeks to year) [Rudnick, 2016] and are capable of carrying a wide range of sensors [Schofield *et al.*, 2015a]. Here we report on the development of a variable fluorescence sensor for an autonomous buoyancy vehicle offering the potential for collecting phytoplankton photophysiology data remotely. This technology was demonstrated during a series of deployments [Carvalho *et al.*, 2016a; Haskins and Schofield, 2015] in the harsh waters off the West Antarctica Peninsula, a region which is experiencing a rapid environmental change [Schofield *et al.*, 2010].

5.3 Autonomous Platform and Sensor integration

5.3.1 Utility of Slocum gliders

There is a critical need to collect regional data (100s-1000s of kilometers), which has been historically collected using research vessels and satellites. Ship-based sampling allows for a wide range of measurements to be made throughout the water column however it represents an extremely expensive (money, time and people) approach. In contrast, satellites can provide regional to global coverage for a wide range of ocean properties (heat, salinity, circulation) for sustained periods of time. Despite these strengths, satellites can only sample the ocean's surface and thus are not well suited for characterizing subsurface and seafloor processes. Therefore, there is a need for integrating new systems into oceanographic instruments that are capable of cost effectively maintaining a sustained subsurface presence that can collect a wide diversity of data over 1000's of kilometers.

Teledyne Webb Research (TWR) Slocum electric gliders are a robust technology capable of mapping properties within the upper water column [Schofield *et al.*, 2007] that are increasingly filling mesoscale sampling needs for ocean science. Gliders maneuver through the ocean at a forward speed of 20 – 30 cm/s in a sawtooth-shaped gliding trajectory, deriving its forward propulsion by means of a buoyancy change and steering by means of a tail fin rudder. Pitch is regulated by shifting batteries back and forth within the glider. An altimeter and depth sensor enable preprogrammed sampling of depth ranges from ~10 meters to 1500 meters. Sensors carried by the gliders continuously record data during the glider descents/ascents, and a typical mission can collect thousands of profiles of data. This allows the glider to collect high-resolution data in both time and space.

5.3.2 Integrating variable fluorescence measurements into a glider

Bio-optical measurements of photosynthetic rates and physiological characteristics of phytoplankton are based on the use of variable fluorescence techniques, including the Fluorescence Induction and Relaxation (FIRe) technique. FIRe measurements are sensitive, fast, non-destructive, and can be done in real-time and *in situ*. The FIRe technique records a comprehensive suite of photosynthetic and physiological characteristics of the organism [Gorbunov and Falkowski, 2004]. The measured parameters characterize the excitonic energy transfer in photosynthetic light-harvesting antennae, photochemical processes in Photosystem II (PSII), and the photosynthetic electron transport to carbon fixation (Figure 5.1). These parameters

(Figure 5.1, Table 5.1) are used to quantify the phytoplankton-specific photosynthetic performance in natural assemblages in aquatic ecosystems [Schofield *et al.*, 2007].

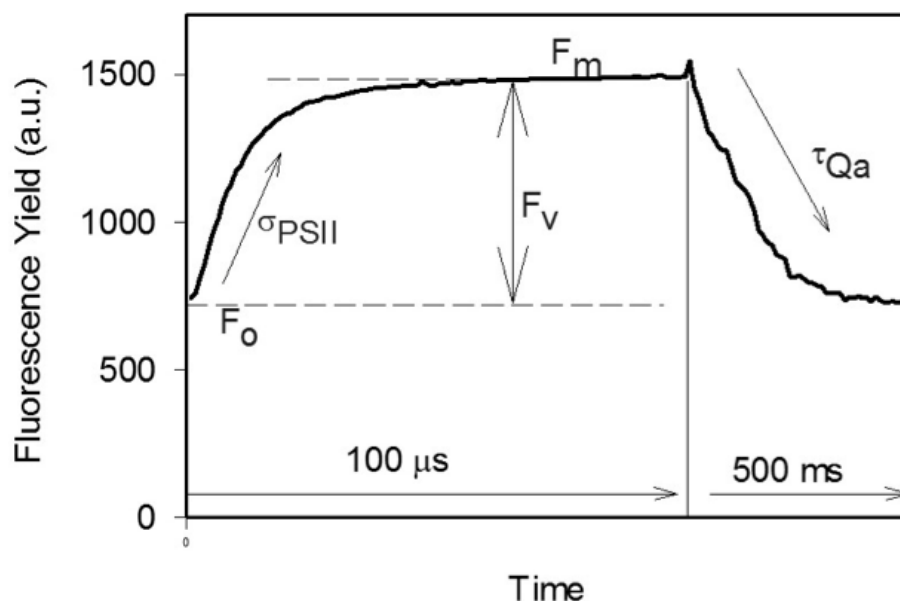


Figure 5.1: An example of Fv/Fm profile. The quantum yield of photochemistry in PSII (i.e., photosynthetic efficiency) is deduced from a relative change in fluorescence yield (F_v/F_m) and the functional absorption cross-section of PSII (σ_{PSII}) - from the rate of fluorescence rise during fluorescence induction (100 μ s phase). The subsequent relaxation in fluorescence yield on millisecond time scale reflects the rates of photosynthetic electron transport down to carbon fixation. Minimum (F_0) and maximum (F_m) fluorescence yields corresponding to the states with open and closed reaction centers of PSII, respectively.

Table 5.1: Notation of important Fv/Fm variables

Abr.	Description	Abr.	Description
σ_{PSII}	Functional absorption cross section of PSII (\AA^2) in a dark-adapted state	σ_{PSII}'	Functional absorption cross section of PSII in a light-adapted state (\AA^2)
F_0, F_m	Minimum and maximum yields of Chl <i>a</i> fluorescence (arbitrary units)	F_0', F', F_m'	Minimum, steady-state, and maximum yields of Chl <i>a</i> fluorescence measured under ambient light (arbitrary units)
F_v	Variable fluorescence ($=F_m - F_0$)	F_v'	Variable fluorescence measured under ambient light ($=F_m' - F_0'$)
F_v/F_m	Maximum quantum yield of photochemistry in PSII, measured in a dark-adapted state (dimensionless)	$\Delta F'/F_m'$	Quantum yield of photochemistry in PSII, measured under ambient light [$= (F_m' - F')/F_m'$] (dimensionless)
E_k	Light-saturation parameter ($\mu\text{mol quanta m}^{-2} \text{s}^{-1}$)	$\Delta F'$	Change in the fluorescence yield measured under ambient light ($=F_m' - F'$)
'	Prime indicates that measurements are collected under ambient light	$\Delta F'/F_v'$	Coefficient of photochemical quenching characterizing the fraction of open reaction centers in a light-adapted state

Fluorescence signals are excited by flashes from blue (450 nm) light emitting diodes (LEDs). The computer controlled LED driver delivers pulses with varied duration from 0.5 μ s to 50 ms, which ensures fast saturation of PSII within a single photosynthetic turnover (<100 μ s). The fluorescence signal, isolated by a red (680 nm) interference filter, is detected by a sensitive avalanche photodiode module [Gorbunov and Falkowski, 2004].

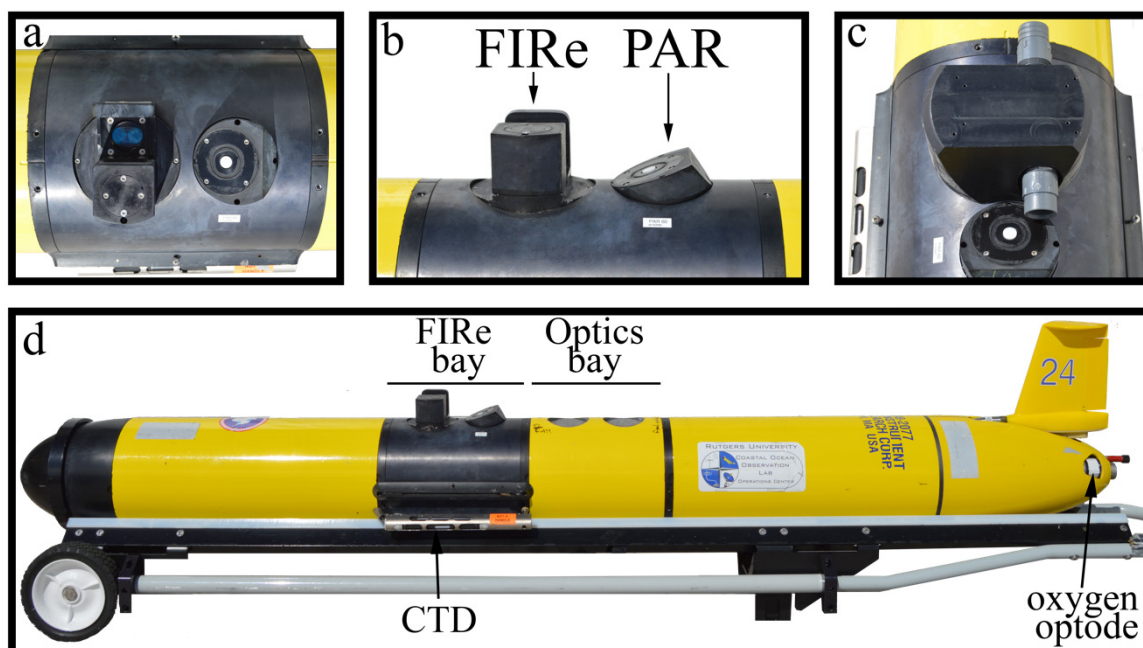


Figure 5.2: Top (a) and side (b) view of the Fluorescence Induction and Relaxation (FIRe) and Photosynthetic Active Radiation (PAR) sensors integrated into a Slocum glider FIRe bay (black section). (c) Optional add-on cap used to evaluate physiological stress in a dark-adapted state. (d) Extended Slocum glider with double science bay configuration with FIRe bay in front and Optics bay with Wetlab ECO pucks (measuring chlorophyll fluorescence, backscatter and colored dissolved organic matter, CDOM) in the aft, Conductivity-Temperature Depth (CTD) sensor and oxygen optode. The glider is shown without its two lateral wings that connect to the black FIRe bay.

In partnership with TWR and Satlantic Inc., a FIRe sensor was integrated into a Slocum glider science payload bay (Figure 5.2), from now on referred to as FIRe glider.

Merging these two platforms together allows for high-resolution continuous mapping of phytoplankton physiological responses to variable light/nutrient regimes in the water column.

5.3.3 Other sensors pairings

A Photosynthetically Active Radiation (PAR) sensor is also present in the glider science bay and it is critical to the interpretation of the FIRE data. An optional double science bay pairing with a WET Labs Inc. Environmental Characterization Optics (ECO) pucks, measuring chlorophyll fluorescence, backscatter at several wavelengths and colored dissolved organic matter (CDOM) fluorescence, permits further analyses involving particle size and community composition. The standard Seabird Conductivity-Temperature-Depth (CTD) package present in all gliders allows a high-resolution characterization of the physical setting, which provides critical data to relate physiological responses to water column stability and mixed layer depth [Carvalho *et al.*, 2017].

5.4 Reference Profile Calibration

Like the bench-top FIRE instrument, the FIRE glider sensor requires a reference excitation profile, which is used to normalize the collected fluorescence intensities and to deduce fluorescence yields. To acquire this reference file, a sample fluorescent dye (e.g., Rose Bengal) is measured and the profile is saved as a reference file. When processing the data collected during the deployment, the FIRE processing program will

use this profile to calculate fluorescence yields. This reference profile is updated every 6 to 12 months.

5.5 Post-deployment processing

5.5.1 Blanks

A “blank” is the background signal recorded from the sample without phytoplankton. It includes a small amount of fluorescence from dissolved organic matter (DOM) and phytoplankton degradation products dissolved in the water.

Although in FRe sensors, the magnitude and variability of the “blank” is usually small compared to chlorophyll fluorescence signals from phytoplankton [Bibby *et al.*, 2008], blanks should be routinely collected and subtracted from the fluorescence signals. When fluorescence signals are much larger than the blank, the blank correction can be neglected. However, if the blanks are high (e.g. in DOM-rich waters) the blank correction may become critical for accurate retrievals of photosynthetic parameters [Bibby *et al.*, 2008].

While it is impossible to measure appropriate *in situ* blanks concurrently with the FRe glider measurements during deployment, *in situ* discrete water samples are collected and analyzed in the lab bench before and after deployment. Measurements of blank are made on filtered seawater collected from at least the surface and from a depth below the deep chlorophyll maximum (DCM) and these blank values are subtracted from the fluorescence profiles from the surface to the DCM and below the DCM, respectively.

5.5.2 Functional absorption cross-sections (σ_{PSII})

To convert the measured σ_{PSII} (collected in arbitrary units) into absolute units (\AA^2), a correction coefficient must be determined by cross-calibrating the FIRE glider sensor against a “standard” calibrated bench-top FIRE instrument.

5.5.3 Determination of chlorophyll concentrations

As for any fluorometer, the FIRE glider records fluorescence yields in arbitrary units. For these data to be used to assess phytoplankton biomass, maximum fluorescence yields (F_m) needs to be calibrated against standard chemical measurements of chlorophyll concentration ($\mu\text{g L}^{-1}$), a proxy of phytoplankton biomass. Discrete water samples are collected and run on both systems (glider and bench-top) before deployment and after recovery. Note that this can be done in parallel with the blanks measurements. Water samples are filtered onto 25 mm Whatman GF/F filters and extracted using 90% acetone following the fluorometric method for phytoplankton chlorophyll determination [*Yentsch and Menzel, 1963*]. As F_m fluorescence yield is much less susceptible to variations in phytoplankton physiological state than F_o , the best linear correlation is observed between chlorophyll concentration and maximum fluorescence yield.

5.6 Hardware configurations

Variable fluorescence measurements under ambient light provide information about the actual rates of photosynthetic electron transport (ETR) as a function of PAR. The ETRs normalized per PSII reaction center are calculated as described in [Gorbunov *et al.*, 2000; Gorbunov *et al.*, 2001]. The FRe retrievals of the functional absorption cross sections allow us to deduce ETRs in absolute units – electrons per second normalized per PSII reaction center [Gorbunov *et al.*, 2000]. These irradiance dependencies of photosynthetic rates in combination with vertical profiles of *in situ* PAR can be used to reconstruct vertical profiles of photosynthetic rates over the euphotic zone. Also, these measurements provide the background to model the rates of primary production in the water column [Falkowski *et al.*, 2004].

Depending on the research question, two different configurations can be used in the FRe glider. One of the biggest advantages of the FRe integration on a glider is the ability to make measurements under ambient light. An optional cap can be used to cover the optical chamber, allowing one to conduct measurements in dark. Such measurements are more informative for assessment of the impact of nutrient stress on phytoplankton physiology [6] (Figure 5.3b). The physiological characteristics available under these two configurations are presented in Figure 5.3 and described in Table 5.1.

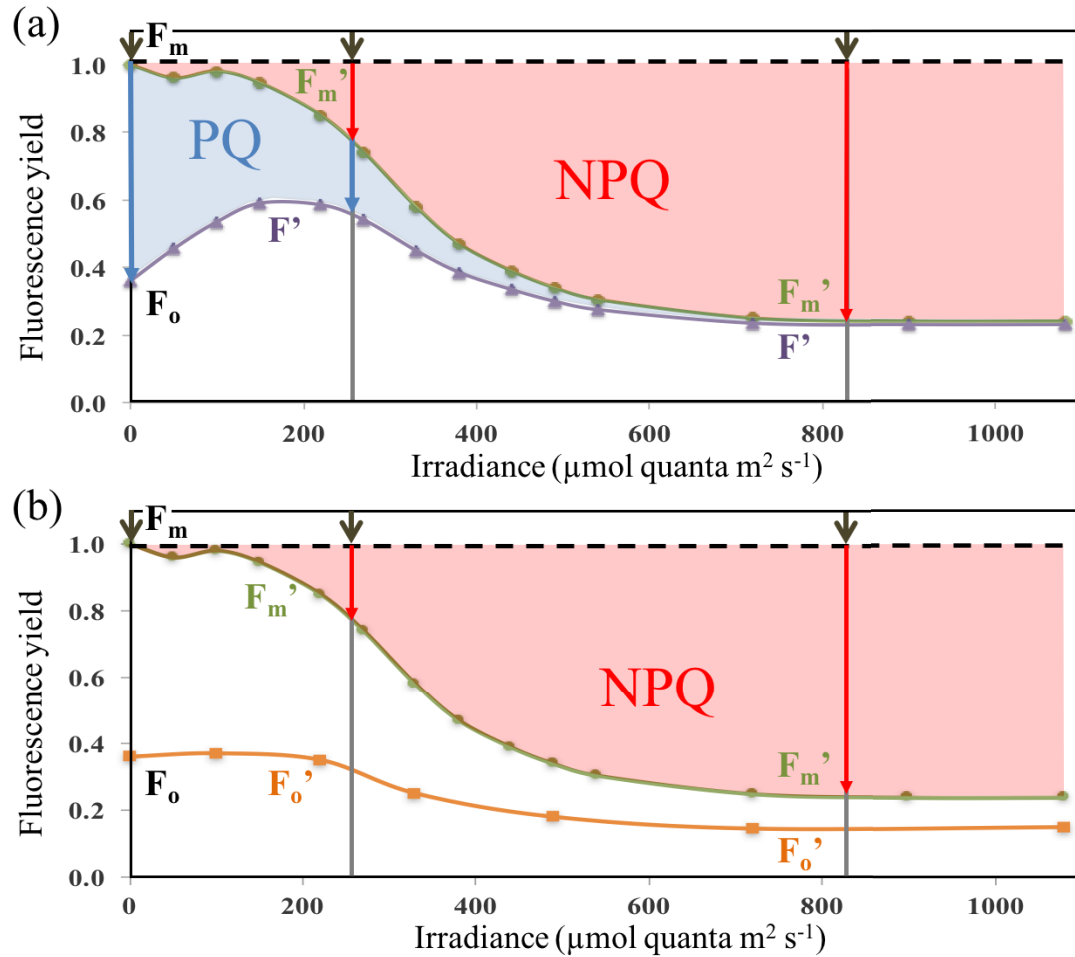


Figure 5.3: Example of irradiance dependence of chlorophyll fluorescence yields recorded in two different FRe glider configurations. Measurements in: (a) light-adapted state, i.e., the optical chamber with cap “off” and (b) dark-adapted state, i.e., the optical chamber with cap “on”. F_0 and F_m are minimum (open reaction centers) and maximum (closed reaction centers) fluorescence yields measured in dark-adapted cells. F_0' and F_m' are the minimum and maximum fluorescence yields in a light adapted state. F' is the actual fluorescence yield measured under ambient light. PQ and NPQ are photochemical quenching and non-photochemical quenching, respectively. Top grey arrows indicate example irradiances and its corresponding fraction of NPQ and PQ.

While measurements in a dark-adapted state (cap “on”) are crucial data to evaluate nutrient stress [Falkowski and Kolber, 1995], flying the glider with the cap “on” hinders the ability to evaluate light effects during that deployment. When interested in evaluating environmental stresses in general, with timescales of 1-2 days, the cap “off” configuration provides more flexibility (Figure 5.3) where the night profiles can be used

as the dark-adapted state measurements. In this situation, nutrient stress can be assessed using nighttime profiles only and both PQ and NPQ can be evaluated throughout the deployment.

5.7 Mission designs

Fluorescence yields measured in a dark chamber provide changes in maximal (F_m') and minimal (F_o') fluorescence in the water column over a diel cycle [Runcie and Riddle, 2011]. These diel cycles allows for a better understanding of the light effect on phytoplankton physiology by isolating the effect of supra-irradiance during peak daytime hours. Two FRe glider missions have been designed to evaluate physiological responses at different temporal and spatial scales, as follows.

5.7.1 The “drift mission”

Phytoplankton community structure features such as cell size and taxonomy influence photosynthetic rates and therefore variable fluorescence signals [Suggett *et al.*, 2009]. When evaluating the temporal pattern (e.g. diel cycles) in the photosynthetic efficiency of a phytoplankton community *in situ*, it is important to make sure that the measurements are constrained to the same phytoplankton community. The best way to accomplish this *in situ* is to use a Lagrangian approach and follow the same water mass over time. A 100 m glider cycle takes around 20 minutes to finish a “yo” (dive and climb). Every hour, a corkscrew dive and climb (fin set all the way to one side) and drift

at the surface the remaining time between dives. This allows the collection of approximately 24 profiles to characterize a diel cycle.

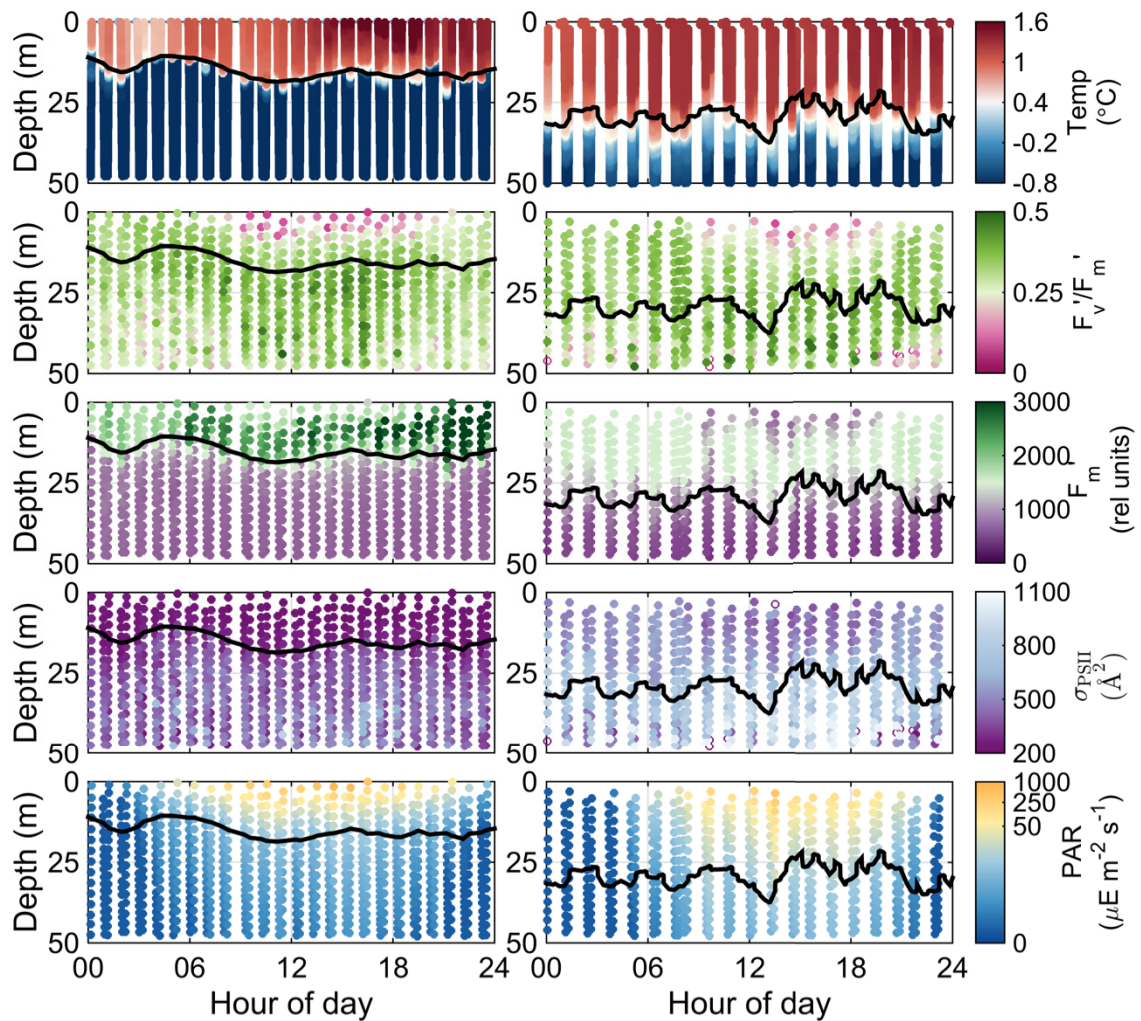


Figure 5.4: Example of diel cycles collected during the drift mission for shallow (left panels) and deeper (right panels) mixing regimes. The depth of the mixed layer is shown with a black line. Gaps in data show times where glider was drifting at the surface. One profile was collected every hour. Effects of high irradiance periods (hours 10-16) shown in yellow in the Photosynthetically Active Radiation panels (E) are evident by the low values seen in F_v'/F_m' (B, photosynthetic efficiency), F_m' (C, proxy for biomass) and σ_{PSII} (D, functional absorption cross-section). This is evidence of Non-Photochemical Quenching (NPQ), with the deepest penetration occurring during peak irradiance (hour 13-14). A warming of the upper ocean (A, Temperature) is also seen during the highest irradiances.

Stratification, Mixed Layer Depth (MLD) and rates of vertical mixing have been extensively identified as controls on primary productions and phytoplankton dynamics [Carvalho *et al.*, 2016b; Lewis *et al.*, 1984; MacIntyre *et al.*, 2000]. Phytoplankton acclimate to light levels averaged over the MLD [Lewis *et al.*, 1984]. A relatively stable light environment as a result of a shallow MLD allows phytoplankton to photoacclimate on timescales of 1-2 days [Schofield *et al.*, 1995]. During intense mixing events, dim-light adapted phytoplankton may be brought towards the surface where they are exposed to supra-optimal irradiances and identified by a decrease in both F_m and F_v/F_m .

Photoadaptive parameters respond at different rates to changes in irradiance. Photoinhibition can be assessed in the fluorescence signal on time-scales of seconds to minutes while it takes several hours for the photosynthetic capacity to be compromised [Lewis *et al.*, 1984]. The collection of high-resolution photophysiology parameters over a diel cycle permits the evaluation of Non-photochemical quenching (NPQ) under supra-irradiances as seen by a decrease of F_v'/F_m' , F_m' and σ_{PSII} (Figure 5.4).

5.7.2 The “station keeping mission”

Often, the irradiance regime experienced by phytoplankton is a result of the interaction between incident radiation, turbulent mixing and variations in water column vertical structure (changes in water column stability and MLD due to varying wind stress and water mass types as well as heat from insolation) [Neale *et al.*, 2003]. For a given temperature and nutrient status, phytoplankton have means to regulate photosynthetic rates based on the light field they are exposed to by alterations in constituents of the

photosynthetic apparatus. As an example, the chlorophyll content is usually higher when the cells have been growing under low light [Lewis *et al.*, 1984; MacIntyre *et al.*, 2000]. It is then informative to analyze phytoplankton physiology in the context of the physical setting they are exposed to.

The ability of the FIRE glider to collect, at high resolution, physiological data together with physical oceanographic parameters allows further analyses on the physical drivers of primary production. Gliders also offer an advantage compared to other oceanographic platforms in providing more flexibility in how, when and where they sample. It is sometimes beneficial to use gliders as virtual moorings when the scientific question involves a spatial comparison. An Eulerian approach allows data collection that isolates the temporal signal by removing space from the equation. Deploying the FIRE glider in station keeping (virtual mooring) mode in locations with different physical settings one can infer how environmental variables affect phytoplankton physiology (Figure 5.5).

A concern regarding the FIRE glider deployment is its energy consumption. The FIRE sensor requires 6W of power, roughly 9 times more energy than a regular Wetlabs fluorometer. This reduces the mission time considerably and so, the FIRE sampling duty cycle needs to be optimized to maximize the data collection to better address the science question. Contrary to the drift mission, in the station-keeping mission the glider is flying and collecting physical data continuously. A FIRE “yo” every hour or so is a good compromise between the collection of high-resolution diel cycles of phytoplankton physiology and the mission longevity.

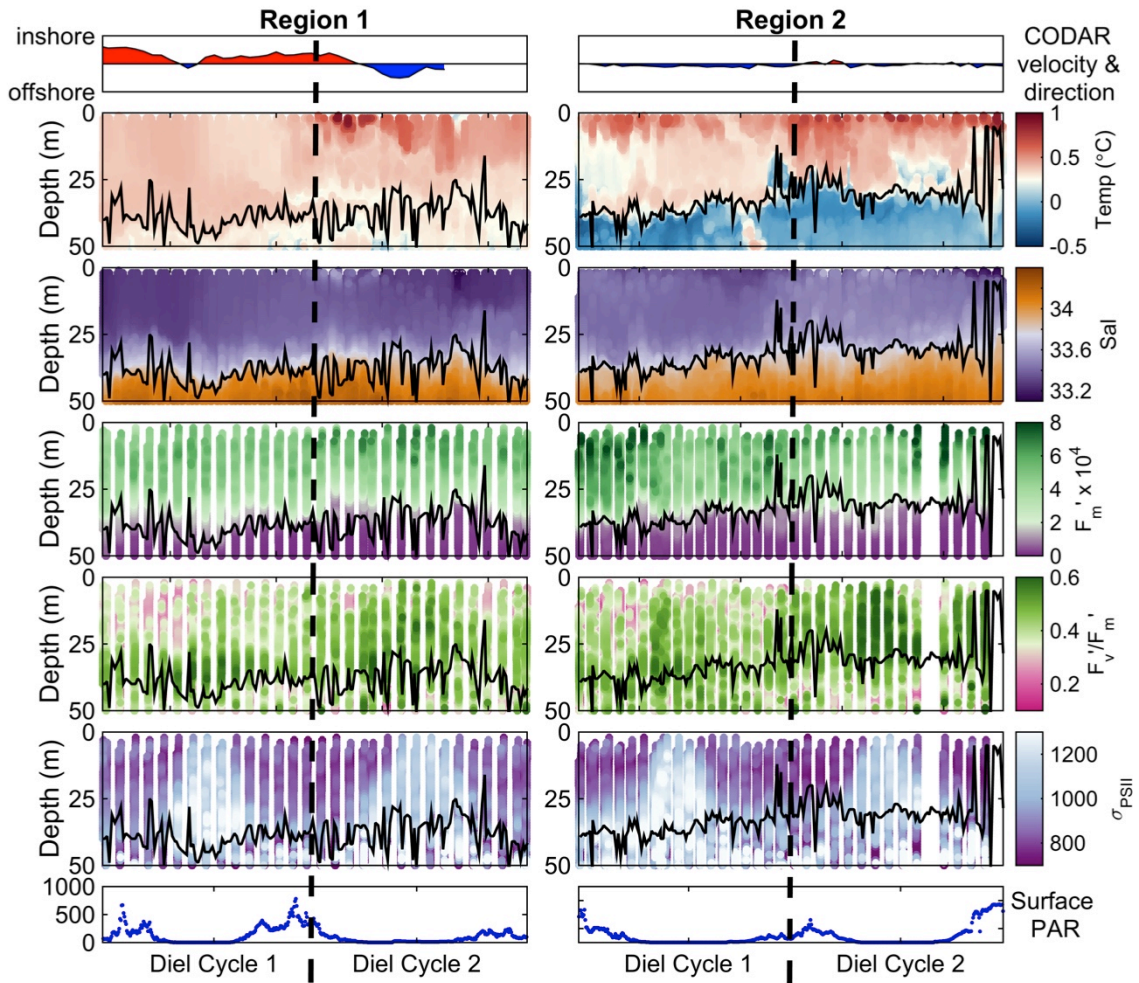


Figure 5.5: Two diel cycles (as outlined in the surface PAR, G) collected in two regions with different oceanographic conditions. Direction and magnitude of the dominant surface currents (A, from HF Radars) are in part responsible for changes in the vertical structure of the water column as demonstrated by the temperature (B) and salinity (C) panels and the depth of the ML (black line). Remaining rows report FIRE measurements - F_m' (C, relative units), F_v'/F_m' (D, dimensionless) and σ_{PSII} (E, functional absorption cross-section of PSII, \AA^2). While the irradiance effect is not very clear in the noisy F_v'/F_m' data (likely due to lower biomass), a depth-dependent diel signal is present in σ_{PSII} (showing high values during nighttime and a decrease during daytime). By analyzing high-resolution photophysiology data in context of our concurrent physical data we can better understand and evaluate the role of mixing and the water column vertical structure in phytoplankton primary production.

5.8 Photoacclimation mechanisms evaluation

To cope with high light-induced stresses (i.e. to optimize light absorption under low light conditions or even to reduce total photon utilization under supra-optimal

irradiance) phytoplankton have developed a suite of photoadaptation mechanisms. Preliminary FIRE data have shown different photoacclimation responses resulting from different MLD dynamics (varying solar radiation exposure conditions, both time and intensity). Bio-optical models [Jassby and Platt, 1976; Webb et al., 1974] have described the relationship between photosynthesis and irradiance. When cells photoacclimate, they adjust their photosynthetic machinery to operate at the highest quantum yield possible that allows for the maximal rate of photosynthesis. This occurs at the inflection point in the photosynthesis irradiance curve, the light saturation parameter (E_k) [Dubinsky and Schofield, 2009]. The hyperbolic tangent model has become one of the most widely used models for predicting photosynthetic rates in natural phytoplankton assemblages. The photosynthetic rates (P) as a function of PAR are described by the following equation [Jassby and Platt, 1976]:

$$P = P_{max} \left[\tanh \left(\frac{PAR}{E_k} \right) \right] \quad (5.1)$$

where PAR is Photosynthetically Active Radiation, P_{max} is the maximum rate achieved at saturating light, and E_k is the light saturation parameter. The quantum yield ($\Delta F'/F_m'$) is, by definition, proportional to the ratio of P to PAR :

$$\frac{\Delta F'}{F_m'} = c \frac{E_k}{PAR} \left[\tanh \left(\frac{PAR}{E_k} \right) \right] \quad (5.2)$$

where $\Delta F'/F_m'$ is the quantum yield of photochemistry in PSII, measured under ambient light and c is F_v/F_m measured in a dark-adapted state at $PAR=0$. Applying this

model to the FRe data we can estimate E_k and explore photoacclimatory responses of phytoplankton to changes in MLD dynamics regimes (Figure 5.6).

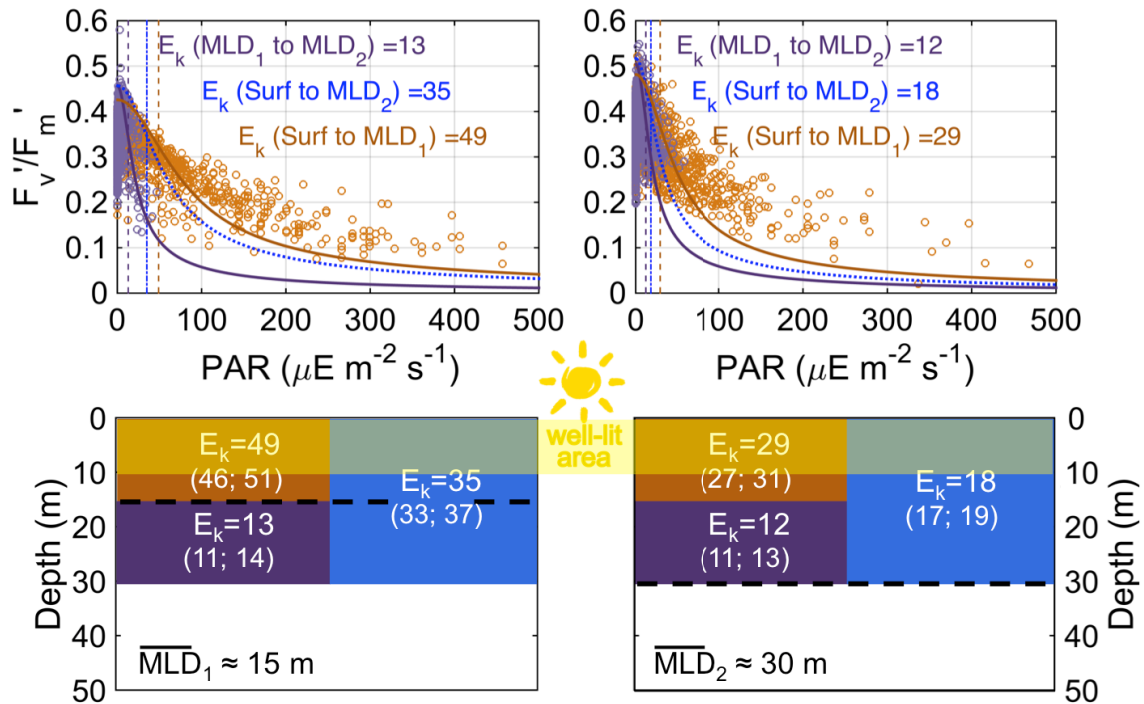


Figure 5.6: Top: Scatter plots of F_v/F_m and PAR with curve fits (Equation 5.2) for the two MLD regimes collected during the drift mission (Section 5.7.1; Figure 5.4). Left, 1: average MLD is 15 m (shallower). Right, 2: average MLD is 30 m (deeper). Three depth bins (surface to MLD₁ – orange, MLD₁ to MLD₂ – black, and surface to MLD₂ – purple) were created to evaluate potential different phytoplankton photoacclimation regimes. Light saturation parameter (E_k) for each fitting are also presented. Bottom: schematics on difference in photoacclimation regimes presented in the plots on top, evaluating E_k in relation to the MLD (black dashed line). 95% confidence intervals are presented in brackets for the E_k parameter estimation. Under a shallow MLD regime, where the light penetration (yellow layer in bottom panel) reaches closer to the bottom of the ML, there is likelihood of two potential different physiological communities (i.e., communities with different photoacclimation regimes) as evaluated by the different E_k (compare orange and purple layers). The much higher E_k seen at the surface gives an indication of phytoplankton acclimated to high irradiances while the lower E_k seen below the MLD shows low light acclimation. Under deeper MLD conditions, E_k values are much closer indicating photoacclimation is similar between the 2 layers.

Changes in E_k values provide insight on photoacclimation regimes due to a combination of the light field that phytoplankton are exposed and the mixing scales that can dominate the kinetics of primary productivity over the time-course of a day. This

method can also be useful to evaluate the role of mixing in the competition between algal species [Falkowski and Woodhead, 2013].

Underwater gliders have proven their usefulness as a robust technology providing an autonomous means to collect high-resolution ocean data. The integration of a Fluorescence Induction and Relaxation sensor in a Slocum glider allows the evaluation of phytoplankton physiology in the context of the physical conditions. It also has the added advantage of collecting *in situ* data under ambient light. Using a variable chlorophyll fluorescence method, physiological parameters can be evaluated in order to assess environmental variables controlling phytoplankton. Gliders provide an added sampling flexibility in terms of both steering and endurance, by providing an opportunity to design missions to target specific scientific goals such as assessing the progression of a phytoplankton population through time or evaluate how different physical settings drive potentially different physiological responses. The high-resolution capabilities in both time and space permit the collection of diel cycles that allow a better understanding how phytoplankton react to light levels over different timescales. Analysis of the irradiance dependencies of variable fluorescence signals provides insight into photoacclimation responses of phytoplankton to variations in vertical mixing regimes. Future adaptation of a recently developed miniaturized multi-color FRe sensor with enhanced sensitivity [Lin *et al.*, 2016] for a glider platform would also offer potential to further improve sampling resolution, as well as to monitor changes in taxonomic composition of phytoplankton communities and to assess taxa-specific physiological characteristics.

5.9 Funding

This work was supported by National Science Foundation (NSF Palmer LTER program) (grant 0823101), National Oceanographic Partnership Program (NOPP) (grant NA05OAR4601089), and NASA Ocean Biology and Biogeochemistry Program (grant NNX16AT54G). Filipa Carvalho was funded by a Portuguese doctoral fellowship from Fundação para a Ciência e Tecnologia (FCT) (grant DFRH - SFRH/BD/72705/2010) and a Teledyne Graduate Fellowship.

5.10 Acknowledgements

The authors would like to thank Rutgers field team (in particular to Nicole Couto, Nicole Waite and Mike Brown), Palmer Station personnel and ARSV Laurence M. Gould crew for support during deployments and recoveries. We would like to thank Kevin Wyman for his comments on the manuscript.

Chapter 6: Conclusions

Coastal waters of the West Antarctic Peninsula are a highly productive ecosystem [Schofield *et al.*, 2010] with cross-shelf canyon systems playing a crucial role in driving increased primary production [Kavanaugh *et al.*, 2015; Schofield *et al.*, 2013] and penguin foraging locations [Fraser and Trivelpiece, 1996]. Previous studies [Prézelin *et al.*, 2000; Prézelin *et al.*, 2004; Schofield *et al.*, 2013] have linked this increased production to the upwelling of warm nutrient enriched modified Upper Circumpolar Deep Water (mUCDW), yet the exact physical mechanisms driving the physiology and composition of phytoplankton blooms in these regions are still not well understood. This dissertation integrates observations (underwater gliders, HF radars, weather data), shipboard incubation experiments and new sensor integration developments to improve the understanding of phytoplankton bloom dynamics in the productive coastal waters of the WAP.

In Chapter 2, shipboard incubation experiments were used to test the “Canyon Hypothesis”, where the upwelling of nutrient-enriched deep water was hypothesized to support the increased production seen at the canyon heads. Results from the incubation experiments suggest instead that light plays a crucial role in phytoplankton growth, with shallow MLD and stratified water columns providing a stable light environment [Mitchell and Holm-Hansen, 1991; Moline and Prézelin, 1996] for phytoplankton photoacclimate and thus, thrive [Sakshaug and Holm-Hansen, 1986; Schofield *et al.*, 1995]. Data also showed, consistent with previous observations [Annett *et al.*, 2015; Carvalho *et al.*, 2016b; Serebrennikova and Fanning, 2004], that macro- and especially micronutrients are abundant in surface waters and did not limit primary production in any of the

canyon systems tested. Mixed Layer Depths are associated with the light levels to which phytoplankton cells acclimate to [Mitchell and Holm-Hansen, 1991] and are thus an important metric in phytoplankton dynamics studies.

Chapter 3 determines an ecologically relevant MLD metric from several glider deployments around Antarctic coastal waters, where the depth of the maximum buoyancy frequency, or $\max(N^2)$ explains best the depth to which phytoplankton can be mixed in coastal Antarctica. Together with a quality index that evaluates the quality of the MLD computation, standardizing this metric will facilitate the inter-comparison among region-specific studies.

Chapter 4 examined the spatiotemporal variability of the phytoplankton spring bloom at Palmer Deep Canyon using the high-resolution dataset of 6-years of glider deployments. Based on the MLD metric described before, it was found that the shoaling of the MLD in early in the season results in increased chlorophyll a concentrations and as MLD gradually deepens due to wind forcing, phytoplankton concentrations decrease, likely due to decreased light availability. Spatial differences were recorded at the head of the canyon and result from the local circulation, with fresher surface waters with more coastal influence linked to increased chlorophyll concentrations. Intrusions of warm deep water to the upper water column were recorded later in the season and seen preferentially in regions with lower chlorophyll concentrations. Further work involves understanding the circulation dynamics at the head of these cross-shelf canyons to try to understand the importance of advective processes in the observed primary production.

Gliders technologies continue to improve our understanding of the ocean by providing autonomous sampling in high-resolution. Chapter 5 describes the first integration of a Fluorescence Induction and Relaxation (FIRe) sensor on a glider that allows autonomous, vertically resolved, high-resolution characterization of phytoplankton physiological responses to physical forcing, based on fluorescence kinetics. The capabilities of the FIRe glider are demonstrated with a series of deployments designed to evaluate *in situ* phytoplankton community response to the dynamic light environment that Antarctic phytoplankton are exposed to during the growing season. Modeling the *in situ* physiological responses of phytoplankton to ambient light provides insight into the photoacclimation mechanisms driven by variations in vertical mixing regimes over different timescales.

This dissertation provides a robust understanding of some of the mesoscale physical processes driving primary production in these “biological hotspots” in the West Antarctic Peninsula. It also provides insight on the physiological responses and photoacclimation mechanisms utilized to thrive in an environment that is ongoing rapid climatic change. Identifying the mechanisms driving these blooms will help assess the feedbacks associated with a changing climate, such as warming temperatures, increased winds or sea ice reduction. Changes in the MLD and water column stability have already been recorded for northern regions of the WAP, where due to increased winds and reduced sea ice cover, deeper MLD and less stable water columns have already been associated with decreases in phytoplankton success. Understanding how the primary

producers are going to react and adjust to the forecasted environmental changes is crucial to the entire Antarctic ecosystem and the associated biogeochemical cycling.

Acknowledgement of Previous Publications

Chapter 2 is soon to be submitted to the scientific journal *Limnology and Oceanography*:

Carvalho et al. Bottom-up controls of the phytoplankton spring bloom in biological hotspots in the West Antarctic Peninsula

Chapter 3 has been published in the scientific journal *Geophysical Research Letters*:

Carvalho, F., J. Kohut, M. J. Oliver, and O. Schofield (2017), Defining the ecologically relevant mixed layer depth for Antarctica's Coastal Seas, *Geophysical Research Letters*, 44, doi: 10.1002/2016GL071205.

Chapter 4 has been published in the scientific journal *Journal of Geophysical Research: Oceans*:

Carvalho, F., J. Kohut, M. J. Oliver, R. M. Sherrell, and O. Schofield (2016), Mixing and phytoplankton dynamics in a submarine canyon in the West Antarctic Peninsula, *Journal of Geophysical Research: Oceans*, 121(7), 5069-5083, doi: 10.1002/2016JC011650.

Chapter 5 is currently in revision for publication in the scientific journal *Optics Express*:

Carvalho, F., M. Gorbunov, M.J. Oliver, C. Haskins, D. Aragon, J. Kohut and O. Schofield. Mapping in situ chlorophyll variable fluorescence using autonomous underwater gliders, *Optics Express* (in revision).

References

- Alderkamp, A., G. L. van Dijken, K. E. Lowry, T. L. Connelly, M. Lagerström, R. M. Sherrell, C. Haskins, E. Rogalsky, O. Schofield, and S. E. Stammerjohn (2015), Fe availability drives phytoplankton photosynthesis rates during spring bloom in the Amundsen Sea Polynya, Antarctica, *Elementa: Science of the Anthropocene*, 3(1), 000043.
- Allen, S. E., and X. D. de Madron (2009), A review of the role of submarine canyons in deep-ocean exchange with the shelf, *Ocean Sci*, 5(4), 607-620.
- Allen, S. E., C. Vindeirinho, R. E. Thomson, M. G. G. Foreman, and D. L. Mackas (2001), Physical and biological processes over a submarine canyon during an upwelling event, *Canadian Journal of Fisheries and Aquatic Sciences*, 58(4), 671-684, doi:DOI 10.1139/cjfas-58-4-671.
- Annett, A. L., J. N. Fitzsimmons, M. Séguret, M. Lagerström, M. Meredith, O. Schofield, and R. Sherrell (submitted), Controls on dissolved and particulate iron distributions in surface waters of the Western Antarctic Peninsula shelf, *Manuscript submitted to Marine Chemistry (MS number MARCHE_2016_29)*.
- Annett, A. L., M. Skiba, S. F. Henley, H. J. Venables, M. P. Meredith, P. J. Statham, and R. S. Ganeshram (2015), Comparative roles of upwelling and glacial iron sources in Ryder Bay, coastal western Antarctic Peninsula, *Marine Chemistry*, 176, 21-33, doi:10.1016/j.marchem.2015.06.017.
- Arrigo, K. R., M. M. Mills, L. R. Kropuenske, G. L. van Dijken, A.-C. Alderkamp, and D. H. Robinson (2010), Photophysiology in two major Southern Ocean phytoplankton taxa: photosynthesis and growth of *Phaeocystis antarctica* and *Fragilariopsis cylindrus* under different irradiance levels, *Integrative and comparative biology*, 50(6), 950-966, doi:10.1093/icb/icq021.
- Arrigo, K. R., G. L. van Dijken, and A. L. Strong (2015), Environmental controls of marine productivity hot spots around Antarctica, *J Geophys Res-Oceans*, 120(8), 5545-5565, doi:10.1002/2015jc010888.
- Behrenfeld, M., E. Boss, D. A. Siegel, and D. M. Shea (2005), Carbon-based ocean productivity and phytoplankton physiology from space, *Global Biogeochem Cy*, 19(1), doi:10.1029/2004gb002299.
- Behrenfeld, M. J., and E. S. Boss (2014), Resurrecting the ecological underpinnings of ocean plankton blooms, *Annual Review of Marine Science*, 6, 167-194, doi:10.1146/annurev-marine-052913-021325.

Bernard, K. S., and D. K. Steinberg (2013), Krill biomass and aggregation structure in relation to tidal cycle in a penguin foraging region off the Western Antarctic Peninsula, *Ices Journal of Marine Science*, 70(4), 834-849, doi:10.1093/icesjms/fst088.

Bibby, T. S., M. Y. Gorbunov, K. W. Wyman, and P. G. Falkowski (2008), Photosynthetic community responses to upwelling in mesoscale eddies in the subtropical North Atlantic and Pacific Oceans, *Deep-Sea Res Pt II*, 55(10), 1310-1320, doi:10.1016/j.dsr2.2008.01.014.

Bown, J., P. Laan, S. Ossebaar, K. Bakker, P. Rozema, and H. J. W. de Baar (2016), Bioactive trace metal time series during Austral summer in Ryder Bay, Western Antarctic Peninsula, *Deep Sea Research Part II: Topical Studies in Oceanography*, doi:http://dx.doi.org/10.1016/j.dsr2.2016.07.004.

Boyd, P. W., K. R. Arrigo, R. Strzepek, and G. L. van Dijken (2012), Mapping phytoplankton iron utilization: Insights into Southern Ocean supply mechanisms, *J Geophys Res-Oceans*, 117(C6), doi:10.1029/2011jc007726.

Brainerd, K. E., and M. C. Gregg (1995), Surface Mixed and Mixing Layer Depths, *Deep-Sea Res Pt I*, 42(9), 1521-1543, doi:10.1016/0967-0637(95)00068-H.

Brunet, C., J. M. Brylinski, and Y. Lemoine (1993), In-Situ Variations of the Xanthophylls Diatoxanthin and Diadinoxanthin - Photoadaptation and Relationships with a Hydrodynamical System in the Eastern English-Channel, *Marine Ecology Progress Series*, 102(1-2), 69-77, doi:DOI 10.3354/meps102069.

Bruno, M., A. Vazquez, J. Gomez-Enri, J. M. Vargas, J. G. Lafuente, A. Ruiz-Canavate, L. Mariscal, and J. Vidal (2006), Observations of internal waves and associated mixing phenomena in the Portimao Canyon area, *Deep-Sea Res Pt II*, 53(11-13), 1219-1240, doi:10.1016/j.dsr2.2006.04.015.

Carvalho, F., J. Kohut, M. Gorbunov, O. Schofield, and M. J. Oliver (2016a), Mapping Antarctic phytoplankton physiology using autonomous gliders, paper presented at OCEANS 2016 MTS/IEEE Monterey, 19-23 Sept. 2016.

Carvalho, F., J. Kohut, M. J. Oliver, and O. Schofield (2017), Defining the ecologically relevant mixed-layer depth for Antarctica's coastal seas, *Geophysical Research Letters*, 44(1), 338-345, doi:10.1002/2016gl071205.

Carvalho, F., J. Kohut, M. J. Oliver, R. M. Sherrell, and O. Schofield (2016b), Mixing and phytoplankton dynamics in a submarine canyon in the West Antarctic Peninsula, *J Geophys Res-Oceans*, 121(7), 5069-5083, doi:10.1002/2016jc011650.

Chu, P. C., and C. W. Fan (2011), Maximum angle method for determining mixed layer depth from seaglider data, *J Oceanogr*, 67(2), 219-230, doi:10.1007/s10872-011-0019-2.

Cimino, M. A., M. A. Moline, W. R. Fraser, D. L. Patterson-Fraser, and M. J. Oliver (2016), Climate-driven sympatry may not lead to foraging competition between congeneric top-predators, *Scientific reports*, 6.

Clarke, A., M. P. Meredith, M. I. Wallace, M. A. Brandon, and D. N. Thomas (2008), Seasonal and interannual variability in temperature, chlorophyll and macronutrients in northern Marguerite Bay, Antarctica, *Deep-Sea Res Pt II*, 55(18-19), 1988-2006, doi:10.1016/j.dsr2.2008.04.035.

Cullen, J. J., and M. R. Lewis (1988), The kinetics of algal photoadaptation in the context of vertical mixing, *Journal of Plankton Research*, 10(5), 1039-1063.

de Boyer Montégut, C., G. Madec, A. S. Fischer, A. Lazar, and D. Iudicone (2004), Mixed layer depth over the global ocean: An examination of profile data and a profile - based climatology, *Journal of Geophysical Research: Oceans (1978-2012)*, 109(C12).

Demers, S., S. Roy, R. Gagnon, and C. Vignault (1991), Rapid light-induced changes in cell fluorescence and in xanthophyll-cycle pigments of *Alexandrium excavatum* (Dinophyceae) and *Thalassiosira pseudonana* (Bacillariophyceae): A photo-protection mechanism, *Mar. Ecol. Prog. Ser.*, 76, 185-193.

Denman, K., and A. Gargett (1983), Time and space scales of vertical mixing and advection of phytoplankton in the upper ocean, *Oceanography*, 28(5).

Dierssen, H. M., R. C. Smith, and M. Vernet (2002), Glacial meltwater dynamics in coastal waters west of the Antarctic peninsula, *Proc Natl Acad Sci U S A*, 99(4), 1790-1795, doi:10.1073/pnas.032206999.

Dong, S., J. Sprintall, S. T. Gille, and L. Talley (2008), Southern Ocean mixed-layer depth from Argo float profiles, *Journal of Geophysical Research*, 113(C6), doi:10.1029/2006jc004051.

Dubinsky, Z., and O. Schofield (2009), From the light to the darkness: thriving at the light extremes in the oceans, *Hydrobiologia*, 639(1), 153-171.

Ducklow, H., K. S. Baker, D. G. Martinson, L. Quetin, R. Ross, R. C. Smith, S. E. Stammerjohn, M. Vernet, and W. Fraser (2007), Marine pelagic ecosystems: the west Antarctic Peninsula, *Philos Trans R Soc Lond B Biol Sci*, 362(1477), 67-94.

Ducklow, H., et al. (2012), The Marine System of the Western Antarctic Peninsula, in *Antarctic Ecosystems*, edited, pp. 121-159, John Wiley & Sons, Ltd, doi:10.1002/9781444347241.ch5.

Erdmann, E. S., C. A. Ribic, D. L. Patterson-Fraser, and W. R. Fraser (2011), Characterization of winter foraging locations of Adelie penguins along the Western Antarctic Peninsula, 2001-2002, *Deep-Sea Res Pt II*, 58(13-16), 1710-1718, doi:10.1016/j.dsr2.2010.10.054.

Falkowski, P. G., M. Koblizek, M. Gorbunov, and Z. Kolber (2004), Development and application of variable chlorophyll fluorescence techniques in marine ecosystems, in *Chlorophyll a Fluorescence*, edited, pp. 757-778, Springer.

Falkowski, P. G., and Z. Kolber (1995), Variations in chlorophyll fluorescence yields in phytoplankton in the world oceans, *Functional Plant Biology*, 22(2), 341-355.

Falkowski, P. G., and J. Raven (2007), *Aquatic photosynthesis*, 484 pp., Princeton University Press.

Falkowski, P. G., and A. D. Woodhead (2013), *Primary productivity and biogeochemical cycles in the sea*, Springer Science & Business Media.

Fragoso, G. M., and W. O. Smith (2012), Influence of hydrography on phytoplankton distribution in the Amundsen and Ross Seas, Antarctica, *Journal of Marine Systems*, 89(1), 19-29, doi:10.1016/j.jmarsys.2011.07.008.

Fraser, W. R., and W. Z. Trivelpiece (1996), Factors controlling the distribution of seabirds: Winter-summer heterogeneity in the distribution of adélie penguin populations, *Antarctic Research Series*, 70, 257-272.

Fujiki, T., T. Toda, T. Kikuchi, and S. Taguchi (2003), Photoprotective response of xanthophyll pigments during phytoplankton blooms in Sagami Bay, Japan, *Journal of Plankton Research*, 25(3), 317-322, doi:10.1093/plankt/25.3.317.

Garibotti, I., M. Vernet, M. E. Ferrario, R. C. Smith, R. M. Ross, and L. B. Quetin (2003a), Phytoplankton spatial distribution patterns along the western Antarctic Peninsula (Southern Ocean), *Marine Ecology Progress Series*, 261, 21-39, doi:DOI 10.3354/meps261021.

Garibotti, I., M. Vernet, W. A. Kozlowski, and M. E. Ferrario (2003b), Composition and biomass of phytoplankton assemblages in coastal Antarctic waters: a comparison of chemotaxonomic and microscopic analyses, *Marine Ecology Progress Series*, 247, 27-42.

Gorbunov, M. Y., and P. G. Falkowski (2004), Fluorescence induction and relaxation (FIRe) technique and instrumentation for monitoring photosynthetic processes and primary production in aquatic ecosystems, paper presented at Photosynthesis: Fundamental Aspects to Global Perspectives—Proc. 13th International Congress of Photosynthesis, Montreal, Aug.

Gorbunov, M. Y., P. G. Falkowski, and Z. S. Kolber (2000), Measurement of photosynthetic parameters in benthic organisms in situ using a SCUBA - based fast repetition rate fluorometer, *Limnol Oceanogr*, 45(1), 242-245.

Gorbunov, M. Y., Z. S. Kolber, M. P. Lesser, and P. G. Falkowski (2001), Photosynthesis and photoprotection in symbiotic corals, *Limnol Oceanogr*, 46(1), 75-85.

Griffiths, G., C. Jones, J. Ferguson, and N. Bose (2007), Undersea gliders, *Journal of Ocean Technology*, 2(2), 64-75.

Harris, P. T., and T. Whiteway (2011), Global distribution of large submarine canyons: Geomorphic differences between active and passive continental margins, *Marine Geology*, 285(1-4), 69-86, doi:10.1016/j.margeo.2011.05.008.

Haskins, C., and O. Schofield (2015), Glider measurements of phytoplankton physiology in penguin foraging zones along the Western Antarctic Peninsula, paper presented at OCEANS 2015 - MTS/IEEE Washington, IEEE, Washington, DC, 19-22 Oct. 2015.

Hawkings, J. R., J. L. Wadham, M. Tranter, R. Raiswell, L. G. Benning, P. J. Statham, A. Tedstone, P. Nienow, K. Lee, and J. Telling (2014), Ice sheets as a significant source of highly reactive nanoparticulate iron to the oceans, *Nature Communications*, 5, doi:10.1038/ncomms4929.

Helbling, E. W., V. Villafane, and O. Holm Hansen (1991), Effect of Iron on Productivity and Size Distribution of Antarctic Phytoplankton, *Limnol Oceanogr*, 36(8), 1879-1885.

Hofmann, E. E., J. M. Klinck, C. M. Lascara, and D. A. Smith (1996), Water mass distribution and circulation west of the Antarctic Peninsula and including Bransfield Strait, in *Foundations for Ecological Research West of the Antarctic Peninsula*, edited by R. M. Ross, E. E. Hofmann and L. B. Quetin, American Geophysical Union, Washington, D.C., doi:10.1029/AR070p0061.

Holm-Hansen, O., and B. Mitchell (1991), Spatial and temporal distribution of phytoplankton and primary production in the western Bransfield Strait region, *Deep Sea Research Part A. Oceanographic Research Papers*, 38(8), 961-980.

Hopkinson, B. M., B. G. Mitchell, R. A. Reynolds, H. Wang, K. E. Selph, C. I. Measures, C. D. Hewes, O. Holm-Hansen, and K. A. Barbeau (2007), Iron limitation across chlorophyll gradients in the southern Drake Passage: Phytoplankton responses to iron addition and photosynthetic indicators of iron stress, *Limnol Oceanogr*, 52(6), 2540-2554, doi:10.4319/lo.2007.52.6.2540.

Jassby, A. D., and T. Platt (1976), Mathematical formulation of the relationship between photosynthesis and light for phytoplankton, *Limnol Oceanogr*, 21(4), 540-547, doi:10.4319/lo.1976.21.4.0540.

Kahl, A. L., O. Schofield, and W. R. Fraser (2010), Autonomous gliders reveal features of the water column associated with foraging by adelic penguins, *Integr Comp Biol*, 50(6), 1041-1050, doi:10.1093/icb/icq098.

Kara, A. B., P. A. Rochford, and H. E. Hurlburt (2000), An optimal definition for ocean mixed layer depth, *Journal of Geophysical Research: Oceans*, 105(C7), 16803-16821, doi:10.1029/2000JC900072.

Kavanaugh, M. T., F. N. Abdala, H. W. Ducklow, D. Glover, W. Fraser, D. G. Martinson, S. Stammerjohn, O. Schofield, and S. C. Doney (2015), Effect of continental shelf canyons on phytoplankton biomass and community composition along the western Antarctic Peninsula, *Marine Ecology Progress Series*, 524, 11-26, doi:10.3354/meps11189.

Kim, H., S. C. Doney, R. A. Iannuzzi, M. P. Meredith, D. G. Martinson, and H. W. Ducklow (2016), Climate forcing for dynamics of dissolved inorganic nutrients at Palmer Station, Antarctica: An interdecadal (1993–2013) analysis, *Journal of Geophysical Research: Biogeosciences*, 121(9), 2369-2389, doi:10.1002/2015JG003311.

Kohut, J., K. Bernard, W. Fraser, M. J. Oliver, H. Statscevvich, P. Winsor, and T. Miles (2014a), Studying the Impacts of Local Oceanographic Processes on Adelie Penguin Foraging Ecology, *Mar Technol Soc J*, 48(5), 25-34.

Kohut, J., C. Haldeman, and J. Kerfoot (2014b), Monitoring dissolved oxygen in New Jersey Coastal waters using autonomous gliders. U.S. Environmental Protection Agency Rep. EPA/600/R-13/180, Washington, DC.

Kohut, J., E. Hunter, and B. Huber (2013), Small - scale variability of the cross - shelf flow over the outer shelf of the Ross Sea, *Journal of Geophysical Research: Oceans*, 118(4), 1863-1876.

Kolber, Z., O. Prášil, and P. G. Falkowski (1998), Measurements of variable chlorophyll fluorescence using fast repetition rate techniques: defining methodology and experimental protocols, *Biochimica et Biophysica Acta (BBA)-Bioenergetics*, 1367(1), 88-106.

Kolber, Z., J. Zehr, and P. Falkowski (1988), Effects of growth irradiance and nitrogen limitation on photosynthetic energy conversion in photosystem II, *Plant Physiology*, 88(3), 923-929.

Kozlowski, W. A., D. Deutschman, I. Garibotti, C. Trees, and M. Vernet (2011), An evaluation of the application of CHEMTAX to Antarctic coastal pigment data, *Deep Sea Research Part I: Oceanographic Research Papers*, 58(4), 350-364, doi:<http://dx.doi.org/10.1016/j.dsr.2011.01.008>.

Kunze, E., L. K. Rosenfeld, G. S. Carter, and M. C. Gregg (2002), Internal waves in Monterey Submarine Canyon, *J Phys Oceanogr*, 32(6), 1890-1913, doi:Doi 10.1175/1520-0485(2002)032<1890:lwimsc>2.0.Co;2.

Lagerström, M., M. Field, M. Séguet, L. Fischer, S. Hann, and R. Sherrell (2013), Automated on-line flow-injection ICP-MS determination of trace metals (Mn, Fe, Co, Ni, Cu and Zn) in open ocean seawater: Application to the GEOTRACES program, *Marine Chemistry*, 155, 71-80.

Lewis, M., J. Cullen, and T. Platt (1984), Relationships between vertical mixing and photoadaptation of phytoplankton: similarity criteria, *Marine ecology progress series. Oldendorf*.

Lin, H., F. I. Kuzminov, J. Park, S. Lee, P. G. Falkowski, and M. Y. Gorbunov (2016), The fate of photons absorbed by phytoplankton in the global ocean, *Science*, 351(6270), 264-267.

Long, M. C., L. N. Thomas, and R. B. Dunbar (2012), Control of phytoplankton bloom inception in the Ross Sea, Antarctica, by Ekman restratification, *Global Biogeochem Cy*, 26(1).

Lorbacher, K., D. Dommenges, P. P. Niiler, and A. Köhl (2006), Ocean mixed layer depth: A subsurface proxy of ocean-atmosphere variability, *Journal of Geophysical Research*, 111(C7), doi:10.1029/2003jc002157.

Lorenzen, C. J. (1966), A method for the continuous measurement of in vivo chlorophyll concentration, paper presented at Deep Sea Research and Oceanographic Abstracts, Elsevier.

MacIntyre, H. L., T. M. Kana, and R. J. Geider (2000), The effect of water motion on short-term rates of photosynthesis by marine phytoplankton, *Trends in plant science*, 5(1), 12-17.

Martin, J. H., S. E. Fitzwater, and R. M. Gordon (1990), Iron deficiency limits phytoplankton growth in Antarctic waters, *Global Biogeochem Cy*, 4(1), 5-12.

Martinson, D. G., and R. A. Iannuzzi (1998), *Antarctic Ocean - ice interaction: Implications from ocean bulk property distributions in the Weddell Gyre*, Wiley Online Library.

Martinson, D. G., and D. C. McKee (2012), Transport of warm Upper Circumpolar Deep Water onto the western Antarctic Peninsula continental shelf, *Ocean Sci*, 8(4), 433-442, doi:10.5194/os-8-433-2012.

Martinson, D. G., S. E. Stammerjohn, R. A. Iannuzzi, R. Smith, and M. Vernet (2008), Western Antarctic Peninsula physical oceanography and spatio-temporal variability, *Deep-Sea Res Pt II*, 55(18-19), 1964-1987, doi:10.1016/j.dsr2.2008.04.038.

Meredith, M. P., M. A. Brandon, M. I. Wallace, A. Clarke, M. J. Leng, I. A. Renfrew, N. P. Van Lipzig, and J. C. King (2008), Variability in the freshwater balance of northern Marguerite Bay, Antarctic Peninsula: Results from $\delta^{18}\text{O}$, *Deep Sea Research Part II: Topical Studies in Oceanography*, 55(3), 309-322.

Mills, M. M., L. R. Kropuenske, G. L. van Dijken, A.-C. Alderkamp, G. M. Berg, D. H. Robinson, N. A. Welschmeyer, and K. R. Arrigo (2010), Photophysiology in two Southern Ocean phytoplankton taxa: photosynthesis of *Phaeocystis antarctica* (Prymnesiophyceae) and *Fragilariopsis cylindrus* (Bacillariophyceae) under simulated mixed-layer irradiance, *Journal of Phycology*, 46(6), 1114-1127, doi:10.1111/j.1529-8817.2010.00923.x.

Mitchell, B. G., E. A. Brody, O. Holm-Hansen, C. McClain, and J. Bishop (1991), Light limitation of phytoplankton biomass and macronutrient utilization in the Southern Ocean, *Limnol Oceanogr*, 36(8), 1662-1677.

Mitchell, B. G., and O. Holm-Hansen (1991), Observations of modeling of the Antarctic phytoplankton crop in relation to mixing depth, *Deep Sea Research Part A. Oceanographic Research Papers*, 38(8), 981-1007.

Mobley, C. D. (1994), *Light and water: Radiative transfer in natural waters*, Academic press San Diego.

Moline, M. (1998), Photoadaptive response during the development of a coastal Antarctic diatom bloom and relationship to water column stability, *Limnol Oceanogr*, 43(1), 146-153.

Moline, M., H. Claustre, T. K. Frazer, O. Schofield, and M. Vernet (2004), Alteration of the food web along the Antarctic Peninsula in response to a regional warming trend, *Global Change Biology*, 10(12), 1973-1980.

Moline, M., and B. B. Prezelin (1996), Long-term monitoring and analyses of physical factors regulating variability in coastal Antarctic phytoplankton biomass, in situ productivity and taxonomic composition over subseasonal, seasonal and interannual time scales, *Marine Ecology Progress Series*, 145(1-3), 143-160, doi:DOI 10.3354/meps145143.

Moline, M., B. B. Prezelin, and H. Claustre (1996), Light-saturated primary production in antarctic coastal waters, *Antarctic Journal of the United States*, 31(5), 105-107.

Moline, M., B. B. Prezelin, O. Schofield, and R. C. Smith (1997), Temporal Dynamics of Coastal Antarctic Phytoplankton: Environmental Driving Forces and Impact of 1991/92 Summer Diatom Bloom on the Nutrient Regimes, in *Antarctic Communities: Species, Structure and Survival*, edited by B. Battaglia, J. Valencia and D. W. H. Walton, pp. 67-72, Cambridge University Press, Cambridge.

Montes-Hugo, M. A., S. C. Doney, H. W. Ducklow, W. Fraser, D. Martinson, S. E. Stammerjohn, and O. Schofield (2009), Recent changes in phytoplankton communities associated with rapid regional climate change along the western Antarctic Peninsula, *Science*, 323(5920), 1470-1473, doi:10.1126/science.1164533.

Montes-Hugo, M. A., M. Vernet, D. G. Martinson, R. Smith, and R. A. Iannuzzi (2008), Variability on phytoplankton size structure in the western Antarctic Peninsula (1997-2006), *Deep-Sea Res Pt II*, 55(18-19), 2106-2117, doi:10.1016/j.dsr2.2008.04.036.

Montes - Hugo, M. A., C. Sweeney, S. C. Doney, H. W. Ducklow, R. Frouin, D. G. Martinson, S. Stammerjohn, and O. Schofield (2010), Seasonal forcing of summer dissolved inorganic carbon and chlorophyll a on the western shelf of the Antarctic Peninsula, *Journal of Geophysical Research: Oceans* (1978–2012), 115(C3), doi:10.1029/2009JC005267.

Neale, P. J., E. W. Helbling, and H. E. Zagarese (2003), Modulation of UVR exposure and effects by vertical mixing and advection, in *UV Effects in Aquatic Organisms and Ecosystems*, edited by E. W. Helbling and H. Zagarese, pp. 107-134, The Royal Society of Chemistry, doi:10.1039/9781847552266-00107.

Nelson, D. M., and W. Smith (1991), The role of light and major nutrients, *Limnol. Oceanogr*, 36, 1650-1661.

Ohad, I., N. Adir, H. Koike, D. J. Kyle, and Y. Inoue (1990), Mechanism of photoinhibition in vivo. A reversible light-induced conformational change of reaction center II is related to an irreversible modification of the D1 protein, *Journal of Biological Chemistry*, 265(4), 1972-1979.

Oliver, M. J., A. Irwin, M. A. Moline, W. Fraser, D. Patterson, O. Schofield, and J. Kohut (2013), Adelie penguin foraging location predicted by tidal regime switching, *PLoS One*, 8(1), e55163, doi:10.1371/journal.pone.0055163.

Oliver, M. J., M. A. Moline, I. Robbins, W. Fraser, D. Patterson, and O. Schofield (2012), Letting Penguins Lead: Dynamic Modeling of Penguin Locations Guides Autonomous Robotic Sampling, *Oceanography*, 25(3), 120-121.

Olson, R. J., H. M. Sosik, A. M. Chekalyuk, and A. Shalapyonok (2000), Effects of iron enrichment on phytoplankton in the Southern Ocean during late summer: active fluorescence and flow cytometric analyses, *Deep Sea Research Part II: Topical Studies in Oceanography*, 47(15-16), 3181-3200, doi: 10.1016/S0967-0645(00)00064-3.

Prézelin, B. B., E. E. Hofmann, C. Mengelt, and J. M. Klinck (2000), The linkage between Upper Circumpolar Deep Water (UCDW) and phytoplankton assemblages on the west Antarctic Peninsula continental shelf, *Journal of Marine Research*, 58(2), 165-202.

Prézelin, B. B., E. E. Hofmann, M. Moline, and J. M. Klinck (2004), Physical forcing of phytoplankton community structure and primary production in continental shelf waters of the Western Antarctic Peninsula, *Journal of Marine Research*, 62(3), 419-460.

Rozema, P. D., H. J. Venables, W. H. van de Poll, A. Clarke, M. P. Meredith, and A. G. J. Buma (2017), Interannual variability in phytoplankton biomass and species composition in northern Marguerite Bay (West Antarctic Peninsula) is governed by both winter sea ice cover and summer stratification, *Limnol Oceanogr*, 62(1), 235-252, doi:10.1002/lno.10391.

Rudnick, D. L. (2016), Ocean research enabled by underwater gliders, *Annual review of marine science*, 8, 519-541.

Runcie, J. W., and M. J. Riddle (2011), Distinguishing downregulation from other non-photochemical quenching of an Antarctic benthic macroalga using in situ fluorometry, *European Journal of Phycology*, 46(3), 171-180.

Saba, G. K., et al. (2014), Winter and spring controls on the summer food web of the coastal West Antarctic Peninsula, *Nat Commun*, 5, 4318, doi:10.1038/ncomms5318.

Sakshaug, E., and O. Holm-Hansen (1986), Photoadaptation in Antarctic phytoplankton: variations in growth rate, chemical composition and P versus I curves, *Journal of Plankton Research*, 8(3), 459-473.

Sakshaug, E., G. Johnsen, K. Andresen, and M. Vernet (1991), Modeling of light-dependent algal photosynthesis and growth: experiments with the Barents sea diatoms *Thalassiosira nordenskioldii* and *Chaetoceros furcellatus*, *Deep Sea Research Part A. Oceanographic Research Papers*, 38(4), 415-430.

Sakshaug, E., and D. Slagstad (1991), Light and productivity of phytoplankton in polar marine ecosystems: a physiological view, *Polar Research*, 10(1), 69-86.

Sallée, J. B., K. G. Speer, and S. R. Rintoul (2010), Zonally asymmetric response of the Southern Ocean mixed-layer depth to the Southern Annular Mode, *Nature Geoscience*, 3(4), 273-279, doi:10.1038/ngeo812.

Schofield, O., et al. (2013), Penguin Biogeography Along the West Antarctic Peninsula Testing the Canyon Hypothesis with Palmer LTER Observations, *Oceanography*, 26(3), 204-206.

Schofield, O., H. W. Ducklow, D. G. Martinson, M. P. Meredith, M. A. Moline, and W. R. Fraser (2010), How do polar marine ecosystems respond to rapid climate change?, *Science*, 328(5985), 1520-1523.

Schofield, O., C. Jones, J. Kohut, U. Kremer, T. Miles, G. Saba, D. Webb, and S. Glenn (2015a), Developing coordinated communities of autonomous gliders for sampling coastal ecosystems, *Mar Technol Soc J*, 49(3), 9-16.

Schofield, O., et al. (2007), Slocum Gliders: Robust and ready, *J Field Robot*, 24(6), 473-485, doi:10.1002/rob.20200.

Schofield, O., T. Miles, A.-C. Alderkamp, S. Lee, C. Haskins, E. Rogalsky, R. Sipler, R. M. Sherrell, and P. L. Yager (2015b), In situ phytoplankton distributions in the Amundsen

Sea Polynya measured by autonomous gliders, *Elementa: Science of the Anthropocene*, 3(1), 000073.

Schofield, O., M. A. Moline, and B. B. Prezelin (1995), Palmer LTER: Photoacclimation in a coastal phytoplankton bloom, *Biological Sciences*, 130.

Schofield, O., et al. (in review), Decadal variability in coastal phytoplankton community composition in a changing West Antarctic Peninsula, *Deep Sea Research Part II: Topical Studies in Oceanography*.

Sedwick, P. N., A. R. Bowie, and T. W. Trull (2008), Dissolved iron in the Australian sector of the Southern Ocean (CLIVAR SR3 section): Meridional and seasonal trends, *Deep-Sea Res Pt I*, 55(8), 911-925, doi:10.1016/j.dsr.2008.03.011.

Serebrennikova, Y. M., and K. A. Fanning (2004), Nutrients in the Southern Ocean GLOBEC region: variations, water circulation, and cycling, *Deep-Sea Res Pt II*, 51(17-19), 1981-2002, doi:10.1016/j.dsr2.2004.07.023.

Smith, R., K. S. Baker, and M. Vernet (1998), Seasonal and interannual variability of phytoplankton biomass west of the Antarctic Peninsula, *Journal of Marine Systems*, 17(1-4), 229-243, doi:10.1016/S0924-7963(98)00040-2.

Smith, R., D. G. Martinson, S. E. Stammerjohn, R. A. Iannuzzi, and K. Ireson (2008), Bellingshausen and western Antarctic Peninsula region: Pigment biomass and sea-ice spatial/temporal distributions and interannual variability, *Deep-Sea Res Pt II*, 55(18-19), 1949-1963, doi:10.1016/j.dsr2.2008.04.027.

Smith, W., D. G. Ainley, K. R. Arrigo, and M. S. Dinniman (2014), The oceanography and ecology of the Ross Sea, *Annual review of marine science*, 6, 469-487.

Smith, W., and R. M. Jones (2015), Vertical mixing, critical depths, and phytoplankton growth in the Ross Sea, *ICES Journal of Marine Science: Journal du Conseil*, 72(6), 1952-1960, doi:10.1093/icesjms/fsu234.

Smith, W., and E. Sakshaug (2013), 9. Polar Phytoplankton, in *Polar Oceanography: Chemistry, Biology, and Geology*, edited by W. Smith, pp. 477-526, Academic Press, San Diego, CA.

Smith, W., S. Tozzi, M. C. Long, P. N. Sedwick, J. A. Peloquin, R. B. Dunbar, D. A. Hutchins, Z. Kolber, and G. R. DiTullio (2013), Spatial and temporal variations in variable

fluorescence in the Ross Sea (Antarctica): Oceanographic correlates and bloom dynamics, *Deep Sea Research Part I: Oceanographic Research Papers*, 79, 141-155.

Stammerjohn, S. E., D. G. Martinson, R. C. Smith, and R. A. Iannuzzi (2008), Sea ice in the western Antarctic Peninsula region: Spatio-temporal variability from ecological and climate change perspectives, *Deep-Sea Res Pt II*, 55(18-19), 2041-2058, doi:10.1016/j.dsr2.2008.04.026.

Suggett, D. J., C. M. Moore, and R. J. Geider (2010), Estimating aquatic productivity from active fluorescence measurements, in *Chlorophyll a fluorescence in aquatic sciences: methods and applications*, edited, pp. 103-127, Springer.

Suggett, D. J., C. M. Moore, A. E. Hickman, and R. J. Geider (2009), Interpretation of fast repetition rate (FRR) fluorescence: signatures of phytoplankton community structure versus physiological state, *Marine Ecology Progress Series*, 376, 1-19.

Sverdrup, H. (1953), On conditions for the vernal blooming of phytoplankton, *Journal du Conseil*, 18(3), 287-295.

Todoroff, K., J. Kohut, P. Winsor, and H. Statscewich (2015), Spatial circulation patterns over Palmer Deep canyon and the effects on Adélie Penguin foraging, paper presented at OCEANS 2015 - MTS/IEEE Washington, 19-22 Oct. 2015.

Twining, B. S., and S. B. Baines (2013), The trace metal composition of marine phytoplankton, *Ann Rev Mar Sci*, 5, 191-215, doi:10.1146/annurev-marine-121211-172322.

Venables, H. J., A. Clarke, and M. P. Meredith (2013), Wintertime controls on summer stratification and productivity at the western Antarctic Peninsula, *Limnol. Oceanogr*, 58(3), 1035-1047.

Vernet, M., D. G. Martinson, R. A. Iannuzzi, S. E. Stammerjohn, W. Kozlowski, K. Sines, R. C. Smith, and I. Garibotti (2008), Primary production within the sea-ice zone west of the Antarctic Peninsula: I-Sea ice, summer mixed layer, and irradiance, *Deep-Sea Res Pt II*, 55(18-19), 2068-2085, doi:10.1016/j.dsr2.2008.05.021.

Walsh, J. J., D. A. Dieterle, and J. Lenos (2001), A numerical analysis of carbon dynamics of the Southern Ocean phytoplankton community: the roles of light and grazing in effecting both sequestration of atmospheric CO₂ and food availability to larval krill, *Deep Sea Research Part I: Oceanographic Research Papers*, 48(1), 1-48.

Webb, W. L., M. Newton, and D. Starr (1974), Carbon dioxide exchange of *Alnus rubra*, *Oecologia*, 17(4), 281-291.

Yentsch, C. S., and D. W. Menzel (1963), A method for the determination of phytoplankton chlorophyll and phaeophytin by fluorescence, paper presented at Deep Sea Research and Oceanographic Abstracts, Elsevier.